[Cover]

Non-Negative Matrix Decomposition for single-channel source separation in biomedical signal processing applications

Memoria de la Tesis Doctoral realizada por

Maciej Niegowski

Y dirigida por el

Dr. Miroslav Zivanovic

Para optar al grado de

Doctor

Departamento de Ingeniería Eléctrica y Electrónica

Universidad Pública de Navarra

Pamplona, Noviembre 2017

Non-Negative Matrix Decomposition for single-channel source separation in biomedical signal processing applications

Memoria de la Tesis Doctoral realizada por

Maciej Niegowski

Y dirigida por el

Dr. Miroslav Zivanovic

Para optar al grado de

Doctor

Departamento de Ingeniería Eléctrica y Electrónica

Universidad Pública de Navarra

Pamplona, Noviembre 2017

Resumen

La separación de fuentes en el procesamiento de señales digitales, consiste en encontrar las mejores aproximaciones de las componentes de una mezcla de señales. Aunque en la mayoría de los casos no se dispone de antemano de una información detallada sobre las fuentes, es posible realizar una separación parcial. Uno de los posibles métodos es la factorización de matrices no negativa (NMF). A pesar de su creciente popularidad en la comunidad de procesamiento de señales biomédicas, se presta poca atención a los importantes inconvenientes que a menudo impiden su uso de forma directa.

Uno de estos inconvenientes es la inicialización aleatoria del algoritmo, lo que a menudo lleva a un mínimo local y a resultados irreproducibles. La selección del rango de las fuentes individuales es a menudo engañosa. Una solución habitual para este problema es asignar el rango de acuerdo con la cantidad de fuentes y luego ajustarlo mediante un procedimiento iterativo de prueba y error. Desafortunadamente, este procedimiento es computacionalmente costoso y no hay garantía de que converja al rango óptimo para cada fuente. Otro aspecto importante es la transformación utilizada para pasar del dominio del tiempo a la representación no negativa (matricial) y viceversa.

En la presente tesis se abordan los problemas mencionados y se proponen nuevas características para algoritmo, tales como: estimación inequívoca del rango no-negativo e inicialización con estructuras cuidadosamente diseñadas. Todos los métodos propuestos se han comparado con al menos dos de referencia.

Summary

Source separation in digital signal processing consists of finding best estimates of the signals involved in a signal mixture. Although, in most cases a detailed information about the sources is not known in advance, a partial separation is still possible. One of possible methods is non-negative matrix factorization NMF. In spite of its increasing popularity in the biomedical signal processing community, a little attention is paid to its serious drawbacks which often make impossible the straightforward use of the available “off-shelf” algorithm.

One of them is a random initialization of an algorithm what often leads to a local minimum and irreproducible results. The selection of the non-negative rank of individual sources is often misleading. A usual shortcut to this problem is to assign rank according to the number of sources and then to tune it up by some iterative trial-and-error input matrix decomposition procedure. Such an approach is computationally costly and is not guaranteed to converge to optimal rank for each source. Moreover, a synthesis of time-domain waveforms from the low-rank source descriptions is often hard, due to the fact that the original phases are unknown.

In the present thesis we address the aforementioned drawbacks and introduce new algorithm features, namely: unambiguous non-negative rank estimation and initialization with carefully designed structures. All proposed methods have been compared to at least two-state-of art reference methods.

Acknowledgements

The author of this thesis expresses a deep debt of gratitude for the contribution of my promoter Dr. Miroslav Zivanovic, namely for his support and substantial investment of his time and effort during the whole research. I am also indebted to Dr. Marisol Gomez who was always there, to motivate me and to find an appropriate solution to all critical situations.

To Dr. Luis Serrano my former tutor, without his initial economical support and encouragement I would not have had joined university community and would not have started thinking of pursuing the Ph.D degree.

I would like to acknowledge my beloved wife Ewa for a great amount of patience and understanding during the whole research.

Of course, to my dear parents Grażyna, Marek, and granny Eugenia for their unconditional love and respect that they have shown me regarding my decisions. Thank you for your support even being so far away.

I should not finish this section without expressing my gratitude to the Universidad Pública de Navarra for hosting me during this educational process and the Gobierno de Navarra for its financial support through the grant.

CONTENTS

“Where there's a will, there's a way.”

Chapter 1

INTRODUCTION

This chapter is intended to provide the general framework of the present research work. The motivation of the source separation and the state of the art are herein discussed. Finally, objectives and structure of the thesis are presented.

1.1 Motivation

Source separation in digital signal processing consists of finding best estimates of the signals involved in a signal mixture. It has found a wide range of applications in different areas i.e. biomedical signal identification, astronomical imaging, communication, speech or audio signal processing. An example is a cocktail party problem, where a number of people are talking simultaneously in a room and a listener is trying to follow one of the conversations [1]. In a biomedical scenario, for instance, the role of the listener can play a set of electrodes attached to the patient during electrocardiogram test. Unwanted artifacts and noise may easily be introduced with patient movements or by power line interferences (PLI). Therefore, source separation treats the signal and artifacts as a source mixture which has to be resolved.

Although, in most cases a detailed information about the source signals present in a mixture is not known in advance, partial separation is still possible by using methods based on parametric or nonparametric approaches. Parametric approaches are based on modeling of the sources involved in a signal mixture. An example of a parametric method is [2] where modeled signals are represented by a set of sinusoids with adjustable amplitude and phase coefficients.

The non-parametric approaches do not use explicit signal models and require less prior knowledge about the mixed sources. The basic ones include all kinds of filtering, whilst the

more advanced employ unsupervised learning algorithms that exploit a priori knowledge about true nature, morphology or structure of latent (hidden) variables or sources such as nonnegativity, sparseness, spatiotemporal decorrelation, statistical independence, smoothness or lowest possible complexity. The key issue is to find such a transformation or coding which has true physical meaning and interpretation [3]. The most popular unsupervised approaches are based either on statistical signal processing, as for example independent component analysis (ICA), or on decomposition principles as matrix factorization (MF). The former methods focus on source signals that are statistically independent, which means that a value of one of the source signals gives no information on the value of other source signals [1] present in the signal mixture. One of the techniques based on MF approach that actually involves nonnegative constrained is called Non-Negative Matrix Factorization (NMF). Starting from an initial guess, NMF decomposes iteratively the intensity representation (e.g. spectrogram) of an input signal mixture into a sum of non-negative components that may naturally correspond to organic properties of the data [4].

Another aspect is a number of data channels available for the measurements: source signal mixture can be given either as a single-channel or multichannel data. Dealing with multichannel data usually requires massive computational resources, since commonly applied signal processing techniques involve complex mathematical algorithms, conditioned by a set of parameters that needs to be adequately tuned. Our experience, resulting from a number of collaborations with medical and sports institutions, shows that end users prefer simple single-channel based approaches with a small number of control parameters. Not only computational complexity may influence long processing time but also the size of the data; modern ambulatory system for physiological research can record up to 32 channels e.g. Electroencephalography (EEG) data sets can occupy more than 1 GB of memory. What is more, a data availability itself may be an issue. In case of surface electromyography (EMG) i.e. electrical activity of muscles, the multichannel data is seldom available. In a vast majority of scenarios, the signals are recorded using a monopolar/bipolar EMG.

In a view of the aforementioned discussion, we decided to focus our research on single-channel source separation only.

1.2 The State of the art

In this section, we will discuss the single-channel source separation techniques already employed in biomedical applications. The methods based on matrix decomposition approach proposed in the present doctoral study and the comparison methods used to evaluate their performance operate on single-channel data only.

The most common parametric method is a sinusoidal modeling which makes use of explicit quasi-harmonic time-variant modeling of the source signals. In biomedical applications, it has been successfully used for modeling the PLI and base line wander (BW) and their removal from ECG and EMG [5]. In more complex case ECG was modeled as high order polynomial with coefficients obtained from solving a linear system of equations in a way that enabled its suppression in EMG [2]. This method exhibits also drawbacks i.e. a proper adjustment of window size together with correct selection of polynomial order for a given scenario and the estimation of the fundamental frequency of a modeled signal especially in a noisy surrounding.

On the other hand, there are non-parametric approaches which are usually based on some kind of signal decomposition. Regarding EMG-ECG separation [6] the simplest approaches include gating [7] subtraction [8] and filtering [9] [10], However, they lack efficiency due to the simplistic approach to the issue of time-frequency signal overlap.

More sophisticated approaches include singular spectrum analysis (SSA) [11] [12] and various noise cancelling algorithms based on the theory of adaptive filtering [13] [14] [15] [16] [17]. They can achieve a good separation quality at the expense of making use of external reference signals and supplementary electrodes.

The use of wavelets in ECG signal processing applications (e.g. QRS detection, compression, denoising [18] [19] [20] [21] [22]) has inspired a number of EMG-ECG separation approaches where the temporal features of an electrocardiogram are captured in the multiresolution time-scale domain. Such an analysis is typically carried out by performing the Discrete Wavelet Transform (DWT) with thresholding of the input signal, followed by adaptive filtering [23] [24], independent component analysis [25] [26], matching pursuit [27], and pitch-synchronous extraction [28]. An interesting approach used in smoothing of ECG Signals is based on Savitzky-Golay filtering [29] [30].

When suppressing PLI the most commonly used techniques are fixed-frequency digital notch filters [31] [32] [33] [34] [35] [36] [37] [38] or the spectral Hampel filter [39], which replaces PLI outliers in the frequency domain with the average of a set of local values. The efficiency of this approach, however, is strongly dependent on the robustness of the outlier detector [39] [40]. More advanced methods use adaptive filters [41] [42] [43] [44] [13] [45] and versions of the Kalman filter [46] [47]. In this application approaches based on WDT [48] [49] [50], time-frequency nonlinear analysis of nonstationary signals [51] [52] [53] and neural networks [54] [55] were also used. In addition, some researches made use of ICA [56] [57] [58] and the subtraction procedure [59] [60].

1.3 The focus of the research

Once the state of the art has been reviewed, we will focus on the single-channel separation approach based on matrix decomposition, in particular the Non-Negative Matrix Factorization (NMF). In spite of its increasing popularity in the biomedical signal processing community, a little attention is paid to its serious drawbacks which often make impossible the straightforward use of the available “off-shelf” algorithms.

The initialization of the classical NMF [61] is performed through matrices containing random non-negative entries. Such an initialization is very general and easy to implement, because it does not assume any kind of a priori information about the input signal. However, it often leads to convergence to a local minimum and accordingly results in unsatisfactory source separation. In the literature, there are only a few attempts at non-random initialization that aim at reaching smaller convergence overall error e.g. the methods based on PCA, fuzzy clustering or wavelets [62].

Optimal non-negative rank is another key factor in non-negative matrix decomposition because it provides a way to drastically reduce problem dimensionality without losing any relevant characteristic of the underlying source. Surprisingly, in the literature this issue is seldom dealt with.

Furthermore, the NMF sensitivity to the non-negative representation of the input signal mixture is another concern to be addressed. The most popular choice is the squared

magnitude of the Short time Fourier Transform (STFT) of the input signal – the spectrogram. However, it turns out that even very small changes of spectrogram parameters (size, type of the window or analysis frame overlap) influence strongly the separation efficiency. Moreover, the spectrogram does not preserve information of the phase which is needed by inverse STFT.

Many users are not aware of the mentioned drawbacks, which inevitably gives rise to irreproducible results. Our goal is to thoroughly analyze the mechanisms behind the NMF algorithms and to come up with a solution to the mentioned drawbacks so that NMF analysis becomes reliable and adequate tool for a number of biomedical applications.

1.4 Outline of the thesis

The thesis contains six hierarchically organized chapters: at the beginning the reader is introduced into the source separation problematic; next, we discuss the classical matrix decomposition approach and its drawbacks. In the following chapters, the reader keeps track on the evolution of the proposed approaches/methods. Each chapter describes a methodology-algorithm based on a carefully chosen example and performance evaluation against at least two state-of-art methods. A brief description of the chapters follows.

Chapter 1 is devoted to the state-of-art of single-channel methods, together with their biomedical applications and main drawbacks. The objectives of this thesis have also been formulated here.

Chapter 2 gives an overview of classical non-negative matrix factorization algorithms [61], where initialization matrices have random entries and multiplicative update rules with a cost function are based on Euclidean distance. At the end of the chapter, the influence of the key parameters selection on the analysis outcome has been discussed.

In Chapter 3 we present our first attempt to address the concerns of the classical NMF outlined in Chapter 2. The approach was focused on enhancing the sparsity of the spectrogram by filtering and downsampling the input mixture signal, thus bringing out a characteristic pattern of one of the constituent signals in the mixture. The STFT was applied in order to satisfy the non-negativity constraint.

In Chapter 4 we work with the Wavelet Transform instead of the popular STFT. The adequately chosen basis functions, Cauchy-type non-linearly scaled wavelets, captured the basis of a desired waveform shapes with a relatively small number of wavelet coefficients. Accordingly, the matrix initialization is strongly improved by confining the algorithm's starting point in the very neighborhood of the global minimum of the cost function.

In Chapter 5 we propose a novel method which treats the harmonic and baseline noise removal task as a source separation problem. The proposed method overcomes the aforementioned drawbacks by introducing new algorithm features, namely: unambiguous non-negative rank estimation of individual sources in the data and phase-preserving spectrogram segmentation.

Finally, general conclusions and future lines of the research will be discussed.

Chapter 1: INTRODUCTION

Chapter 2

NON-NEGATIVE MATRIX FACTORIZATION

In this chapter an NMF algorithm for dimensionality reduction and source separation is discussed. The last section presents the performance of the NMF algorithm applied on source separation of real biomedical signals.

2.1 Introduction

In the literature there are a number of matrix decomposition techniques, to name a few, Principle Component Analysis (PCA), Singular Value Decomposition (SVD), Probability Matrix Decomposition (PMD), Non-Negative Matrix Factorization (NMF) etc. They all seek to find important information hidden in a complex system expressed in a matrix form: e.g. PCA is a tool which aligns data with the most important correlated dimensions (dimension reduction).

NMF differs from most decomposition techniques because it imposes additional constraint to a matrix form; all matrix entries must be non-negative which leads to a parts-based representation of data [4]. Initially, it was applied to face recognition, where each image consisted of different combinations of facial parts (eyes, nose, mouth etc.) and those combinations were treated as different image patterns. The variables were mapped to pixel intensities, which are by default non-negative.

In any biomedical signal processing application, the input time domain signal needs to be first converted to an image representation. Typically, it is achieved by means of the STFT. In this way, the corresponding spectrogram is regarded as a combination of time-frequency elements which are, similarly to the face recognition application, used to compose diverse patterns of sources involved in the input mixture.

2.2 Method

An overview of the classical "of-the-shelf" NMF algorithm can be seen in the Figure 2.1, where a time domain input signal mixture has to be transformed into a non-negative representation denoted further as ***V***. Then it is factorized into $\boldsymbol{V_1, V_2, \ldots V_N}$ estimates which in the end are transformed back into time domain waveforms.

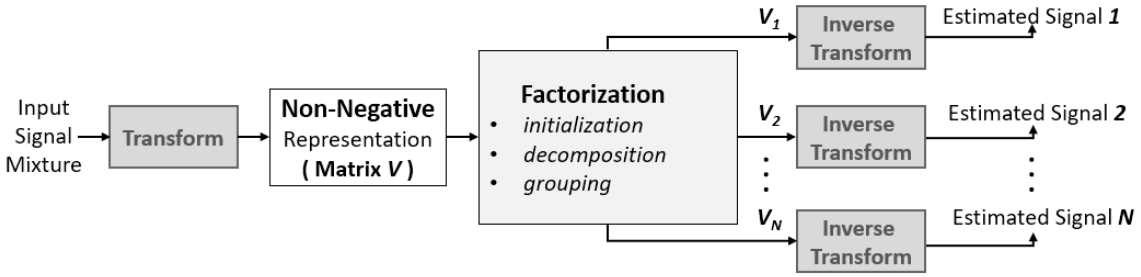

Figure 2.1 Overview of the major steps in the classical NMF algorithm.

The NMF aims at creating a low rank approximation of ***V*** which contains a product of non-negative factors (matrices or vectors) usually called ***W*** and ***H***. It is done by solving the following nonlinear optimization problem:

$$C = min \parallel \boldsymbol{V} - \boldsymbol{WH} \parallel^2 = min\left(\sum_{ij}\left(\boldsymbol{V_{ij}} - (\boldsymbol{WH})_{ij}\right)^2\right) \tag{2.1}$$

where ***C*** is the cost function to be minimized through a number of iterations, with $\boldsymbol{W} \geq 0$ and $\boldsymbol{H} \geq 0$. In the neighborhood of an optimal solution (global minimum) the matrices ***W*** and ***H*** respectively contain the spectrum and the temporal activity information of the input signal s:

$$\boldsymbol{V} \approx \boldsymbol{WH} \tag{2.2}$$

Whether ***W*** and ***H*** are vectors or matrices depends on user-defined factorization rank *r*.

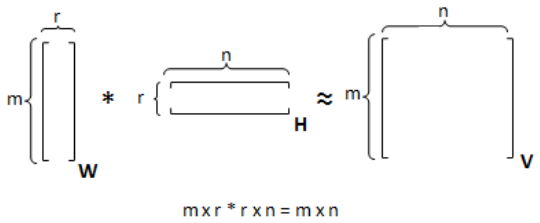

Figure 2.2 Graphical representation of the decomposition given by (2.2).

The authors of the classical NMF algorithm [61] indicate that matrix factorization rank *r* should be chosen so that:

$$(n+m)*r < n*m \tag{2.3}$$

and they add that the product ***WH*** should be regarded as a compressed form of the data ***V***. Unfortunately, no information on how to select an optimal value of *r* was given.

According to Figure 2.1, the factorization part can be divided into three steps:

- initialization,
- decomposition,
- source grouping.

In the classical approach the matrices ***W*** and ***H*** are initialized with the Gaussian noise [61]. The decomposition step is iterative and consists of finding the values of non-negative matrices ***W*** and ***H*** so that their product equals approximately to input matrix ***V*** (2.2).

In particular, initialized matrices ***W*** and ***H*** are modified within in each iteration according to the so called "multiplicative rules" until desired precision of (2.1) is reached. These rules, given by the following expressions, minimize the Euclidean distance between ***V*** and the product ***WH***:

$$\boldsymbol{W_{ia} \leftarrow W_{ia}} \frac{\left(\boldsymbol{VH^T}\right)_{\boldsymbol{ia}}}{\left(\boldsymbol{WHH^T}\right)_{\boldsymbol{ia}}} \tag{2.4}$$

$$\boldsymbol{H_{aj} \leftarrow H_{aj}} \frac{\left(\boldsymbol{W^T V}\right)_{\boldsymbol{aj}}}{\left(\boldsymbol{W^T WH}\right)_{\boldsymbol{ia}}} \tag{2.5}$$

Euclidean distance is invariant under these updates if and only if ***W*** and ***H*** are at a stationary point of the distance [61].

After the decomposition step, (2.2) is expressed as a sum of factorized products $\boldsymbol{w_{r_1}h_{r_1}}, \boldsymbol{w_{r_2}h_{r_2}}, \ldots \boldsymbol{w_{r_N}h_{r_N}}$.

$$\boldsymbol{WH} = \sum_{n=1}^{N} \boldsymbol{w_{r_n}h_{r_n}} \tag{2.6}$$

The matrix factorization grouping *factor* r_n defines how many columns and corresponding rows of the product ***WH*** are to be taken into account in order to estimate correctly each source signal $\boldsymbol{V_n}$:

$$\boldsymbol{V_N} = \boldsymbol{w_{r_N}h_{r_N}} \tag{2.7}$$

As the final step, after factorization of ***V*** into source signal estimates $\boldsymbol{V_1, V_2, \ldots V_N}$ each one of them is transformed back into time domain.

2.2.1 Algorithm summary

(1) Initialization

- Non-negative rank set by a user – typically *r* equals to *N* number of sources.
- Initialization of an algorithm with Gaussian Noise.

(2) Decomposition

- Obtain sub-spectrogram estimates by the Euclidean-distance NMF constrained to the basis vectors matrix and activation coefficients matrix.
- For each estimated source:

(3) Obtain time-waveforms by means of the inverse STFT.

2.3 Critical aspects

It is vey important to have in mind that succesful application of NMF depends mainly on the follwing aspects:

- Non-negative signal represenatation (transform).
- An accurate selection of the factorization rank *r*.
- A proper initialization of martices ***WH***.

If it is necessary to return to a time domain after decomposition, an ***inverse transform*** also plays a significant role in terms of separation quality.

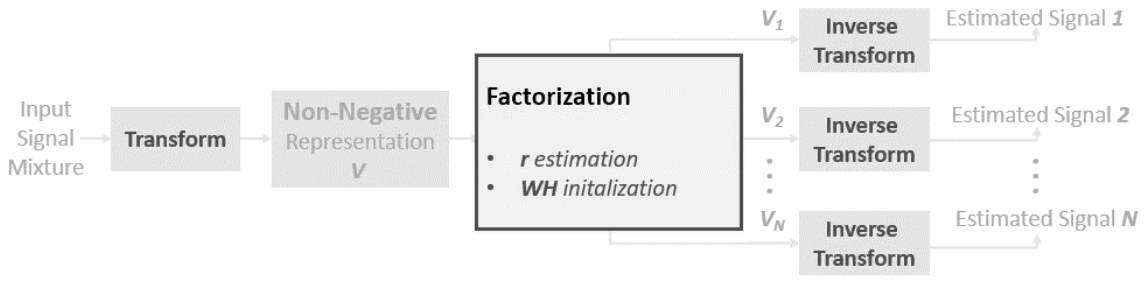

Figure 2.3 Critical aspects in the use of the classical NMF algorithm.

There is a number of NMF variants that add additional constraints to the algorithm as orthogonality [63] [64] [65], temporal continuity [66] or sparseness [67] [68] [69]. An alternative to Euclidean distance may be normalized Kullback-Leibler divergence [61] which was further modified by imposing sparsity and orthogonality [70]. Another interesting approach proposed a convolutive NMF [71]. Unfortunately, unless critical aspects are taken into account (and set correctly according to the available data), there is no guaranty that any of the mentioned NMF methods will work properly.

2.3.1 Transform

The spectral content of biomedical signals is non-stationary (changes over time); thus, applying the Discrete Fourier Transform (DFT) over the whole data record would not reveal transitions in a spectrogram. The way to avoid that is to apply the DFT over short periods of time so that the analyzed signals could be seen as quasi-stationary.

A spectrogram *S(t,ω)* is calculated by dividing the time domain signal *s(τ)* into small frames and performing DFT on each frame:

$$S(t,\omega) = DFT\,\{s(\tau)\gamma(\tau - t)\} \tag{2.8}$$

where $\gamma(\tau - t)$ is a short-time window, whilst the magnitude $\boldsymbol{V}$ is expressed as the norm $\|S(t,\omega)\|$.

In biomedical applications it is often desired to recover time domain waveforms from separated spectrogram estimates $\boldsymbol{V_1, V_2, \ldots V_N}$. To that end, we need the original phase information which, unfortunately, is not contained in the spectrogram.

One of the possibilities to acquire information of phase is to employ a phase generator [72] or a pretrained autoregressive model [73]. The less resource-demanding solution can be found in [74] where it is assumed that at each STFT sample, one of the involved sources is dominant at a given time.

Also note that a spectrogram is very sensitive to the parameters as analysis window type, duration (controls frequency resolution) and overlap between windows. For instance, a time domain ECG-EMG mixture can be shown either in a form of horizontal or vertical lines that stand for a set of harmonics and oriented clusters for QRS complexes of an ECG signal, respectively (Figure 2.4). The blurry background is EMG signal. The short vertical TF pattern of ECG signal was obtained with extremely short analysis window. More examples can be found in the 2.4 section of this chapter.

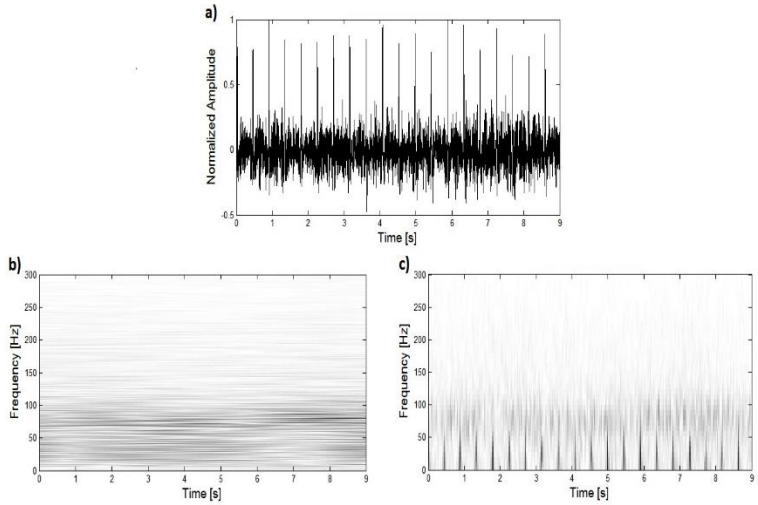

Figure 2.4 ECG-EMG signal mixture spectrogram for different analysis window duration: a) input signal, b) 4 seconds c) 0.1 seconds.

2.3.2 Factorization rank

Non-negative rank *r* provides a way to drastically reduce problem dimensionality without losing any relevant characteristic of the underlying sources; also, it allows for a fast convergence to a global minimum.

The usual rank selection strategy, which seems to work fine in audio domain, sets *r* equal to the number of sources *N* [67] or slightly higher than *N*; once the decomposition has been carried out a correct number is selected [75]. However, this strategy not always holds true for more complex TF patterns in biomedical signal processing domain, even though the number of sources might be known beforehand.

In special cases when TF signal patterns are not too complex e.g. a 50Hz PLI characterized either by a horizontal line or a clean ECG waveform represented as a set of vertical lines for a short spectrogram analysis window (Figure 5), *r* can be set to unity.

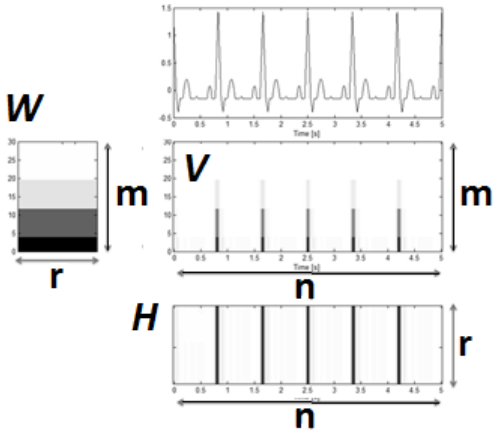

Figure 2.5 In the central part of the figure there is a very short windowed spectrogram V of the clean ECG waveform seen just above it (marked with blue). The vectors W and H were obtained with a classical NMF with r set to unity. Their dimensions m x r and r x n coincide with V dimensions; m x n.

In the Figure 2.5, spectrogram ***V*** of the ECG waveform is decomposed by NMF with $r = 1$ into ***W*** and ***H*** vectors that contain frequency components and the information of spatial occurrence of these components, respectively. Note that lengths of these vectors (m and n, respectively) are also defined by the size of ***V***.

In chapter 5, we develop a study which discusses a general relationship between a standard and the non-negative matrix rank. There is also presented a procedure for estimation of the optimal rank r.

2.3.3 Initialization

The initialization of the classical NMF algorithm [61] is performed through the matrices ***W*** and ***H*** containing random non-negative entries. Such an initialization is very general and easy to implement, because it does not assume any kind of a priori information about the input signal. However, this type of initialization means that the initial point of the iterative process might be close to a global minimum. Since there are typically various local minima in a cost function, the algorithm might never reach the global convergence. In the worst-case scenario, the algorithm can get stuck in a local minimum and even after many iterations the result would not improve at all. Moreover, in series of trails the starting point is often set differently for each trail, even though the algorithm settings remain unchanged.

In order to ensure convergence to a global minimum, a proper initialization of an NMF algorithm is crucial [76]. In the literature, there are only a few attempts at non-random initialization that aim at reaching smaller overall error at convergence e.g. the methods based on PCA, SVD, centroid-based and fuzzy clustering or wavelets [62] [77] [78] [79].

It is our belief that initialization of an algorithm should depend strongly on a data type, in case of biomedical signal applications; the TF patterns of the sources should be taken into account, as we show in the Chapters 3, 4 and 5. Only well-designed initialization structures can guarantee repeatability of an NMF algorithm.

2.4 Separation performance

As an example, let us show how a Euclidean-based NMF performs on real ECG-EMG signal mixtures. We want to show that varying spectrogram parameters (e.g. window duration) as well as the factorization rank *r* can indeed influence separation quality.

As already mentioned, the random initialization often makes NMF produce different outcome in each trail, in terms of the separation quality. There is also no guarantee that estimates $\boldsymbol{V_1, V_2, \ldots V_N}$ will always contain the same separated sources. It means that after one analysis, estimate $\boldsymbol{V_1}$ may represent the estimated source whereas in the other (with exactly the same settings) this source will be placed in another estimate, for example, $\boldsymbol{V_2}$.

2.4.1 Data

The experimental procedure was conducted in accordance with the Declaration of Helsinki and was approved by the Local Ethics Committee. Each subject provided an informed written consent before participation in the study.

The EMG signal was obtained from the vastus medialis obliquus during a sustained fatiguing contraction at 30% of the maximal voluntary contraction (MVC) for ten healthy subjects. The MVC was calculated as the highest value of two MVCs of the right knee extension over a period of 5 seconds, separated by 120 seconds of rest. The signals were recorded using three Ag/AgCl sintered electrodes (4 mm in diameter). The skin surface was abraded before the electrode fixation. Next, the signals were band-pass filtered (−3 dB bandwidth, 1–500 Hz), sampled at

2048 Hz and digitalized with 12 bits resolution. The EMG signal before mixing was downsampled to 1 kHz.

The ECG signals were taken from the PTB Diagnostic ECG database which is a part of the Physionet project [80]. The database contains 549 recordings from 290 subjects, each subject represented by one to five recordings. Each recording includes 15 simultaneously measured signals by the conventional 12 electrodes. The recordings are digitized at 1 kHz with 16-bit resolution over the ±16.384 mV range.

2.4.2 Spectrogram - duration of the window

The duration of the analysis window has a significant impact on how signal sources are represented in a form of TF image. In Figure 2.6 – 2.8 the window duration is set to be 2 seconds, 1 second and finally 0.1 seconds respectively whilst the rest of the settings is kept unchanged. There is a 50% overlap and the window type used is Hanning. The factorization rank *r* equals to 2 i.e. two sources are present in the mixture.

By a visual inspection of these figures, the window size has indeed influence on the separation results. For windows longer than 1 second, the characteristic TF pattern of the ECG is lost and the separation is not possible. A smaller window duration brings out the ECG from a noisy-like EMG yielding better results.

Although the results are far from desired we can clearly see that each of the obtained waveforms can roughly be associated with its original unmixed signal source.

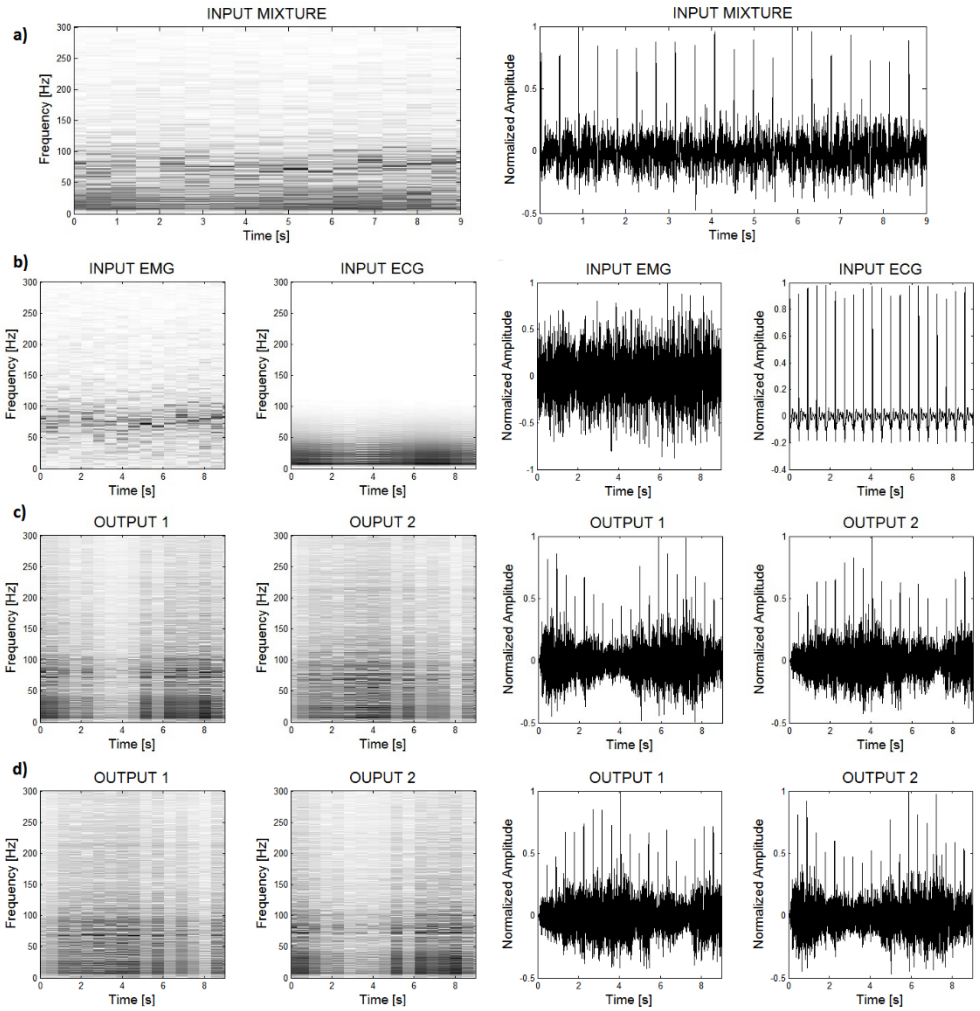

Figure 2.6 On the right-hand side there are waveforms and on the left-hand side there are their corresponding spectrograms (window size equals to 2 seconds). Starting from the top of the figure, a) ECG-EMG input mixture; b) clean ECG and clean EMG input sources; c) and d) represent separation results (output 1&2) obtained by two different NMF analysis with the same settings.

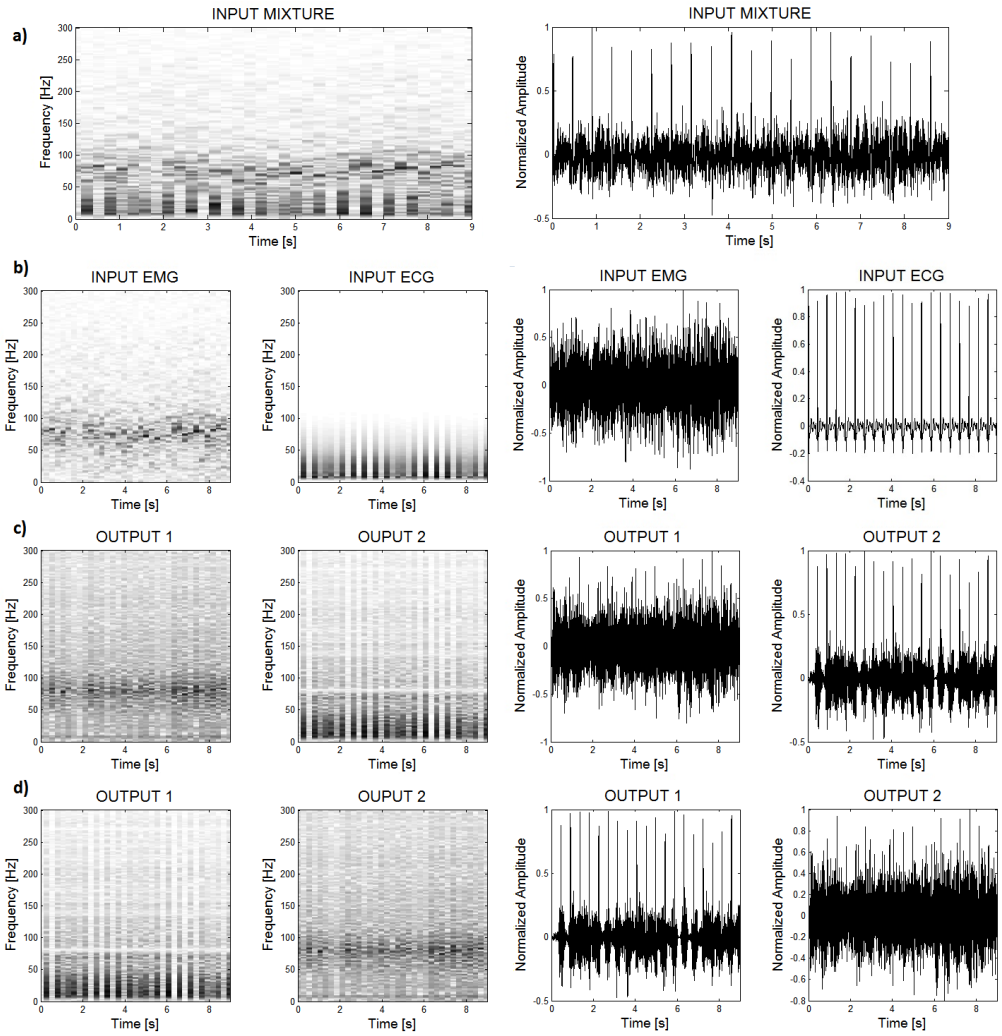

Figure 2.7 On the right-hand side there are waveforms and on the left-hand side there are their corresponding spectrograms (window size equals to 1 second). Starting from the top of the figure, a) ECG-EMG input mixture; b) clean ECG and clean EMG input sources; c) and d) represent separation results (output 1&2) obtained by two different NMF analysis with the same settings.

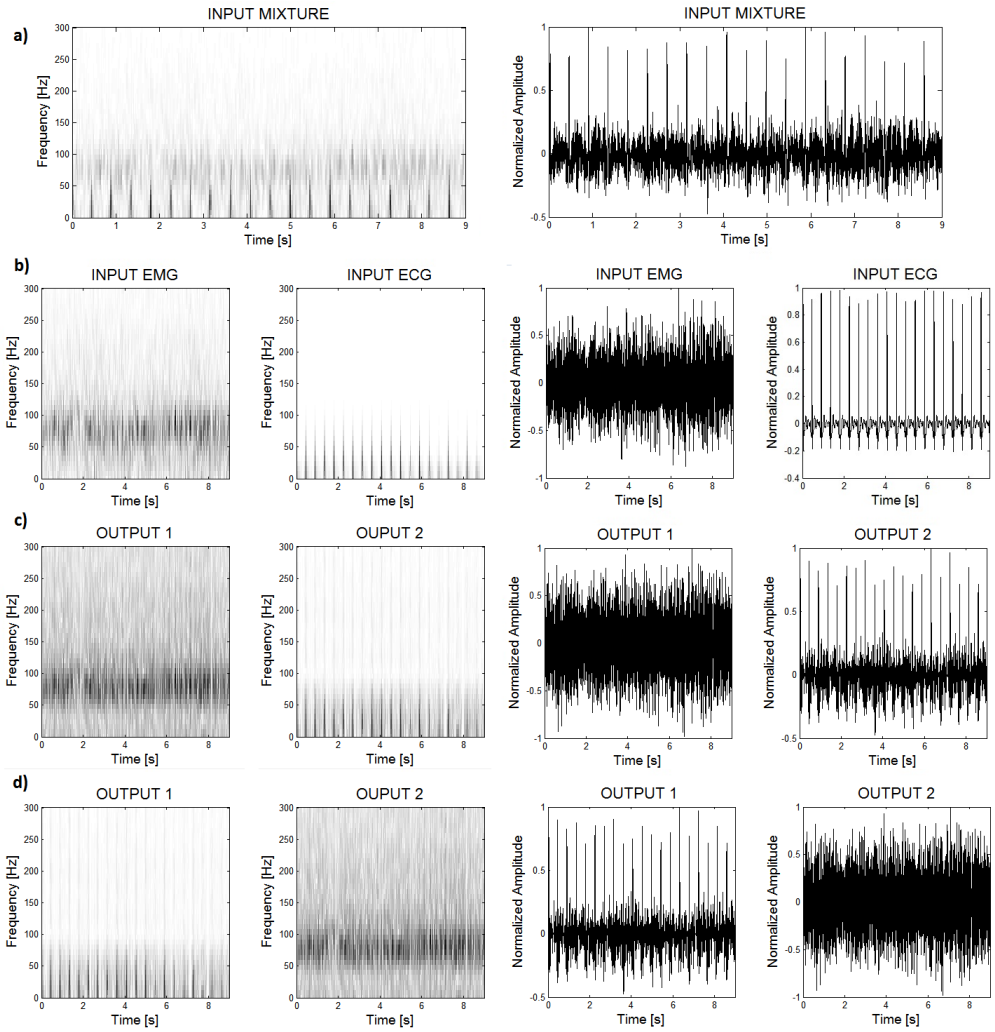

Figure 2.8 On the right-hand side there are waveforms and on the left-hand side there are their corresponding spectrograms (window size equals to 0.1 seconds). Starting from the top of the figure, a) ECG-EMG input mixture; b) clean ECG and clean EMG input sources; c) and d) represent separation results (output 1&2) obtained by two different NMF analysis with the same settings.

2.4.3 Factorization rank

In the previous section, it was shown that the window duration has an impact on the separation quality. Herein, the same experiment has been carried out keeping the window duration unchanged (the 1 second – Hanning window) while letting the factorization rank *r* vary.

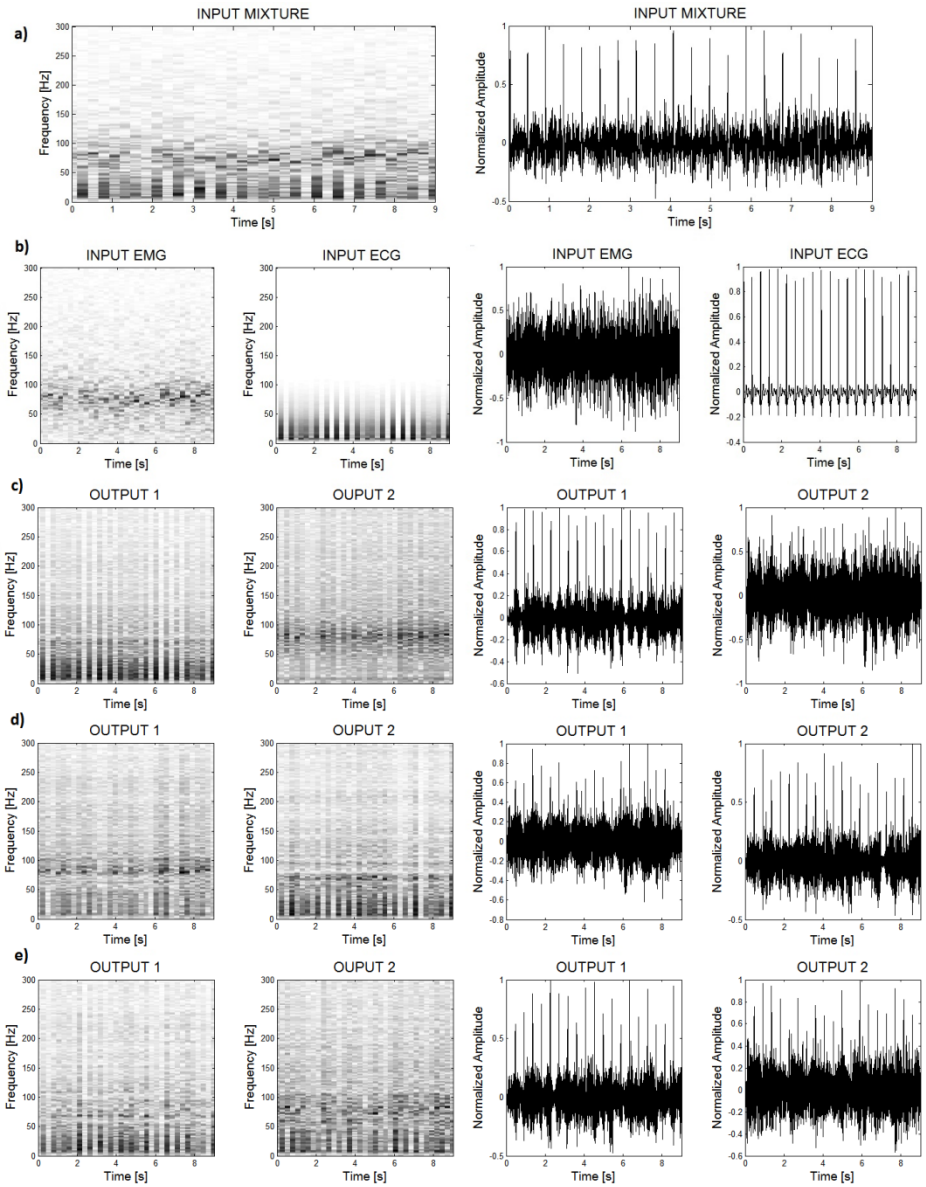

Figure 2.9 On the right-hand side there are waveforms and on the left-hand side there are their corresponding spectrograms (window size equals to 1 second). Starting from the top of the figure, a) ECG-EMG input mixture; b) clean ECG and clean EMG input sources; c), d) and e) represent separation results (output 1&2) obtained by three different NMF analysis with factor *r set to* 2, 8 and 20, respectively.

The poor separation quality is still visible; what is more, increasing of the factorization rank *r* up to 20 has made the result even worse.

It is interesting to note that the factorization rank $r = r_1 + r_2$ does not have to be equally distributed on r_1 and r_2. Each pair of initialization matrices can be composed of pairs of $\boldsymbol{w_1h_1}$ and $\boldsymbol{w_2h_2}$ with different sizes (Figure 2.10).

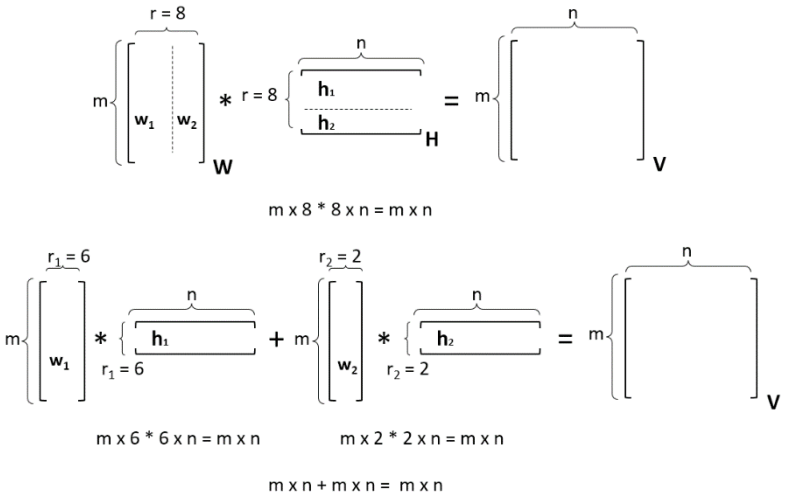

Figure 2.10 ***WH*** Matrices for *r* = 8.

The separation result has not improved because the resulting ***WH*** matrices (composed of merged pairs $\boldsymbol{w_1h_1}$ and $\boldsymbol{w_2h_2}$) were initialized with random entries (Figure 2.9d).

2.5 Summary

We have shown that in biomedical applications involving source separation there are critical aspects to be taken into account while applying NMF. Regardless to the selected NMF algorithm variant, those aspects are: 1) signal transformation, 2) optimal matrix decomposition rank and 3) algorithm initialization.

A transformation of the input data provides an image representation, which is conceived as a combination of elements that compose diverse patterns of sources present in the input. The more prominent differences between source signal patterns the better the separation quality. As it will be shown in the following chapters the initialization with accurately designed TF

structures significantly improves the separation quality. When it is combined with optimal rank selection (chapter 5) NMF becomes a very efficient tool for biomedical source separation applications even for noisy scenarios. On the other hand, a classical random initialization reduces an importance of factorization rank *r* selection and often renders the separation impossible.

Chapter 2: NON-NEGATIVE MATRIX FACTORIZATION

CHAPTER 3

RESHAPED SPECTROGRAM NMF

In this chapter, we present a single-channel approach aimed at separation of mixed biomedical signal sources. The approach is based on a linear decomposition of the input signal spectrogram in two non-negative components, which represent the signal source spectrogram estimates. The non-negative representation of the input mixture was achieved with the STFT; next, the corresponding spectrogram is reshaped in order to bring out characteristic time-frequency (TF) patterns of the sources present in the input data. Furthermore, initialization of an algorithm has been improved when compared to the classical NMF approach [61] which ensured fast convergence to a global minimum of the cost function.

An illustration of this approach is based on Electrocardiogram (ECG) extraction from surface Electromyogram (EMG) signals.

3.1 Method

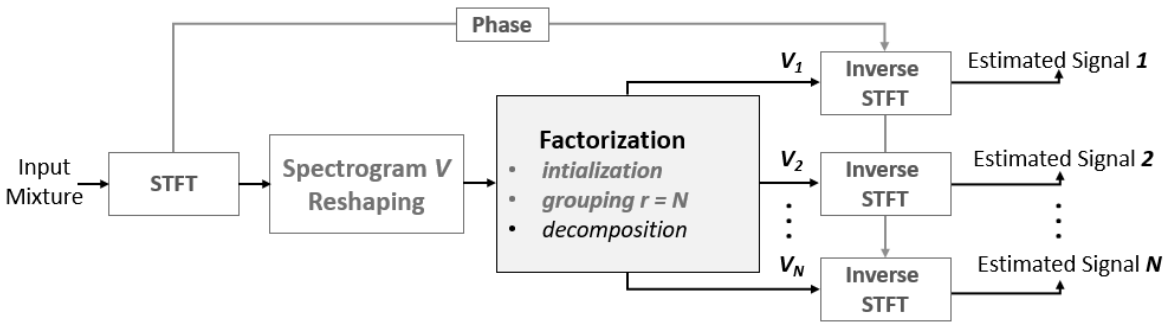

Figure 3.1 Overview of the reshaped spectrogram NMF.

The overview of the reshaped spectrogram NMF analysis can be seen in the Figure 3.1. The input is transformed into a non-negative representation by the STFT. Before the factorization stage, it is reshaped in such a way that characteristic patterns of signal sources are brought out. Then algorithm is initialized with accurately designed TF structures instead of Gaussian noise. These structures are obtained by filtering the input data in such a way that most of the energy of each signal source is captured in one structure. The matrix factorization rank *r* is set equally to *N* number of expected sources. After *decomposition,* each separated signal estimates $\boldsymbol{V_1, V_2 \ldots V_N}$ is transformed back into time domain by the inverse STFT transform. The phase information is obtained directly from the input under assumption that at each STFT sample one of the sources is dominant.

In the present approach, we focus our attention on the initialization of NMF algorithm through input spectrogram reshaping.

3.1.1 Digital Signal Processing (DSP) operations

Before we move to the algorithm details, the DSP operations i.e. ***filtering***, ***resampling*** and ***spectral whiting*** will be briefly discussed.

In the proposed algorithm ***filtering*** is used to limit the signal range i.e. the PLI harmonics can be filtered out in such a way that they become dominant in the spectrogram (right hand side of the Figure 3.2).

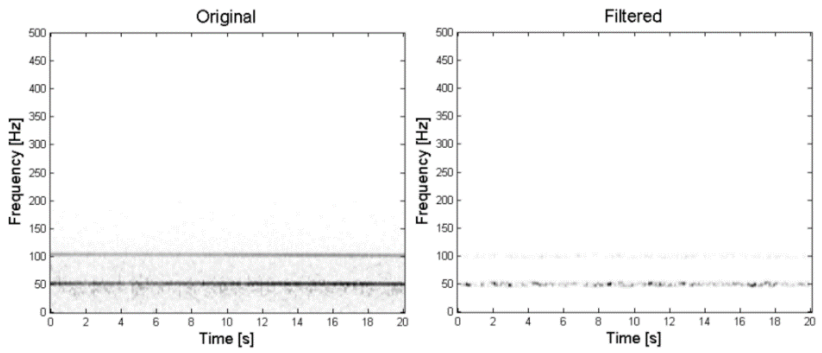

Figure 3.2 Filtering of the two harmonic PLI from the input surface EMG.

Resampling is a general term that refers to changing the sample rate of a digital representation of the signal whilst preserving, as closely as possible, an information contained in the original signal [81]. There are two related operations: decimation and interpolation.

Decimation of discrete time signals is used to reduce the sampling rate by an integer factor *M*. It means that one out of every *M* samples, is retained from the original signal. It is important to note that such operation can provoke aliasing (distortion caused by high-frequency signal components). In order to suppress aliasing, it is often desired to perform anti-alias digital low pass filtering.

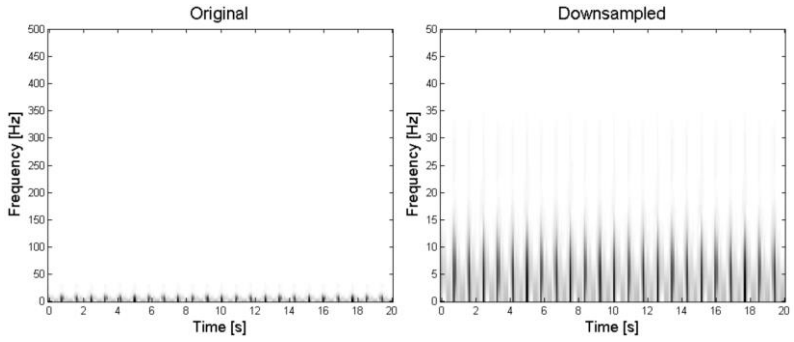

Figure 3.3 Downsampling of the ECG signal by factor *M*.

The decimation can be also called downsampling (Figure 3.3). The opposite operation that increases number of samples of the original signal by integer *M* is denoted as interpolation or upsampling.

The last term discussed in this section is spectral whitening which refers to a spectrogram smoothing and it is applied to balance overall amplitude spectrum.

As it will be shown further, in the practical example section, the objective will be to emphasize the ECG over a noisy like EMG source signal. Take a look at the left-hand side of the Figure 3.4, where the spectrograms of ECG (grey) and EMG (darker grey) are shown. In this case, a simple low pass filtering can preserve most of the ECG energy located in this range.

The situation changes drastically when fatigue occurs and the EMG spectrum moves towards lower frequencies [82]. In the right-hand side of the Figure 3.4, we observe a strong overlap between the ECG and EMG sources; accordingly, low-pass filtering (LPF) alone will not produce a desired outcome.

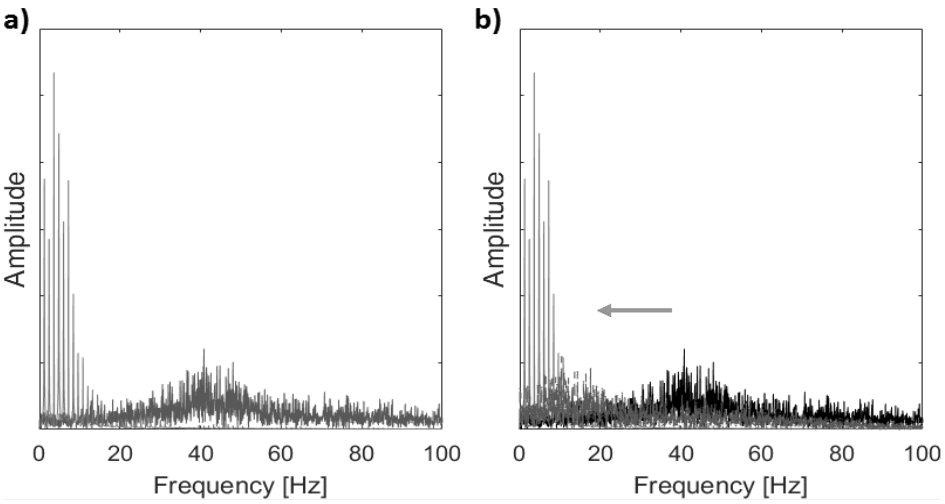

Figure 3.4 ECG and EMG spectrograms marked with red and blue respectively; a) no fatigue, b) fatigue.

The solution is to apply LPF and then ***Linear Predictive Coding*** (LPC) to calculate the spectral envelope of EMG signal still present in low frequency range. Once the LPC coefficients are obtained, they are applied to create an inverse filter which suppresses undesired EMG source. In this way most of the ECG energy is preserved in the low frequency range.

3.1.2. Classical NMF framework

Let $\boldsymbol{V}$ be a non-negative matrix $\boldsymbol{V} \epsilon R^{\geq 0, MxN}$. The decomposition of $\boldsymbol{V}$ can be done in such a way that the product of the resulting non-negative matrices $\boldsymbol{W} \epsilon R^{\geq 0, Mxr}$ and $\boldsymbol{H} \epsilon R^{\geq 0, rxN}$ equals approximately matrix $\boldsymbol{V}$:

$$\boldsymbol{V} \approx \boldsymbol{WH} \tag{3.1}$$

Equation (3.1) can also be expressed in an alternative way:

$$\boldsymbol{WH} = \sum_{n=1}^{N} \boldsymbol{w}_{r_n} \boldsymbol{h}_{r_n} \tag{3.2}$$

where $\boldsymbol{w}_r$ and $\boldsymbol{h}_r$ represent the r^{th} column of $\boldsymbol{W}$ and the r^{th} row of $\boldsymbol{H}$ respectively. Factor r denotes the number of expected signal sources in the given input mixture. The source

separation is performed by a decomposition of the spectrogram of the input signal and then by clustering these products into separate signal sources.

In a general NMF framework the matrices ***W*** and ***H*** are initialized with positive random entries and then alternatively updated with the following multiplicative update rules [61]:

$$\boldsymbol{W_{ia}} \leftarrow \boldsymbol{W_{ia}} \frac{\left(\boldsymbol{VH^T}\right)_{\boldsymbol{ia}}}{\left(\boldsymbol{WHH^T}\right)_{\boldsymbol{ia}}} \tag{3.3}$$

$$\boldsymbol{H_{aj}} \leftarrow \boldsymbol{H_{aj}} \frac{\left(\boldsymbol{W^T V}\right)_{\boldsymbol{aj}}}{\left(\boldsymbol{W^T WH}\right)_{\boldsymbol{ia}}} \tag{3.4}$$

where .* and ./ denote element-wise multiplication and division respectively. The reconstruction error between ***V*** and the product ***WH*** is minimized, while constraining the matrices to be entry-wise non-negative. The quality of the reconstruction is measured by the cost function C, which evaluates the square of the Euclidean distance between ***V*** and ***WH***:

$$C = min \parallel \boldsymbol{V - WH} \parallel^{\boldsymbol{2}} = min\left(\sum_{\boldsymbol{ij}} \left(\boldsymbol{V_{ij}} - \left(\boldsymbol{WH}\right)_{\boldsymbol{ij}}\right)^{\boldsymbol{2}}\right) \tag{3.5}$$

3.1.3 Algorithm summary

The algorithm can be summarized as follows:

(1) Initialization

- Reshape (Filter & Decimate by *M*) input record in such a way to bring TF patterns
- For each source:
  - Filter the input record in such a way that most of its energy is preserved.
  - Non-negative rank *r* set to 1.

(2) Source grouping

- For each source:
  - Decimate and compute sub-spectrogram by
  - Randomly initialized rank-constrained NMF.
- Generate the basis vectors matrix and activation coefficients matrix by stacking the results of the previous step.

(3) Decomposition

- Obtain noise-suppressed sub-spectrogram estimates by the Euclidean-distance NMF constrained to the basis vectors matrix and activation coefficients matrix.
- For each source:

(4) Obtain time-waveforms with inverse STFT.

3.2 Practical case: ECG extraction from EMG

The separation of ECG source from single-channel surface EMG recordings remains an important task for a number of biomedical signal processing applications. The major difficulty arises from the fact that ECG and EMG simultaneously overlap in the time and frequency domain. This overlap is particularly significant in the 0.1 - 50 Hz band, where most of the ECG signal energy is clustered. Thus, ECG-EMG separation is a challenging task that requires an adequate approach.

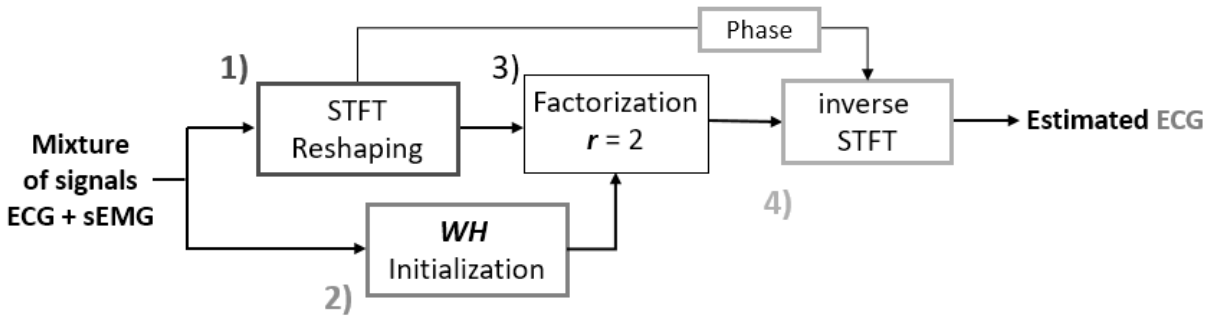

Figure 3.5 Overview of reshaped spectrogram NMF for ECG estimation from surface EMG.

The goal is to identify the electrocardiogram signal component from a single channel mixture of ECG and EMG. The method can be divided into four steps:

1. The input mixture spectrogram reshaping (Figure 3.6),
2. ***W*** and ***H*** accurate initialization (Figure 3.7),
3. Factorization,
4. Time domain source signals recovery (Figure 3.8).

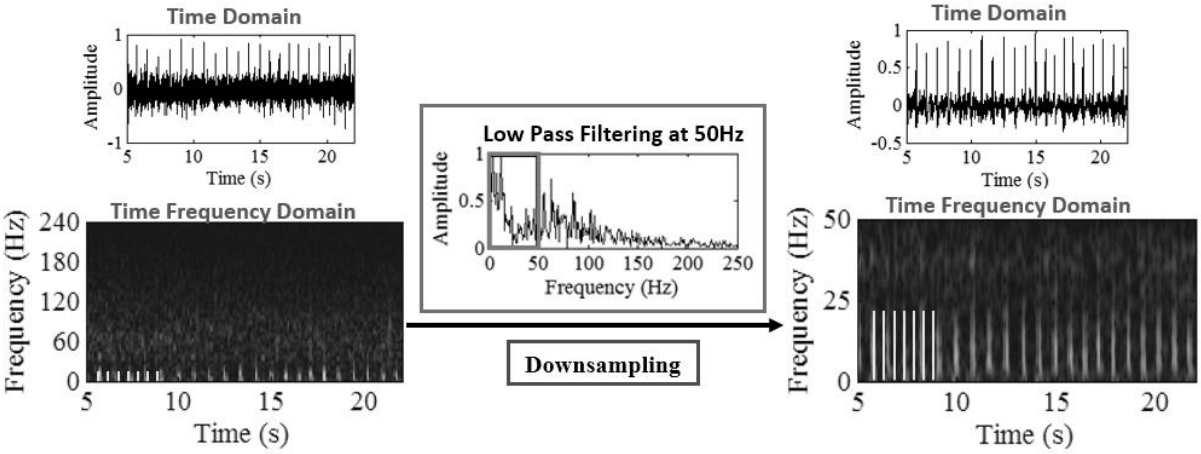

Figure 3.6 Input spectrum reshaping.

Step1. Figure 3.6 shows the reshaping of input ECG-EMG signal; left and right-hand side for situation before and after this operation, respectively. Since we are interested in ECG extraction, its characteristic pattern is of our interest (it is marked with white vertical lines at the bottom of spectrum). The EMG is represented with a blurry background. In order to emphasize the ECG pattern, we applied a 5^{th} order Butterworth Low Pass Filter with a fixed cut-off frequency at 50 Hz (a frame in the middle of the Figure). Next, the signal was downsampled at 100 Hz, with the decimation factor coupled to the original sampling frequency. As a result, in the spectrogram the ECG patterns are clearly enhanced over the EMG (right hand side of the same Figure).

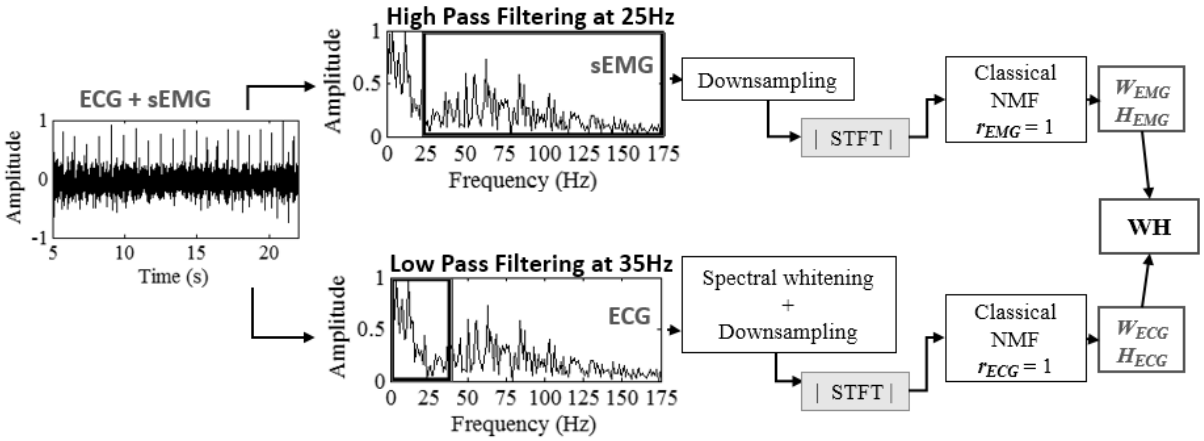

Figure 3.7 W and H matrices initialization.

Step2. The matrices ***W*** and ***H*** were initialized by the rough estimates of the ECG and EMG. First the Input signal is filtered by a high pass filter at fixed cut of frequency equal to 25 Hz - in this way most of remaining EMG energy is preserved. The signal is then downsampled as in the reshaping step, followed by the NMF algorithm (3.1) - (3.5) with $r_{EMG} = 1$. In this way $\boldsymbol{W_{EMG}}$ $\boldsymbol{H_{EMG}}$ contain rough estimation of EMG pattern. Similarly, we obtain the pair $\boldsymbol{W_{ECG}}$ $\boldsymbol{H_{ECG}}$. Observe that the ECG additionally undergoes spectral whitening by means of the linear prediction analysis of order 5, which is meant to further suppress the residual EMG energy at low frequencies. Step2 provides two sets of matrices ($\boldsymbol{W_{ECG}}$ $\boldsymbol{H_{ECG}}$) and ($\boldsymbol{W_{EMG}}$ $\boldsymbol{H_{EMG}}$) which are merged into initial ***W*** and ***H***.

Step3. In this step, the NMF algorithm (3.1) - (3.5) is performed on the reshaped input spectrogram ***V*** with the previously obtained initial ***W*** and ***H*** matrices and source grouping factor $r = r_{ECG} + r_{EMG} = 2$.

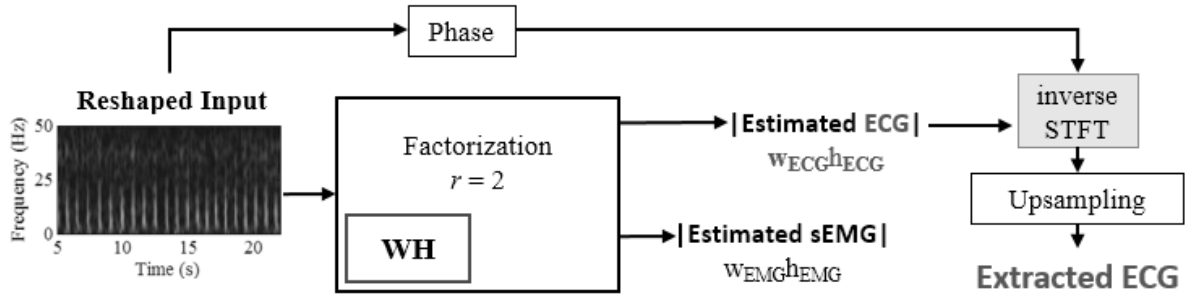

Figure 3.8 The inverse Transform and upsampling.

Step4. The estimated spectrogram of ECG is transformed back into the time domain by means of the inverse STFT. The phase information required by this transform is obtained by assuming that at each STFT sample one of the underlying sources is dominant [74]. Finally, the upsampling of the obtained ECG waveform was done with factor *M* set in such a way to recover the original sampling rate.

3.3 Results

3.3.1 Data

Synthetic Data

The ECG signal was generated with the MATLAB simulation program [83]. The EMG component was created following a general approach described in [14] [23], i.e. by passing a zero-mean unitary-variance Gaussian white noise through an all-poles bandpass filter with filter coefficients: [1,1.9408, 1.3108, –0.2965, –0.0037, 0.0588]. The ECG and EMG components are mixed together according to the chosen signal-to-noise (SNR) ratio level, where signal/noise refers to the ECG and EMG respectively.

Real Data

The experimental procedure was conducted in accordance with the Declaration of Helsinki and was approved by the Local Ethics Committee. Each subject provided an informed written consent before participation in the study. The experimental session was performed with a KinCom Isokinetic Dynamometer (Chattanooga, TN, USA). The subjects performed two maximal voluntary contractions (MVC) of right knee extension over a period of 5 seconds, separated by 2 min of rest. The highest MVC value was used to obtain the submaximal force levels. After 2 min of rest, the subjects were asked to maintain an isometric right-knee extension at 30% MVC for as long as possible. EMG activity during the isometric contraction of the vastus medialis of the right leg was recorded using a grid of 65 surface electrodes (5 columns × 13 electrodes; 2.5 mm interelectrode distance). The grid was placed along the direction of the muscle fibers, between the innervations zone and the distal tendon,

previously identified during a preliminary brief knee isometric contraction. A reference electrode was placed around the right ankle. Before the placement of the electrodes, the skin was shaved, lightly abraded and cleaned with water. The EMG signals were amplified as monopolar derivations (EMG amplifier, LISiN-OT Bioelettronica, Torino, Italy), bandpass filtered (–3dB bandwidth, 1–500 Hz), sampled at 2048 samples/s, and converted to digital data by a 12-bit A/D converter board.

3.3.2 Evaluation parameters

The performance of the proposed method was carried out by Signal-to-Residual Ratio for synthetic data and by High/Low energy ratio, Average Rectified Value and Visual inspection for real scenarios.

Signal-to-Residual Ratio (SRR)

The SRR is defined as:

$$SRR[dB] = 10log_{10}\frac{\sum_n \boldsymbol{S_{ECG}}(\boldsymbol{n})^2}{\sum_n \left|\boldsymbol{S_{ECG}}(\boldsymbol{n}) - \widehat{\boldsymbol{S}}_{\boldsymbol{ECG}}(\boldsymbol{n})\right|^2} \tag{3.6}$$

where $\boldsymbol{S_{ECG}}(\boldsymbol{n})$ and $\widehat{\boldsymbol{S}}_{\boldsymbol{ECG}}(\boldsymbol{n})$ are the original and estimated ECG components. The last expression is the energy ratio of the original signal and the error between the original and separated signal expressed in decibels.

3.3.3 Methods for the comparative study

For the present performance comparative study, we have selected the following reference methods:

(1) Butterworth filter [84],

(2) Method based on wavelets and ICA approach (further denoted as WICA) [26].

The former is a popular 4th order Butterworth filter with the cutoff frequency set to 30Hz. The latter reference method [26], which we will refer to as the WICA, makes use of a non-linearly scaled wavelet basis decomposition of the input electromyogram in order to emphasize the ECG against the EMG in the TF domain. Next, a heuristic criterion for QRS complexes localization is applied to yield intensity patterns with predominantly ECG and EMG energy respectively. Those patterns are fed to a Fast ICA algorithm which calculates two independent source vectors associated to the ECG and EMG respectively. This method, however, provides significantly different outputs for the same input settings. Accordingly, we have taken into account only the best quality separation results.

3.3.4 ECG denoising from EMG

For the reshaped spectrogram NMF analysis, the following settings have been used: signal duration = 10 seconds, original sampling frequency fs = 1000Hz, decimation/interpolation factor *M* = 10, window type Hanning, analysis window size = 0.24 seconds with 50% overlap.

First, the performance comparison was carried out for synthetic data. The SNR was varied in the range –8 dB to 8 dB with 4 dB step.

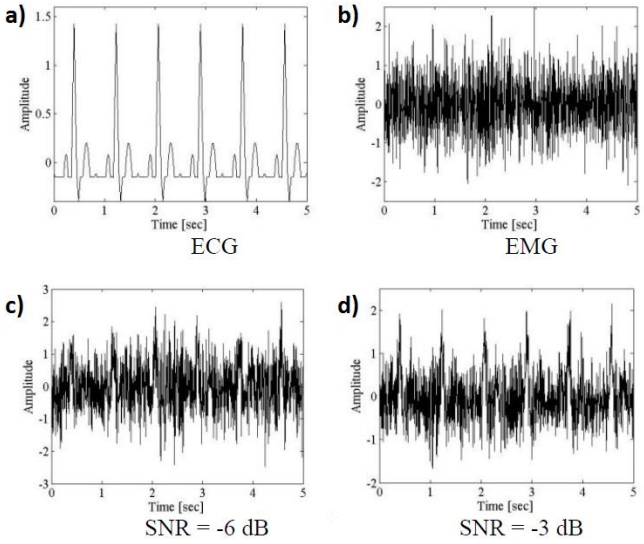

Figure 3.9 Input synthesized signals. a) ECG and b) EMG signals before mixing and c) and d) mixtures with SNR equal to -6 dB and -3dB, respectively.

For each SNR, we evaluated the methods 100 times and calculated the estimated averaged ECG. Since the original sources are available, the quality of separation was evaluated with SRR.

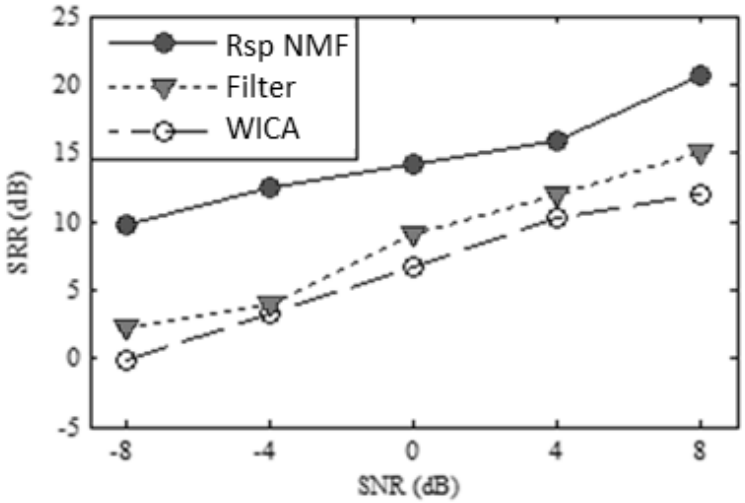

Figure 3.10 SRR versus SNR for the methods involved in the comparative study.

We observe in all performance curves a general trend of ascending SRR towards larger SNR. This is not surprising, as we expected all the methods to perform well in situations of low-impact EMG. The filter and WICA method exhibit a similar performance, although the filter method is slightly better, particularly at higher SNR where it is situated around 3 dB over the WICA. For low SNR both methods undergo important performance degradation, due to the EMG energy increase within the ECG frequency band. Consequently, more EMG energy is retained by the filter, while the wavelet analysis in the WICA fails to properly localize the ECG components in the TF plain. The proposed method clearly outperforms the reference methods in the whole analysis range, and in particular at low SNR. For instance, with SNR = -8 dB it achieves a SRR of about 10 dB over the reference methods. The methods were also tested beyond the analysis range. For SNR lower than -8dB, dominating EMG source made separation impossible for all of the methods.

For real signals, the use of the SRR was not possible, as the signal components before the mixture were not available. The visual comparison will indicate easily the best performer in this scenario.

For the proposed method, the following settings have been used: signal duration = 5 seconds, original sampling frequency fs = 2048 Hz, decimation/interpolation factor *M* = 20, window type = Hanning, analysis window size = 0.46 seconds with 50% overlap. The performance comparison was carried out for two subjects with different MVC (30% and 80%).

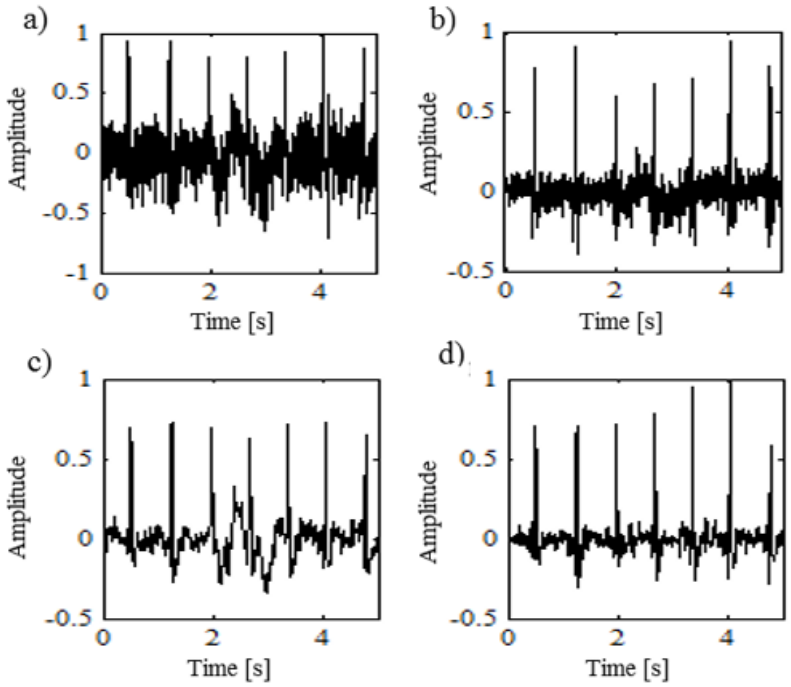

Figure 3.11 (a) Input signal for the subject with MVC 30%, (b) estimated ECG for the WICA, (c) estimated ECG for the filtering and (d) estimated ECG for the proposed method.

Visual inspection of Figure 3.11 and Figure 3.12 brings out the impact of each method on the ECG-EMG separation. In both cases the WICA retains most of the EMG residual energy in the estimated ECG, while the filtering and proposed methods are clearly better, which is in accordance with Figure 3.10.

In addition, observe that the low-frequency movement artifact around t = 2.5 seconds could not be removed by neither the WICA nor filtering method. The proposed method, on the contrary, efficiently pulls it out of the mixture, thus yielding an artifact-free ECG signal.

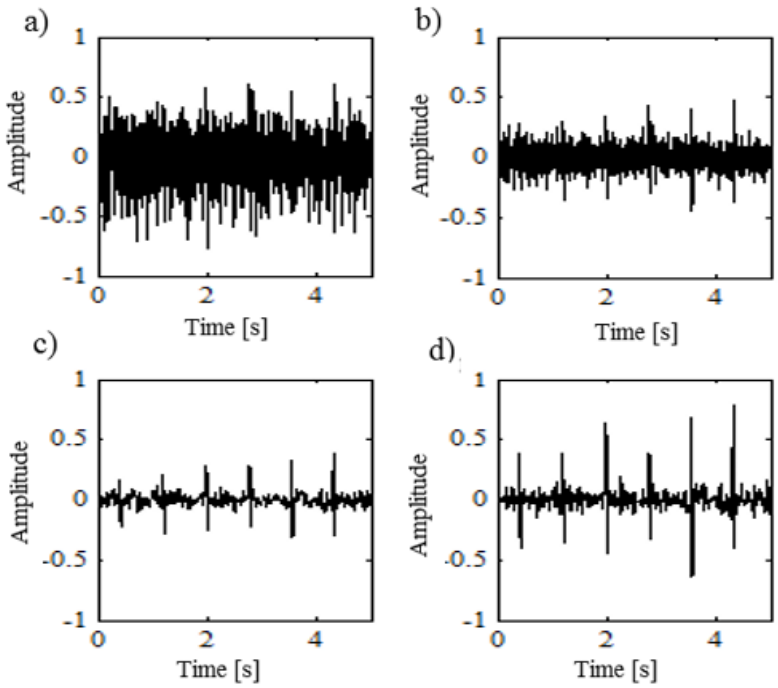

Figure 3.12 (a) Input signal for the subject with MVC 80%, (b) estimated ECG for the WICA, (c) estimated ECG for the filtering and (d) estimated ECG for the proposed method.

3.4 Summary

We have shown that reshaped spectrogram NMF initialized with roughly adjusted TF structures instead of commonly used Gaussian random entries performs well. Thanks to reshaping of the input mixture spectrogram, the ECG pattern became more visible and there was no need to use more complex solution for adequate estimation of low rank factor *r*. However, it had a cost in a form of large sensitivity to the spectrogram parameter settings. A very short window used in the STFT left small margin in adjustment of the overlap, what influenced the overall performance. Nevertheless, the reshaped NMF has proven to be useful for ECG denoising tasks.

Relatively limited performance of the wavelet-based ICA method has not come as a total surprise. In fact, it is known that the Fast ICA separation algorithm is very sensitive to initial guess [85]. In the context of the present application, we have observed that for marginal ECG contamination, the Fast ICA provided physically meaningful results. Otherwise, a non-convergence was met and it was necessary to re-run the algorithm a number of times until

consistent components were obtained. The spectrogram-based NMF turned out to be a much better choice for ECG-EMG separation, although it must be kept in mind that all spectrogram-based separation methods are often conditioned by the choice of user-defined analysis parameters e.g. the length and type of the window, overlap between contiguous frames. Different parameter settings will give rise to different intensity images, which can compromise the initialization of a non-negative matrix factorization algorithm.

CHAPTER 4

WAVELET BASED NMF

We have already seen (Chapter 2) that the spectrogram is very sensitive to the choice of analysis parameters: the duration of the window and overlap between contiguous analysis frames. This means that rather small value changes in those parameters can give rise to important variations in the TF decomposition of the input signal. Another problem that needs to be tackled when working with spectrograms is the back-conversion to the time domain. A vast majority of applications requires time-domain waveforms in order to properly characterize the corresponding scenarios. Since NMF operates on spectrograms, the phase information, which is crucial for recovering time-domain waveforms, is lost. Moreover, the classical NMF initialization is performed through matrices containing random non-negative entries [61] what often leads to convergence to a local minimum and accordingly results in an unsatisfactory source separation.

In the current work, we present two novelties which can successfully circumvent the aforementioned drawbacks: 1) we design a robust initialization algorithm to NMF in order to ensure convergence to the global minimum of the cost function, 2) we carry out a low-rank matrix decomposition over wavelet-based intensity patterns, which in turn ensures a correct reconstruction of the time-waveforms by means of the inverse transform.

The approach was aimed at removing the ECG perturbation from single-channel surface electromyogram EMG recordings.

4.1 Method

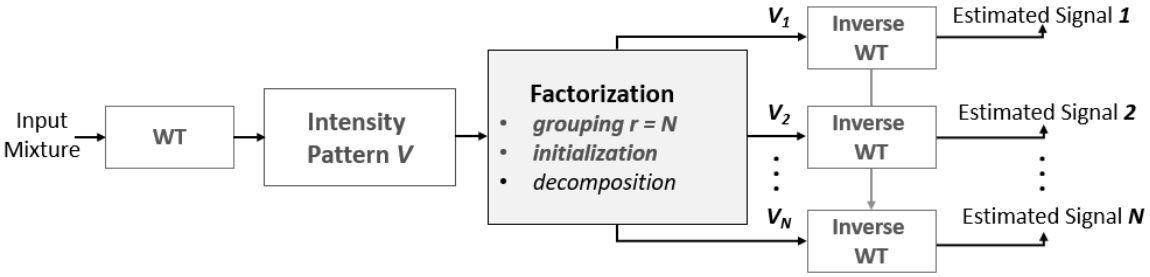

Figure 4.1 Overview of the major processing steps in the wavelet-based NMF.

The overview of the wavelet-based NMF (WNMF) is shown in Figure 4.1. The input is transformed by means of the wavelet transform (WT). This transform, as its name indicates, makes use of a basis of the scaled wavelets in contrast to the complex exponential in case of the STFT. Wavelets are functions with a determined shape, but can be shifted and dilated in time.

The continuous WT of the signal ***x(t)*** is given as:

$$W(a;b) = \frac{1}{\sqrt{a}} \int_{-\infty}^{\infty} \boldsymbol{x}(\boldsymbol{t}) \psi \left(\frac{(t-b)}{a} \right) dt \qquad (4.0)$$

where ψ is the mother wavelet, translated by b and dilated by the factor a. Since this is a convolution, the wavelets can be considered as a set of impulse responses of filters. The dilation factor a is known as the scale factor of the wavelet. The shape of a wavelet can be scaled according to the nature of the treated signal.

The factorization begins after obtaining a non-negative intensity image of the input data by means of the WT and setting the matrix factorization rank r to N equal to the number of expected sources in the mixture. The algorithm starts from an initial guess in the form of two matrices with non-negative entries. Through a number of iterations, those matrices are progressively modified in such a way that their product approximately equals the matrix ***V***, which represents the input signal. A carefully chosen initial guess can bring the algorithm fast

in the neighborhood of a global minimum, where one matrix contains the characteristic features of the constituent sources in the input signal, whereas the other matrix contains their corresponding locations in the time domain. The last step is to return to the time domain; the selected separated signal estimates $\boldsymbol{V_1, V_2 \ldots V_N}$ are transformed back with inverse WT.

4.1.1 Algorithm summary

The algorithm can be summarized as follows:

(1) Initialization

- For each source:
  - Filter the input record in such a way that most of its energy is preserved.
  - Non-negative rank *r* set to 1.

(2) Source grouping

- For each source:
  - Compute wavelet-based intensity pattern decomposition by randomly initialized rank-constrained NMF.
- Generate the basis vectors matrix and activation coefficients matrix by stacking the results of the previous step.

(3) Decomposition

- Obtain noise-suppressed sub-intensity patterns by the Euclidean-distance NMF constrained to the basis vectors matrix and activation coefficients matrix.
- For each source:

(4) Obtain time-waveforms with inverse WT

4.2 Practical case: removing ECG from surface EMG

Analysis of surface electromyography signals is a key issue in a wide range of biomedical signal processing applications e.g. muscle onset/offset detection, conduction velocity estimation, fatigue analysis, to name a few. Often, the presence of electrocardiogram disturbances gives rise to distortions in EMG signals, jeopardizing the accuracy of analysis and possibly leading to misjudgments. Removal of the heart muscle electrical activity from a single-channel surface electromyogram recording remains a challenging task, because the ECG and clean (undistorted) EMG simultaneously overlap in both time and frequency domain.

4.2.1 Wavelet family selection

Wavelets have shown to be an adequate tool for generating local scale dependent descriptions of individual features in the electrocardiogram [26]. Such descriptions are typically supported by a small number of relevant transform coefficients, which in turn provide sparse time-frequency intensity representations.

In the context of the present application, the choice of wavelet family was determined by the following constraints. On one hand, we need non-dyadic wavelet analysis which would provide non-uniform frequency resolution in the band up to 500 Hz approximately. This is due to the fact that most of the ECG-EMG energy overlap is clustered at low frequencies (up to 50 Hz) and there we need more analysis resolution. At higher frequencies the spectrum of the input signal is dominated by the EMG, which can be correctly characterized at low resolution. On the other hand, we need wavelets that would be easy to implement and that would provide fast and efficient direct and inverse transform calculation, in order not to slow down the overall ECG-EMG separation process.

Among a plethora of available wavelet families, probably the most adequate for the problem at hand are so called complex-valued wavelets [86]. Such wavelets, defined either in the time or frequency domain, are known to have good temporal localization properties and at the same time, they can ensure variable user-defined frequency resolution. Unlike the classical dyadic wavelet analysis where the frequency bands are progressively halved from high towards low frequencies, the complex-valued wavelets can be defined more flexibly through

a set of frequency responses of a bank of band-pass filters. Examples of such wavelets are frequency B-spline wavelets [87] and Cauchy-type non-linearly scaled wavelets [26]. Both wavelet classes are characterized by a flexible design of the filter bank by means of orthogonal adjustment of the bandwidth and central frequency. Such an analysis scheme makes these wavelets a valuable tool for single-scale ECG decomposition.

We had no preference when choosing specific wavelets, given that both are well suited for the problem at hand. Our choice has fallen on the Cauchy-type non-linearly scaled wavelets, because they have recently been used in combination with the FastICA algorithm for the same purpose [26].

Those wavelets are characterized by a set of $P = 18$ band-pass filters of the following frequency response $B_k(F)$:

$$B_k(F) = F_k^m e^{(-F_k+1)m}, k = 1 \dots P \tag{4.1}$$

$$F_k = \frac{f}{f_c^{(k)}} \tag{4.2}$$

$$f_c^{(k)} = \frac{1}{m}(1.45 + k)^{1.959} \tag{4.3}$$

where the parameter m represents a scaling factor typically equal to 0.7. The graphical representation of the filter bank is shown in Figure 4.2.

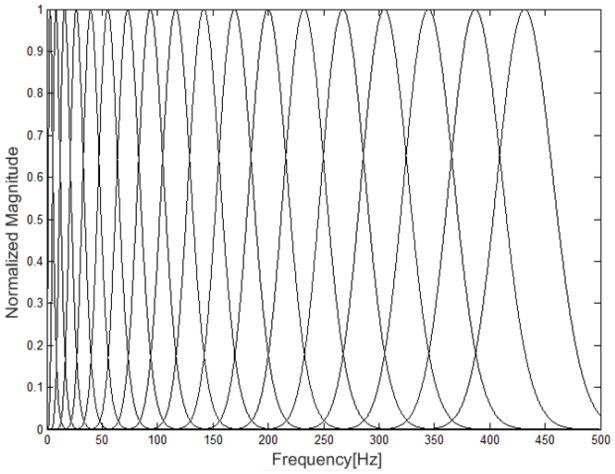

Figure 4.2 The Cauchy-type non-linearly scaled wavelets.

Following [26] the frequency responses (4.1) are inverse-transformed by the inverse Fast Fourier Transform and the corresponding filter impulse responses are obtained. These complex waveforms of length *N* samples are next arranged as the columns of a 36×*N* matrix **B**.

Let ***s*** be an *N*-point vector containing a single-channel recording of a surface electromyogram. Then, we will refer to ***v*** as the wavelet transform of *s* i.e. ***v*** = ***B*** * ***s***, where the symbol '*' stands for row-wise convolution. The corresponding intensity image is obtained by squaring all entries in ***v*** and adding the first 18 rows to the last 18 rows. We will call the resulting 18 × *N* matrix ***V***, which is the basis for the WNMF algorithm described in next section.

4.2.2 The proposed methodology

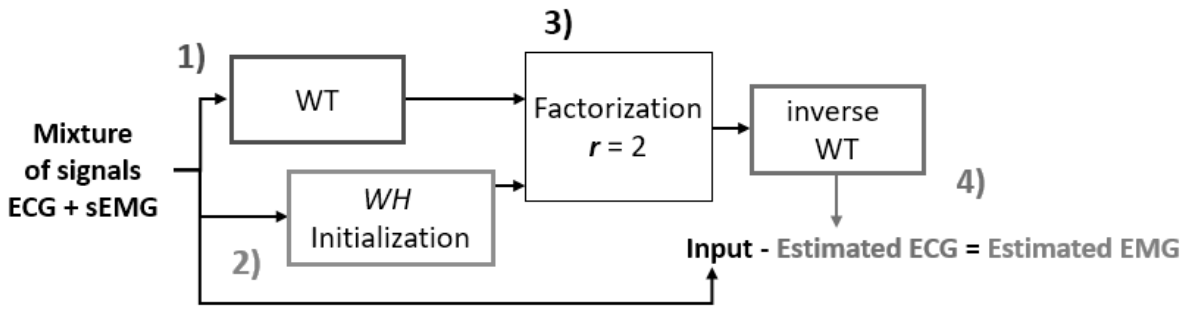

Figure 4.3 Overview of the WNMF for EMG estimation.

As explained in Chapter 2, the NMF aims at creating a low rank approximation to $\boldsymbol{V}$ which contains nonnegative factors (matrices or vectors) usually called $\boldsymbol{W}$ and $\boldsymbol{H}$. The NMF of $\boldsymbol{V}$ is created by solving the nonlinear optimization problem:

$$C = min \parallel \boldsymbol{V} - \boldsymbol{WH} \parallel^2 = min\left(\sum_{ij}\left(\boldsymbol{V_{ij}} - (\boldsymbol{WH})_{ij}\right)^2\right) \tag{4.3}$$

where C is the cost function to be minimized through a number of iterations, with $\boldsymbol{W} \geq 0$ and $\boldsymbol{H} \geq 0$. In the neighborhood of an optimal solution (global minimum) the matrices $\boldsymbol{W}$ and $\boldsymbol{H}$ respectively contain the spectrum and the temporal activity information of the input signal **s**:

$$\boldsymbol{V} \approx \boldsymbol{WH} \tag{4.4}$$

The matrices $\boldsymbol{W}$ and $\boldsymbol{H}$ respectively contain the spectrum and the temporal activity information of the input signal **s**. In this particular application, the (4.4) comes in the following form:

$$\boldsymbol{V^{18\times N}} \approx \boldsymbol{W^{18\times r}H^{r\times N}}, \qquad r \geq 1 \tag{4.5}$$

Because the NMF is an iterative algorithm, it is essential to ensure convergence to the global minimum of C. To that end, we need to provide a good initial guess, which we will call $\boldsymbol{H_{init}}$ and $\boldsymbol{W_{init}}$. These matrices should be generated in such a way to best capture the time-frequency characteristics of the underlying sources (ECG and EMG) in the input recording. This is achieved by the WNMF initialization process schematically shown in Figure 4.4 with a) which corresponds to the generation of $\boldsymbol{w}$ and $\boldsymbol{h}$ and b) where these pairs are rearranged in such a way to get $\boldsymbol{H_{init}}$ and $\boldsymbol{W_{init}}$.

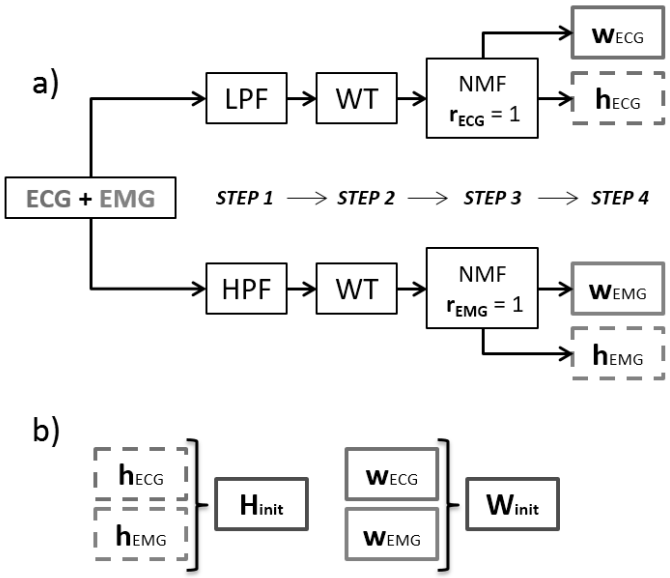

Figure 4.4 Initialization of matrices H_{init} and W_{init}.

Step 1 comprises a simultaneous low-pass (LPF) and high-pass (HPF) filtering of the input signal, with the cutoff frequencies of 35Hz and 25 Hz respectively. These values roughly correspond to the frequency bands where most of the signal component energy is clustered. Such filtering generates coarse estimates for the ECG and EMG signal components in the time domain. Although not very accurate, due to spectral overlap, it will be shown that this filtering provides a sparse representation of the electrocardiogram in the wavelet domain and consequently an accurate basis for further decomposition.

In Step 2 each signal component is wavelet transformed and the corresponding intensity patterns $\boldsymbol{V_{ECG}}$ and $\boldsymbol{V_{EMG}}$ are generated. In Step 3 the intensity patterns are fed to an NMF algorithm with rank r = 1 for both ECG and EMG.

Let us briefly discuss the choice of rank in the context of the present work. A unitary rank for ECG can be considered a correct choice, because of its inherent TF sparse representation. On the other hand, a dense (non-sparse) TF representation of EMG would definitely need a larger rank.

However, it turns out that EMG rank estimation is not really necessary, and the reason for this is twofold:

- It would affect initialization process and overall separation performance in terms of speed, due to increased complexity.
- Since *r* = 1 proved to be sufficient for approximating the ECG, the EMG can be obtained by simply subtracting the estimated ECG waveform from the input mixture.

The cost function (4.3) is iteratively minimized with the following multiplicative update rules [61]:

$$\boldsymbol{W_{ia}} \leftarrow \boldsymbol{W_{ia}} \frac{\left(\boldsymbol{VH^T}\right)_{\boldsymbol{ia}}}{\left(\boldsymbol{WHH^T}\right)_{\boldsymbol{ia}}} \tag{4.6}$$

$$\boldsymbol{H_{aj}} \leftarrow \boldsymbol{H_{aj}} \frac{\left(\boldsymbol{W^T V}\right)_{\boldsymbol{aj}}}{\left(\boldsymbol{W^T WH}\right)_{\boldsymbol{ia}}} \tag{4.7}$$

where .* and ./ denote element-wise multiplication and division respectively. The reconstruction error between ***V*** and the product ***WH*** is minimized, while constraining the matrices to be entry-wise non-negative. The quality of the reconstruction is measured by the cost function *C*, which evaluates the square of the Euclidean distance between ***V*** and ***WH***.

The iterative process stops when certain user-defined reconstruction error threshold is reached. Since the rank *r* = 1, the NMF yields two set of vectors as outcome: $\boldsymbol{(W_{ECG}, H_{ECG})}$ and $\boldsymbol{(W_{EMG}, H_{EMG})}$. These vectors are optimal in the sense that:

$$\boldsymbol{V_{ECG}} \approx \boldsymbol{W_{ECG}} * \boldsymbol{H_{ECG}} \tag{4.8}$$

$$\boldsymbol{V_{EMG}} \approx \boldsymbol{W_{EMG}} * \boldsymbol{H_{EMG}} \tag{4.9}$$

Finally, the vectors (W_{ECG}, H_{ECG}) and (W_{EMG}, H_{EMG}) are merged into the matrices H_{init} and W_{init} (see Figure 4.4.b). As an illustration of the WNMF initialization process the Figure 4.5 presents an example of the intermediate outcomes in the diagram from Figure 4.3.

The top waveform represents an input electromyogram waveform, where the ECG contamination is clearly visible. One level below (Step 1) we see roughly separated ECG and EMG waveforms by means of the filtering. In the next level (Step 2) we see the intensity patterns obtained through the matrix WT. Observe how sparse the ECG pattern is: it consists mostly of short vertical lines at the bottom of the plot whereas the rest is close to zero.

As expected, the EMG intensity pattern is noise-like. In the bottom level (Step 3) we show the content of the vectors (W_{ECG}, H_{ECG}) and (W_{EMG}, H_{EMG}).

Observe how the frequency envelopes of the signal components are captured in W_{ECG} and W_{EMG} whereas the time-domain activity appears in H_{ECG} and H_{EMG}. Further refinement of the ECG-EMG separation is carried out in the second part of the WNMF algorithm, as explained in the following subsection.

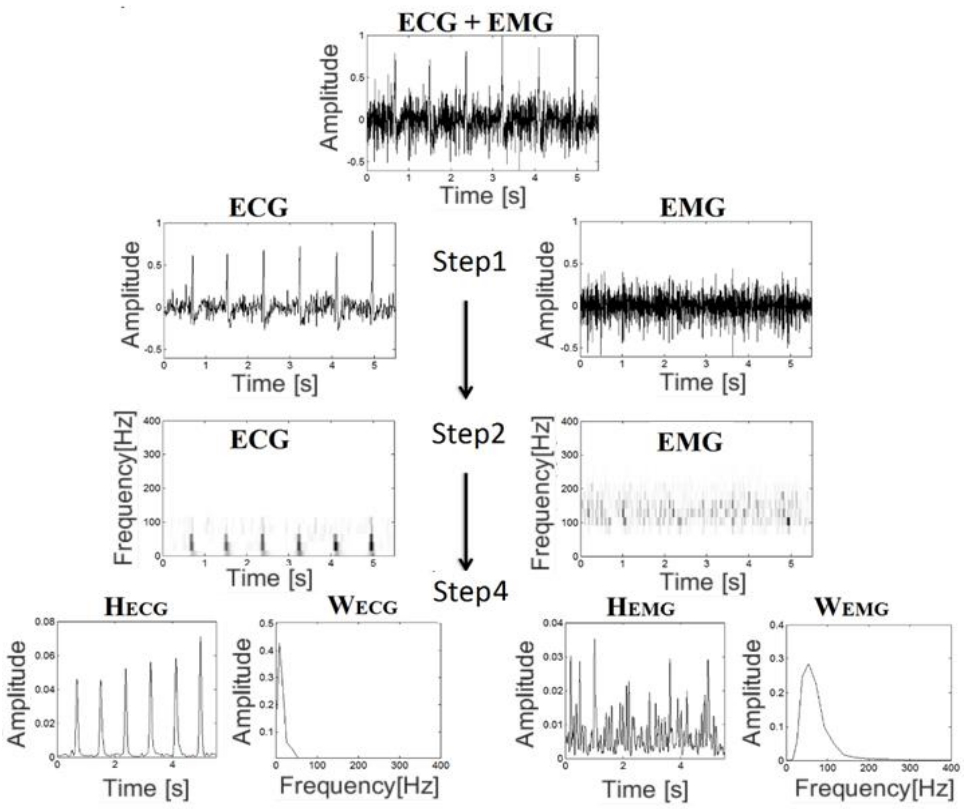

Figure 4.5 The WNMF algorithm Initialization overview – example.

4.2.3 EMG source separation

In order to obtain estimated EMG source, we first concentrate on ECG estimation by following the scheme in Figure 4.5. The upper branch a) of the diagram bears resemblance to Figure 4.4 with a few important differences. The matrix $\boldsymbol{V}$ is now the intensity pattern of the input signal, while the NMF is initialized by compound matrices $\boldsymbol{H_{init}}$ and $\boldsymbol{W_{init}}$. Contrary to the algorithm initialization, we set rank $r = 2$ as we are now dealing with two sources. The iterative procedure follows the multiplicative update rules (4.6) and (4.7) until a convergence criterion is reached. As an outcome, the NMF delivers two matrices $\mathbf{W_{sep}} = (\mathbf{w_{ECG}} \ \ \mathbf{w_{EMG}})$ and $\mathbf{H_{sep}} = (\mathbf{h_{ECG}} \ \mathbf{h_{EMG}})$ whose columns (rows) are mutually related as:

$$\boldsymbol{V} \approx \boldsymbol{w_{ECG}} * \boldsymbol{h_{ECG}} + \boldsymbol{w_{EMG}} * \boldsymbol{h_{EMG}} \tag{4.10}$$

The matrix relationship (4.5), schematically represented in Figure 4.6, holds true when it is seen as a sum of energies. Alternatively, it can be represented as a linear combination of two matrices, namely $\boldsymbol{V_{ECG}}$ and $\boldsymbol{V_{EMG}}$:

$$\boldsymbol{V} \approx \boldsymbol{\alpha} * \boldsymbol{V_{ECG}} + \boldsymbol{\beta} * \boldsymbol{V_{EMG}} \tag{4.11}$$

where α and β are scaling factors. Recalling the aforementioned discussion about choice of matrix rank, the ECG waveform is estimated by means of the Inverse WT and posterior rescaling to mitigate the effect of the factor α:

$$\hat{\boldsymbol{s}}_{\boldsymbol{ECG}} = \boldsymbol{WT^{-1}}\{\boldsymbol{V}.*(\boldsymbol{w_{ECG}} * \boldsymbol{h_{ECG}})\} \tag{4.12}$$

$$\hat{\boldsymbol{s}}_{\boldsymbol{ECG}} \rightarrow \frac{\hat{\boldsymbol{s}}_{\boldsymbol{ECG}}}{max|\hat{\boldsymbol{s}}_{\boldsymbol{ECG}}|} max|\boldsymbol{s}| \tag{4.13}$$

where WT $^{-1}$ stands for the Inverse Wavelet Transform (see Figure 4.3) and "^" denotes an estimation.

The estimated (clean) EMG is straightforwardly obtained by subtracting the estimated ECG from the input signal:

$$\hat{\boldsymbol{s}}_{\boldsymbol{ECG}} = \boldsymbol{s} - \hat{\boldsymbol{s}}_{\boldsymbol{ECG}} \tag{4.14}$$

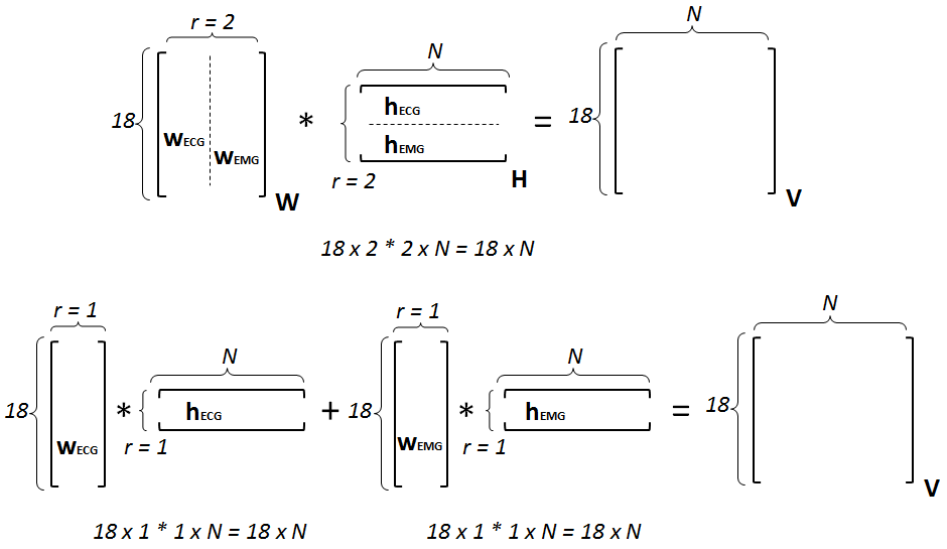

Figure 4.6 Matrix V decomposition with *r* = 2.

4.3 Results

4.3.1 Data

The experimental procedure was conducted in accordance with the Declaration of Helsinki and was approved by the Local Ethics Committee. Each subject provided an informed written consent before participation in the study. The experimental session was performed with a KinCom Isokinetic Dynamometer (Chattanooga, TN, USA). The subjects performed two maximal voluntary contractions (MVC) of right knee extension over a period of 5 seconds, separated by 2 min of rest. The highest MVC value was used to obtain the submaximal force levels. After 2 min of rest, the subjects were asked to maintain an isometric right-knee extension at 30% MVC for as long as possible. EMG activity during the isometric contraction of the vastus medialis of the right leg was recorded using a grid of 65 surface electrodes (5 columns × 13 electrodes; 2.5 mm interelectrode distance). The grid was placed along the direction of the muscle fibers, between the innervations zone and the distal tendon,

previously identified during a preliminary brief knee isometric contraction. A reference electrode was placed around the right ankle. Before the placement of the electrodes, the skin was shaved, lightly abraded and cleaned with water. The EMG signals were amplified as monopolar derivations (EMG amplifier, LISiN-OT Bioelettronica, Torino, Italy), bandpass filtered (–3dB bandwidth, 1–500 Hz), sampled at 2048 samples/s, and converted to digital data by a 12-bit A/D converter board.

4.3.2 Evaluation parameters

The performance of the proposed method was carried out by means of a set of parameters used to characterize electromyograms: High-to-Low power ratio (H/L), normalized median frequency (NMDF), spectral density difference (SPD) and normalized average rectified value (NARV). The last three of them would need a clean EMG signal as a reference, which was obviously not available. We used instead an approximation of a clean EMG signal by selecting segments of the recorded electromyogram between contiguous electrocardiogram QRS complexes [6].

The High/Low energy ratio

It provides rough information about the energy distribution of an EMG signal in the frequency domain. It is defined as energy ratio between high (40-90Hz) and low (2-30Hz) frequency bands. The former encompasses most of the EMG and the latter with dominant ECG signal source.

The Normalized Median Frequency

It is the frequency that divides the EMG power spectrum into two parts of equal power.

This parameter was implemented as a ratio between median frequency of the reference EMG (MDF_{approx}) and median frequency of separated EMG ($MDF_{estim.}$) respectively [88].

$$NMDF = \frac{MDF_{approx.}}{MDF_{estim.}} \tag{4.15}$$

The Spectral Density

It is the power spectral density in low frequency band up to 20Hz. It was defined as:

$$SPD = \frac{\sum_k |\boldsymbol{S_{EMG}(k)} - |\widehat{\boldsymbol{S}}_{\boldsymbol{EMG}}(\boldsymbol{k})|^2}{\boldsymbol{S_{EMG}}\,(\boldsymbol{k})} \tag{4.16}$$

where, $\boldsymbol{S_{EMG}}$ and $\widehat{\boldsymbol{S}}_{\boldsymbol{EMG}}$ are discrete FFT spectrum of reference and separated EMG signal, respectively.

The Normalized Average Rectified Value

It defined as a normalized sum of the signal $\boldsymbol{s}$ of N samples defined in the following way:

$$ARV = \frac{1}{N}\sum_{n=1}^{N}|\boldsymbol{s}(\boldsymbol{n})| \tag{4.17}$$

This parameter was implemented as a ratio between average rectified value of estimated ARV_{estim} and reference $ARV_{approx.}$ EMG signals [88].

$$NARV = \frac{ARV_{estim.}}{ARV_{approx.}} \tag{4.18}$$

4.3.3 Methods for the comparative study

The performance of the proposed approach was evaluated through a comparative study against recent unsupervised learning method and an SSA-based method for ECG-EMG separation. The first reference method [11] further denoted as SSA-ALE, is based on singular spectrum analysis implemented as a first stage of an adaptive line enhancer (ALE). During signal component reconstruction stage in the SSA, the eigentriples are adaptively selected using the delayed version of the input signal in each iteration they are further tuned. The last step is the subtraction of the outcome from the delayed mixture. The performance of the algorithm depends on the correct estimation of the period of ECG (needed for delayed input

signal), overall number of eigentriples and the iteration step size μ_k which is often set manually. The second reference method [89], which we will refer to as the reshaped spectrogram NMF (chapter 3), fits into the classical NMF spectrogram-based approach with improved initial estimates. In order to obtain well localized ECG patterns, the inputs spectrogram is reshaped by means of signal decimation and filtering. This procedure renders intensity spectrogram patterns, which are next used as the initial guess for the NMF separation algorithm. The algorithm outputs two sets of matrices which are merged into the estimated ECG-EMG spectrograms.

In Table 4.1 we show the performance of the four methods evaluated on four subjects. For each subject and method, a total of 64 recording channels were processed in terms of mean and variance of the performance evaluation parameters described in Section 4.3.2.

Throughout the analysis each channel was processed independently from the rest of the channels. In order to generate the spectrograms for the reshaped spectrogram NMF, the original settings were used: decimation/interpolation factor set to 10, window type was Hanning, analysis window duration equal to 0.24 seconds with 50% overlap. For the WNMF the reconstruction error threshold (stopping criterion) was set to 10e-5 for unit-normalized input waveforms.

In order to interpret the results in the context of the present application, let us first comment on the parameter values for the best-case scenario separation – a perfect EMG denoising i.e. after the ECG removal from the input electromyogram, the EMG signal component undergoes no distortion. Accordingly, we expect the H/L ratio and SPD to be small, whereas the NMDF and NAVR should ideally be unitary. Obviously, for real-world separation scenarios we expect the parameter values to deviate from the ideal situation.

Table 4.1 Comparative study outcomes (mean ± standard deviation) for four subjects.

H/L ratio

	Subject1	Subject 2	Subject 3	Subject 4
SSA-ALE	5.01 ± 0.35	9.33 ± 1.21	10.02 ± 1.06	3.97 ± 0.09
RSp NMF	6.22 ± 1.09	14.19 ± 0.49	10.58 ± 3.21	4.10 ± 0.72
WNMF	4.58 ± 0.26	9.84 ± 0.31	8.67 ± 0.81	3.31 ± 0.26

NMDF

	Subject1	Subject 2	Subject 3	Subject 4
SSA-ALE	1.20 ± 0.03	1.13 ± 0.04	0.89 ± 0.03	1.10 ± 0.08
RSp NMF	0.94 ± 0.02	0.92 ± 0.02	0.93 ± 0.02	0.94 ± 0.02
WNMF	0.97 ± 0.02	0.96 ± 0.03	0.96 ± 0.02	0.93 ± 0.02

SPD

	Subject1	Subject 2	Subject 3	Subject 4
SSA-ALE	0.64 ± 0.02	0.71 ± 0.03	0.69 ± 0.02	0.62 ± 0.02
RSp NMF	0.52 ± 0.04	0.53 ± 0.03	0.51 ± 0.01	0.42 ± 0.02
WNMF	0.46 ± 0.03	0.51 ± 0.03	0.49 ± 0.01	0.39 ± 0.02

NARV

	Subject1	Subject 2	Subject 3	Subject 4
SSA-ALE	0.79 ± 0.09	0.76 ± 0.06	0.85 ± 0.06	0.74 ± 0.09
RSp NMF	0.88 ± 0.02	0.92 ± 0.02	0.90 ± 0.02	0.87 ± 0.02
WNMF	0.90 ± 0.01	0.96 ± 0.01	0.93 ± 0.02	0.91 ± 0.01

If we examine the content of Table 4.1, we will see that the proposed WNMF separation method exhibits the best overall performance, followed by the reshaped spectrogram NMF and SSA-ALE method.

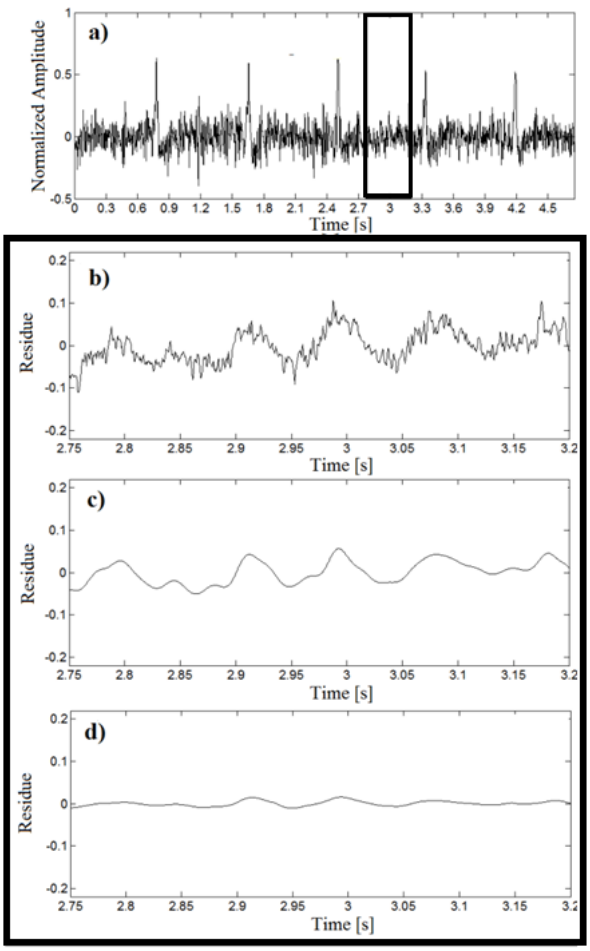

Figure 4.7 Time-domain residual for Subject 2 after the separation performed by each method.

As an illustration of the aforementioned analysis, we show in Figure 4.7 the effect of ECG removal on the EMG signal component for Subject 2. Figure 4.7 *a*) shows a 5-second single-channel input signal, whilst Figure 4.7 *b*) – *d*) show the residuals obtained by subtracting the estimated EMG from the clean EMG.

Both reshaped spectrogram NMF and WNMF residuals exhibit only a low frequency content (up to 10 Hz approximately), with the WNMF providing the best fit (smallest residual) to the clean EMG.

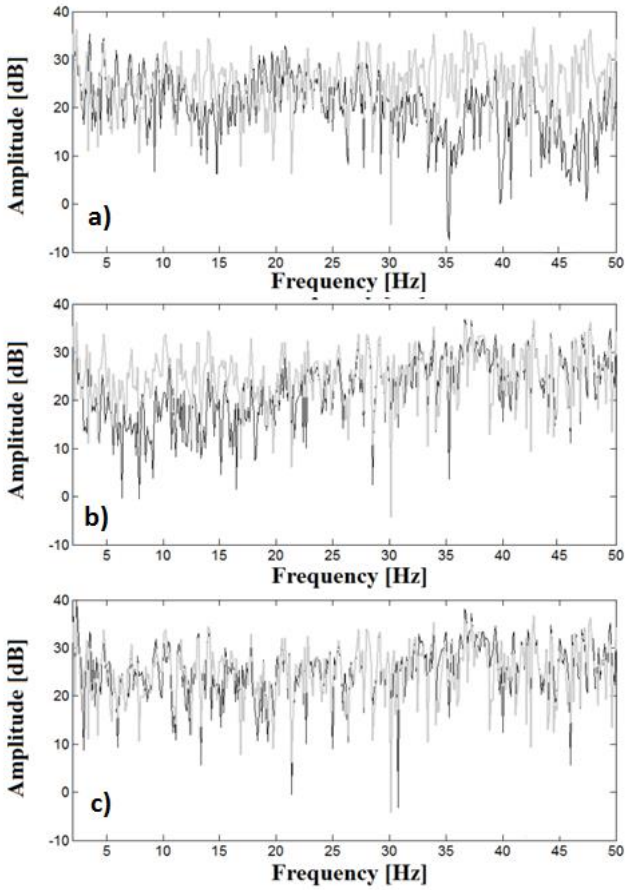

Figure 4.8 Frequency domain comparisons between the methods for subject 3.

In order to provide a deeper insight, the analysis of the previous example was conducted in the frequency domain as well. Figure 4.8(*a*) - (*c*) show the spectrum of the EMG signal segment from Figure 4.7(*a*), together with the spectra of the estimated EMG by the methods involved in the comparative study. The mismatch between these spectra, plotted on the logarithmic amplitude scale, show roughly at which frequency bands the residuals concentrate most of its energy.

4.4 ECG denoising from EMG and other artifacts

In this section, we present a comparison between the reshaped spectrogram NMF and WNMF, shown in the form of block diagram in Figure 4.9. As the noise artifact, we have considered baseline wander (BW) which is often present in real data recordings.

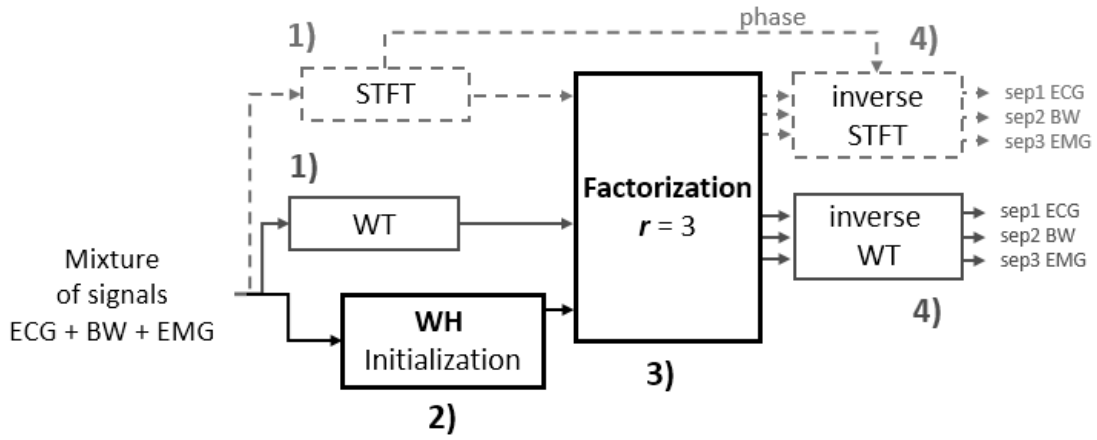

Figure 4.9 EMG denoising with the reshaped spectrogram NMF (dashed line) and WNMF (continuous line).

For the input signal, the initialization is carried out by means of a low-pass filter at cutoff frequency 3 Hz, where most of the BW energy is preserved. The factorization matrix factor r_{Base} = 1 is sufficient to capture a slow varying interference. Next, a band-pass filter between 3-50 Hz is used on the input in order to preserve most of the ECG energy.

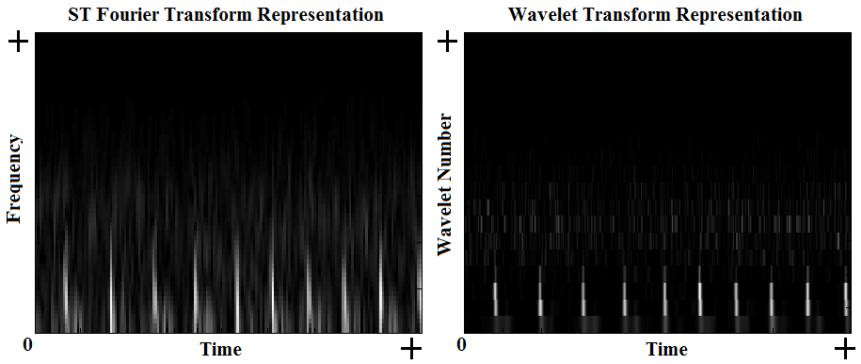

Figure 4.10 Clean ECG image obtained by the STFT with a short window (left) and by WT (right).

As it may be seen in the Figure 4.10 both non-negative representations obtained by the STFT and WT show similar patterns - vertical lines at the bottom of the spectrogram. The factorization matrix factor for ECG is set to 1. The input signal is the same as in section 4.3.1 with MVC 30%. The following settings have been used: signal duration equal to 5 seconds, the sampling frequency fs = 2048 Hz.

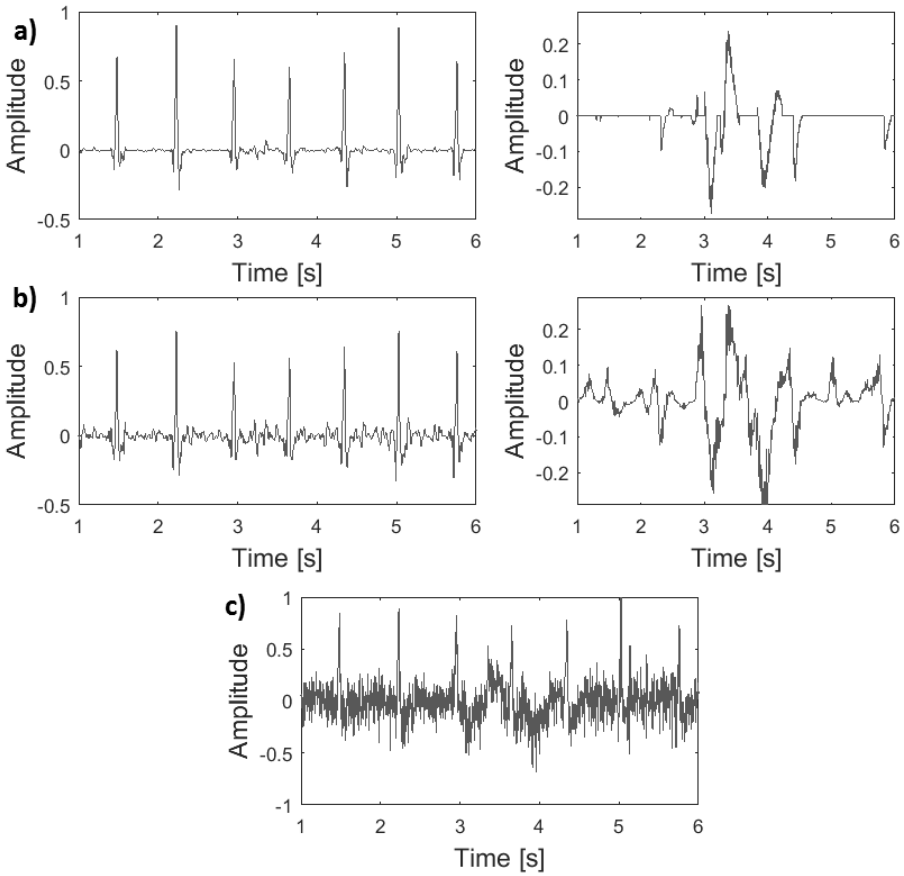

Figure 4.11 ECG and BW extraction from EMG record; a) reshaped spectrogram NMF, b) WNMF and c) input record.

From Figure 4.11 we see that both methods were able to correctly denoise ECG. The ECG the reshaped spectrogram NMF looks somewhat better but it turns out that the QRS is distorted. The EMG signal cannot be obtained directly from the algorithm since the r_{EMG} was set to 1, what is clearly insufficient to correctly describe the signal complexity in the ***WH*** structure.

4.5 Summary

We have presented a novel approach to electrocardiogram removal from single-channel electromyogram recordings by means of the wavelet transform combined with non-negative matrix factorization. We have shown that sparse time-frequency representations, inherent to electrocardiograms, can be efficiently exploited in the context of initialization of a non-negative matrix factorization algorithm. It was shown that such an initial guess ensures low-rank decomposition onto the intensity images, from which the estimated signal components can be easily recovered by means of the inverse wavelet transform.

Validation of the proposed approach was conducted on real electromyogram signals through a comparative study, which included two state-of-the-art methods: a singular spectrum analysis one and reshaped spectrogram based NMF, and four performance evaluation parameters in both the time and frequency domain. In comparison to the reference methods, the proposed method showed the highest performance in terms of high-to-low energy ratio, normalized median frequency, spectral power difference and normalized average rectified value. The proposed approach thus achieves ECG suppression with the smallest EMG distortion amongst the analyzed methods, and this can be highly beneficial for parameter estimate uncertainty reduction in the clinical and sports medicine applications. As most of the low-frequency EMG content is preserved, the frequency-based fatigue evaluation parameters estimates would exhibit less variance, which is advantageous for statistical significance tests [90] [91] . Furthermore, the proposed method can be used for the surface electromyography applications based on time waveform e.g. mean conduction velocity estimation [92], EMG signal classification [93], EMG signal compression [94], to name a few.

CHAPTER 5

LOW-RANK NMF

In two previous chapters, we have presented methods which aimed at separating ECG-EMG signal mixtures by making use of sparsity and unsupervised learning algorithms based on NMF. The former focused on enhancing the sparsity of the ECG spectrogram by filtering and downsampling the input signal, thus bringing out the QRS complexes against the EMG background. The latter processed input data by the wavelet transform with adequately chosen basis functions (Cauchy-type non-linearly scaled wavelets) which captured the basic ECG waveforms shapes with a relatively small number of wavelet coefficients. Both methods provided a sparse ECG TF representation which was used as the initialization for the NMF algorithms and they both achieved a very good ECG-EMG separation compared to the existing state-of-the-art techniques.

However, both methods have important drawbacks, namely:

(1) they do not work with data containing more than two signal sources,

(2) their performance largely depends on the analysis window size used to generate TF representations,

(3) they always consider unitary rank matrix description independent of the signal source dynamics.

Adopting the general approach based on sparsity and unsupervised learning, we propose a novel method which poses the harmonic and baseline noise removal task as a source separation problem (the preliminary research in the context of EMG denoising was discussed in [95]). The proposed method overcomes the aforementioned drawbacks by introducing new algorithm features, namely: unambiguous non-negative rank estimation of individual sources in the data and phase-preserving spectrogram segmentation.

Optimal non-negative rank is a key factor in any non-negative matrix decomposition because:

(1) it provides a way to drastically reduce problem dimensionality without losing any relevant characteristic of the underlying source,

(2) it allows for fast convergence of the NMF algorithms.

However, existing algorithms for computing the non-negative rank introduce a prohibitively high computational cost, which impedes its use in on-line applications.

Herein we develop a study which (1) discusses a general relationship between standard and non-negative matrix rank, and (2) shows under which circumstances those ranks can be used interchangeably in the context of the present application. A major benefit of this study is that the estimation of the non-negative rank can be carried out by economy-size singular value decomposition (SVD), which drastically relaxes the algorithm's overall computational cost. Furthermore, we introduce a spectrogram segmentation procedure which aims at coarse separation of underlying signal sources in the TF domain by means of a set of data-driven spectrogram shaping vectors. Such a segmentation scheme ensures that no spectral phase modification occurs; accordingly, the estimated signal component waveforms are virtually distortionless. By combining these novel features with NMF, our algorithm achieves an unambiguous and physically meaningful signal-noise separation from the spectrogram of the input data in only a few computational iterations. Moreover, such a separation strategy was proven experimentally to be especially efficient in data acquisitions with very low SNR.

The proposed method was tested on real electrocardiogram (ECG) and electromyogram (EMG) signals for different analysis scenarios, against two state-of-the-art reference methods.

5.1 Method

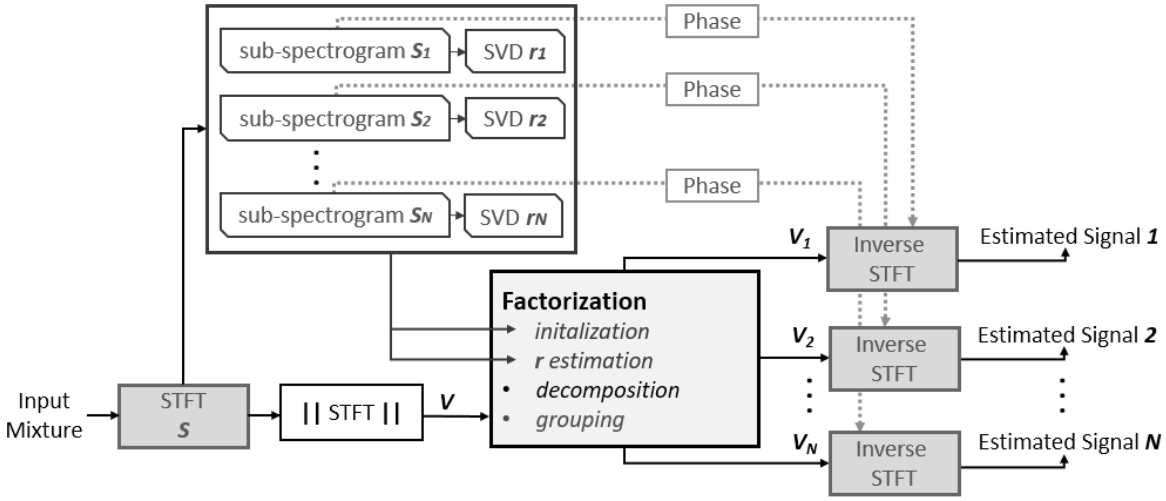

Figure 5.1 Low Rank Matrix Factorization.

The overview of the Low Rank Matrix Factorization analysis can be seen in Figure 5.1. The input mixture is transformed into a non-negative representation by the STFT. It is then segmented in such a way that most of the energy of each source is contained in a sub-spectrogram. Note that no filtering was employed in this stage. After that the Singular Value Decomposition SVD approach is applied in order to extract information of every signal source dynamics. This information is used to set r_N properly and to apply a classical NMF on every sub-spectrogram. The resulting pairs of $\boldsymbol{w_N}$ and $\boldsymbol{h_N}$ are concatenated into initialization matrices $\boldsymbol{W_{init}}$, $\boldsymbol{H_{init}}$. The optimal matrix factorization rank r is a sum of r_1, r_2, …, r_N. After the decomposition, the previously obtained values of r_N are used to group the estimates accordingly. The final step is a recovery of the time domain waveforms.

In this approach we focus our attention on matrix sparsity and non-negative rank r, which are one of the most prominent concepts of the low-rank matrix decomposition theory [96] [97]. Briefly, it states that a large matrix with a small number of significant non-negative entries can be replaced by a lower rank matrix, providing a more efficient representation of the relationship between data elements. Such a matrix brings out the most relevant components of the data while, at the same time, mitigating the effect of possible disturbances.

5.2 Practical case: EMG denoising

Often the quality of recorded surface electromyography signals (EMG) may be compromised by interferences like power line interference (PLI) and baseline wander (BW). Power line coupling, movement artifacts or varying electrode impedance are the most common sources of interferences. Both lie in the same frequency bandwidth as the signal of interest. Therefore, their removal without losing any relevant information contained in the EMG becomes a challenging task.

5.2.1. Initialization

Let *N* be a number of concurrent sources in the input record. Starting from $\boldsymbol{S}$ we seek to obtain *N* sub-spectrograms $\boldsymbol{S_i} \in R_+^{mxn}$, $i = 1, \dots, N$ such that $\boldsymbol{S_i}$ contains most of the energy of the $\boldsymbol{i}^{th}$ source plus energy-attenuated contributions from the remaining sources.

If we express $\boldsymbol{S_i} = (\boldsymbol{s_1}, \dots \boldsymbol{s_n})$ with $\boldsymbol{s_i} \in R_+^m$, $k = 1, \dots, n$ being column vectors, the sub-spectrograms are obtained:

$$\boldsymbol{S_i} = (\boldsymbol{s_1} \circ \boldsymbol{h_i}, \dots \boldsymbol{s_n} \circ \boldsymbol{h_i}), \qquad i = 1, \dots, N \tag{5.1}$$

where $\boldsymbol{h_i} \in R_+^m$ are spectrogram shaping vectors. The shapes of $\boldsymbol{h_i}$ are determined under the assumption that the number and nature of the underlying sources is known. It is very important to highlight that spectrogram shaping is not equivalent to filtering. With spectrogram shaping the phase information is fully preserved, which is crucial for the final time-domain conversion step.

As an illustration, Figure 5.2 shows the vectors $\boldsymbol{h_i}$ for an input EMG recording corrupted by baseline and harmonic noise.

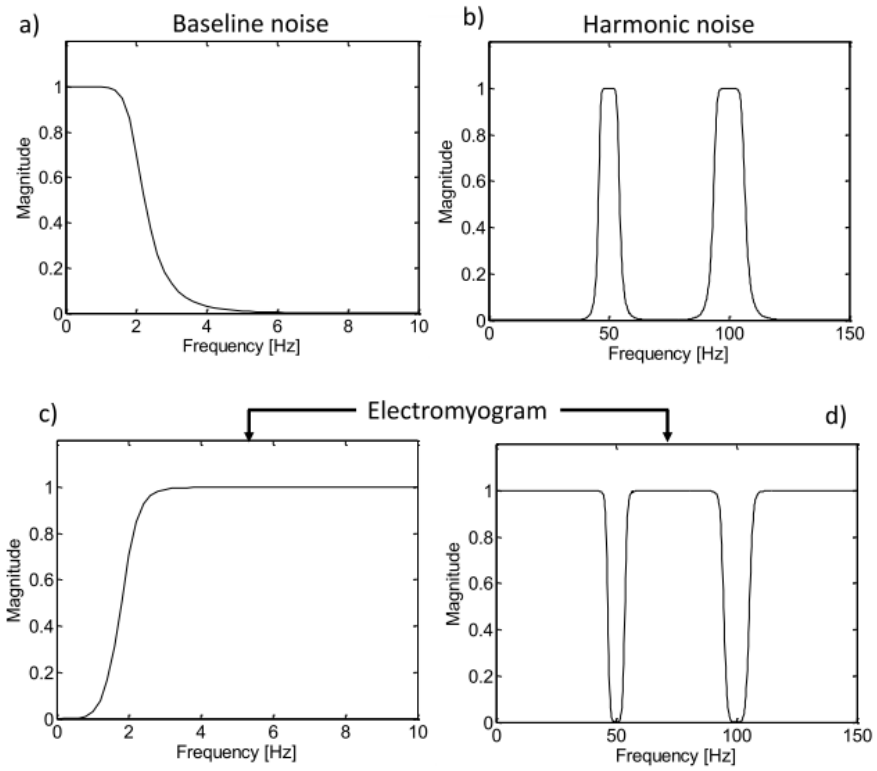

Figure 5.2 Spectrogram shaping example.

Algebraically, the sub-spectrograms are matrices where a certain number of rows (spectra) contain entries close to zero. This is especially true for the noise sub-spectrograms due to the highly selective performance of the shaping vectors. Accordingly, these matrices are almost sparse because rather than being exactly zeros, the entries are relatively small numbers. Such approximately sparse matrices admit important dimensionality reductions where optimal non-negative rank estimation plays a key role.

5.2.2. Non-negative rank estimation

At this point we must first differentiate between standard rank and nonnegative rank. The standard rank of a matrix, as revealed by the SVD for instance, is the size of the largest set of its columns (or rows) that are linearly independent. However, for a non-negative matrix we need to consider the non-negative rank which is defined as follows [98].

> ***Definition 1***. *Given a non-negative matrix* $\boldsymbol{A} \in R_+^{mxn}$ *the non-negative rank of* ***A*** *is the smallest natural number r for which there exist two matrices* $\boldsymbol{V} \in R_+^{mxr}$ *and* $\boldsymbol{U} \in R_+^{rxn}$ *such that* ***A=VU***.

Accordingly, in the case of the non-negative rank, $rank_+(\boldsymbol{A})$ the linear combinations of the columns (or rows) are required to have positive coefficients. Due to this constraint, the non-negative rank may be larger than the standard rank [99]:

$$rank(\boldsymbol{A}) \leq rank_+(\boldsymbol{A}) \leq \min\{\mathrm{m}, \mathrm{n}\} \tag{5.2}$$

Thus, the problem of computing $rank_+(\boldsymbol{A})$ boils down to finding the smallest collection of non-negative vectors that generate columns of ***A*** in a non-negative way. This task, unfortunately, turns out to be NP-hard [100]. On the other hand, the following theorem provides a valuable insight into the relationship between the standard and non-negative rank [101].

> ***Theorem 1***. *Given k < {m, n} let* $R_+(k)$ *denote manifold of non-negative matrices in* R_+^{mxn} *with non-negative rank k. Then, given* $\boldsymbol{A} \in R_+(k)$ *the conditional probability of,* $rank(\boldsymbol{A}) = k$*, is one.*

In other words, this theorem says that the set of matrices whose standard rank is strictly less than their non-negative rank has measure zero. Consequently, even though the matrices with $rank(\boldsymbol{A}) < rank_+(\boldsymbol{A})$ exist, they are isolated points in the space R_+^{mxn} i.e. the probability of coming across such matrices in the present application is zero. In this manuscript, the sub-spectrograms $\boldsymbol{S_i}$ are always in the format of a non-negative matrix. Accordingly, they fall in the class of matrices A from the above theorem. Consequently, their standard rank is the same as the non-negative rank. With respect to the aforementioned discussion, we need to estimate the standard rank of the sub-spectrogram matrices $\boldsymbol{S_i}$.

The SVD provides a diagonalization of an arbitrary matrix $\boldsymbol{A} \in R_+^{mxn}$ in the way

$$\boldsymbol{A} = \boldsymbol{UZV^T} \tag{5.3}$$

where ***U*** and ***V*** are orthogonal matrices, $\boldsymbol{Z} = \begin{pmatrix} \boldsymbol{\Sigma} & \mathbf{0} \\ \mathbf{0} & \mathbf{0} \end{pmatrix} \in R_+^{mxn}$, $\sum = diag(\sigma_1, \ldots \sigma_p) \in R_+^{mxn}$, $\sigma_1 \geq \sigma_2 \geq \cdots \geq \sigma_p > 0$, is the diagonal matrix of the singular values of ***A***.

Since ***U*** and $\boldsymbol{V}^T$ are unitary, their columns can be regarded as basis vectors with associated singular values. The set of singular values form the singular value spectrum, whose weights explain the variance of the associated singular vectors in the data. Typical singular spectrum shapes for a number of biomedical signal components of interest are shown in Figure 5.3.

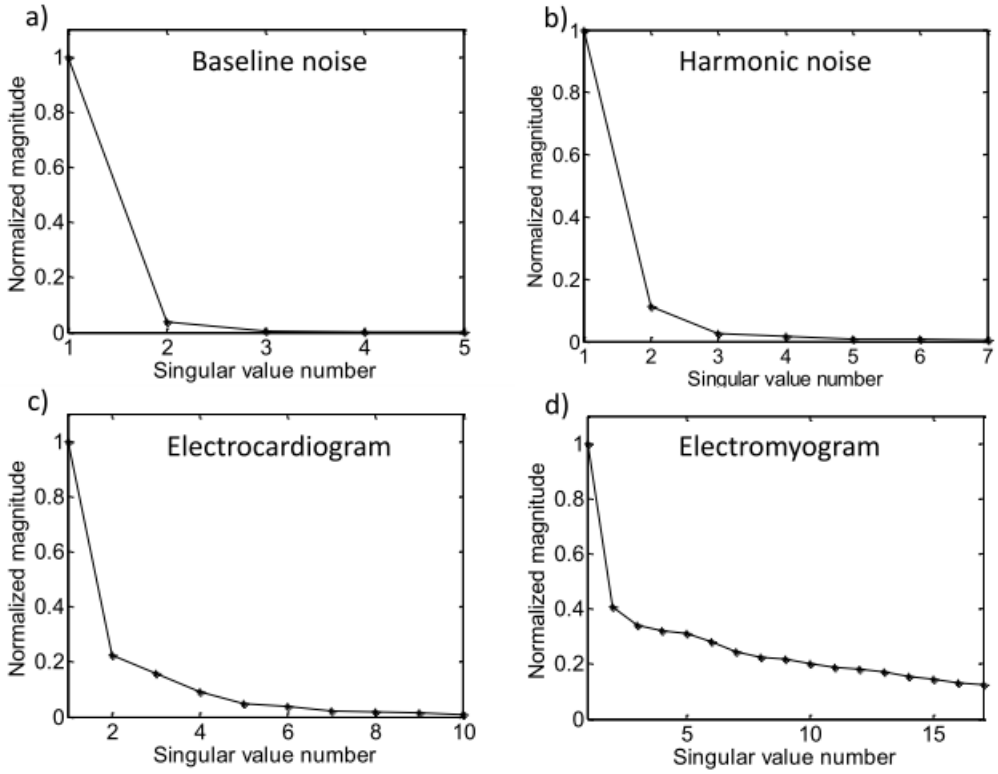

Figure 5.3 Typical singular values for different source signals.

From Figure 5.3 we see that:

1) the first singular value accounts for the most variance,

2) the spectral roll-off depends on the waveform complexity.

The latter is of extreme importance as it states that only *k* < *n* singular values and vectors are enough to capture the essential features of the data i.e. *k* is an optimal approximation to *rank* ***(A)***. This argumentation is readily verified by a visual inspection of the spectra in Figure 5.3.

For example, the sharp almost-zero drop for the baseline noise results from a simple waveform shape (slowly varying DC component). Therefore, we expect the corresponding sub-spectrogram to have a rank not larger than two. On the other hand, the EMG has a noise-like waveform shape, which means that more singular vectors are needed to properly capture the dynamics of the signal. Thus, the rank should definitely be larger than two. Recall that a sub-spectrogram $\boldsymbol{S_i}$ contains information about the signal component of interest $\boldsymbol{A_i}$ (e.g. harmonic noise) plus some interference coming from the rest of the components $\boldsymbol{E_i}$ (e.g. EMG and baseline noise). From the properties of the SVD [38] we have:

$$|\sigma_k(\boldsymbol{S_i}) - \sigma_k(\boldsymbol{A_i})| \leq \sigma_k(\boldsymbol{E_i}) = \|\boldsymbol{E_i}\|_2 \leq \|\boldsymbol{E_i}\|_F, k = 1, \dots n \tag{5.4}$$

The proof of (5.3) can be found in the aforementioned reference. Since $\sigma_{r+1}(\boldsymbol{A_i}) = 0$, we obtain the following:

$$\sigma_{r+1}(\boldsymbol{S_i}) \leq \sigma_1(\boldsymbol{E_i}) \tag{5.5}$$

$$\sigma_r(\boldsymbol{S_i}) \in (\sigma_r(\boldsymbol{A_i}) - \sigma_1(\boldsymbol{E_i}), \sigma_r(\boldsymbol{A_i}) + \sigma_1(\boldsymbol{E_i})) \tag{5.6}$$

Therefore, given $\sigma_r(\boldsymbol{A_i}) > \sigma_1(\boldsymbol{E_i})$, expressions (5.4) - (5.6) show that an appropriate threshold on the singular values yield the rank *r*. Accordingly, provided the spectrogram shaping effectively reduces the level of interference from the rest of the components, the number of significant singular values will be those of the component of interest. In order to estimate the number of relevant singular vectors (i.e. the rank) from the singular value spectra, there are a number of strategies which fall into the commonly known number-of-factor estimation problem: the Kaiser criterion, the scree test, parallel analysis, to name a few [102]. However, these methods do not entirely fit in the context of the present application because they often lead to rank underestimation. More reliable rank estimates are obtained by the explained-variance based approach [103], where a user-defined threshold δ on the accumulated variance $\sigma_{A,i}^2$ determines the number or relevant singular vectors. Analytically,

$$\sigma_r^2 = \sum_{k=1}^{r} \sigma_k^2 \leq \delta \mid \delta \in R_+, rank_+ = r \tag{5.7}$$

The optimal value for δ should keep in balance the parsimony and goodness-of-fit of the solution. Accordingly, we used $\delta = 0.05$, which means that 95% of the signal variance is explained by *r* retained singular values and vectors. The optimal non-negative $rank_+ = r$ obtained in this way ensures that all relevant features of the underlying matrix are preserved by considering only *r* associated basis vectors. Taking $rank_+ < r$ leads to excessive smoothing e.g. a less exact approximation of the matrix. On the other hand, if $rank_+ > r$ overfitting occurs. The *r* largest basis vectors explain the main component, whilst the remaining *n-r* basis vectors characterize the interfering components. Accordingly, considering more than *r* basis vectors would increase the presence of interference in the component of interest. Note, however, that the basis vectors in our estimation will not come from the SVD but from the NMF of the sub-spectrogram (see next section). The SVD is only used to find the non-negative rank *r*.

5.2.3 Source grouping

With the non-negative rank for each sub-spectrogram $\boldsymbol{S_i}$ determined, we need to provide a non-negative dimension reduced representation for each $\boldsymbol{S}$. To that end, we cannot simply utilize the result of the SVD because non-negativity of the singular vectors is not ensured. Instead, we make use of the NMF approach which imposes an additive model (subtractions are not permitted) to compositional data [4]. In particular, the NMF solves the following estimation problem:

$$\boldsymbol{S_i} = \boldsymbol{\psi_i C_i^T} + \boldsymbol{E_i}, i = 1, \dots N \tag{5.8}$$

where, $\boldsymbol{\psi_i} \in R_+^{mxr}$ and $\boldsymbol{C_i^T} \in R_+^{rxn}$ stand for the basis vectors and coefficients respectively, whilst, $\boldsymbol{E_i} \in R_+^{mxn}$ represents the approximation error. Note the similarity to the SVD, where the factors $\boldsymbol{U\Sigma}$ and $\boldsymbol{V^T}$ play the same role as $\boldsymbol{\psi_i}$ and $\boldsymbol{C_i^T}$ respectively. The exact solution of (5.8) cannot be attained; however, we can obtain the estimates $\{\boldsymbol{\psi_{i,0}}, \boldsymbol{C_{i,0}^T}\}$ in the sense of the minimum Frobenius norm of $\boldsymbol{E_i}$:

$$\{\boldsymbol{\psi_{i,0}}, \boldsymbol{C_{i,0}^T}\} = argmin_{\boldsymbol{\psi_i}, \boldsymbol{C_i^T}} \|\boldsymbol{S_i} - \boldsymbol{\psi_i C_i^T}\|_{\boldsymbol{F}}^{\boldsymbol{2}}, i = 1, \dots, N \tag{5.9}$$

The non-linear minimization of (5.9) with respect to *i* and $\boldsymbol{C_i^T}$ is carried out in an iterative manner by means of any available randomly initialized NMF algorithm. Finally, the estimated factors (matrices) are concatenated (grouped) as:

$$\boldsymbol{\psi_0} = \left(\boldsymbol{\psi_{1,0}}, \dots, \boldsymbol{\psi_{N,0}}\right), \boldsymbol{\psi_0} \in R_+^{mxR} \tag{5.10}$$

$$\boldsymbol{C_0^T} = \left(\boldsymbol{C_{i,0}^T}, \dots, \boldsymbol{C_{N,0}^T}\right), \boldsymbol{C_0^T} \in R_+^{Rxn} \tag{5.11}$$

where we assume that the rank R for (5.10) and (5.11) is the sum of the optimal ranks for all $\boldsymbol{S_i}$ as calculated by (5.7). Matrices $\{\boldsymbol{\psi_0}, \boldsymbol{C_0^T}\}$ retain the principal non-negative features of the under- lying sources in the input signal. Nevertheless, some interference (residual) among the sources is still present, due to the coarse sub-spectrogram generation in (5.1). Moreover, for most clinical purposes we need to convert the sub-spectrogram to time waveforms. These tasks are completed in the final algorithm step described in the following section.

5.2.4 Separation

A) Sub-spectrograms interference removal

As mentioned in the previous section, the goal of the present algorithm step is to mitigate the interferences among the signal sources by adequately modifying the matrices $\{\boldsymbol{\psi_0}, \boldsymbol{C_0^T}\}$. These matrices contain the optimal number of basis vectors and coefficients respectively which generate all the sub-spectrograms $\boldsymbol{S_i}$, *i = 1, …N* plus unwanted residual (interferences). Recalling the sub-spectrogram additivity assumption, we can establish the relationship between $\boldsymbol{S}$ and $\{\boldsymbol{\psi_0}, \boldsymbol{C_0^T}\}$:

$$\boldsymbol{S} \approx \sum_i^N \boldsymbol{S_i} = \boldsymbol{\psi_0 C_0^T} + \boldsymbol{e_i}, i = 1, \dots, N \tag{5.12}$$

where e is the overall residual from all sub-spectrograms that should be minimized.

Let us express the basis coefficient matrix through its columns $\boldsymbol{C_0^T} = \left(\boldsymbol{C_{0,1}^T}, \dots, \boldsymbol{C_{0,n}^T}\right), \boldsymbol{C_{0,k}^T} \in R_+^R$, *k = 1, …n*. Recalling $\boldsymbol{S_i} = (\boldsymbol{s_1}, \dots \boldsymbol{s_n})$ we can express each column of $\boldsymbol{S}$ as an over determined linear system:

$$\boldsymbol{s_j} = \boldsymbol{\psi_0}\, \boldsymbol{C_{0,k}^T}, k = 1, \dots n \tag{5.13}$$

The last expression says that the data in the first column of the input spectrogram can be represented as a linear combination of *R* basis vectors weighted by the corresponding coefficients. Finding the best linear combination is then a least-squares projection problem resulting in the following minimum-norm solution for the coefficients:

$$\widehat{\boldsymbol{C}}_{\boldsymbol{0,k}}^{\boldsymbol{T}} = \left(\boldsymbol{\psi}_{\boldsymbol{0}}^{\boldsymbol{T}}\boldsymbol{\psi_0}\right)^{-\mathbf{1}}\boldsymbol{\psi}_{\boldsymbol{0}}^{\boldsymbol{T}}\boldsymbol{s_k}, k = 1, \dots, n \tag{5.14}$$

where we project $\boldsymbol{s_k}$ onto the space spanned by the columns of $\boldsymbol{\psi_0}$The basis vectors are linearly independent, which is ensured by the spectrogram segmentation; therefore $\left(\boldsymbol{\psi}_{\boldsymbol{0}}^{\boldsymbol{T}}\boldsymbol{\psi_0}\right)$ is non-singular and it follows that individual sub-spectrograms can be estimated column-wise:

$$\hat{\boldsymbol{s}}_{\boldsymbol{i,k}} = \boldsymbol{\psi}_{\boldsymbol{i,0}}\widehat{\boldsymbol{C}}_{\boldsymbol{0,k}}^{\boldsymbol{T}}(r_{i-1} + 1{:}\, r_i), i = 1, \dots, N, k = 1, \dots, n, r_0 = 0 \tag{5.15}$$

where the operator (:) in MATLAB notation selects a subvector with corresponding indices. In this way, we would accomplish the source separation by running the least-squares estimation algorithm n times. Such an approach, unfortunately, is not feasible be cause $\widehat{\boldsymbol{C}}_{\boldsymbol{0,k}}^{\boldsymbol{T}}$ are not constrained in sign. This is due to the fact that $\boldsymbol{\psi_0}$ is usually not a monomial non-negative matrix [104]. Therefore, an alternative approach constrained to non-negativity is needed to solve the problem (5.12). This goal is achieved by the Euclidean-distance NMF algorithm with $\{\boldsymbol{\psi}_{\boldsymbol{i,0}}, \boldsymbol{C}_{\boldsymbol{i,0}}^{\boldsymbol{T}}\}$ being the initial conditions for the first iteration. This algorithm performs a non-linear non-negative cost function minimization where in subsequent iterations the following updates are performed [61]:

$$\boldsymbol{\psi_t} = \boldsymbol{\psi_{t-1}} \circ \frac{[\boldsymbol{SC_{t-1}}]}{\left[\boldsymbol{\psi}_{\boldsymbol{t-1}}^{\boldsymbol{T}}\boldsymbol{\psi_{t-1}}\boldsymbol{C}_{\boldsymbol{t-1}}^{\boldsymbol{T}}\right]} = \left(\boldsymbol{\psi_{1,t}}, \dots, \boldsymbol{\psi_{N,t}}\right) \tag{5.16}$$

$$\boldsymbol{C_t^T} = \boldsymbol{C_{t-1}^T} \circ \frac{\left[\boldsymbol{\psi}_{\boldsymbol{t-1}}^{\boldsymbol{T}}\boldsymbol{S}\right]}{\left[\boldsymbol{\psi}_{\boldsymbol{t-1}}^{\boldsymbol{T}}\boldsymbol{\psi_{t-1}}\boldsymbol{C}_{\boldsymbol{t-1}}^{\boldsymbol{T}}\right]} = \left(\boldsymbol{C_{1,t}^T}, \dots, \boldsymbol{C_{N,t}^T}\right) \tag{5.17}$$

where the bracket operator [.] stands for element-wise division and t is the iteration number. Compared to the classical least-squares approach (5.13) - (5.15) the present algorithm presents the following benefits:

- It preserves the non-negativity in each iteration,
- It starts with the matrices $\{\boldsymbol{\psi}_{i,0}, \boldsymbol{C}_{i,0}^{T}\}$ which place the initial solution in the neighborhood of the cost function minimum,
- In each iteration both basis vectors and coefficients are modified in the sense of the minimum gradient of the cost function.

As a result, the algorithm converges after very few iterations (typically 29-32), providing a significant reduction of the residuals in the sub-spectrograms. The refined sub-spectrograms are obtained as follows:

$$\widehat{\boldsymbol{S}}_{\boldsymbol{i}} = \boldsymbol{\psi}_{i,t}, \boldsymbol{C}_{i,t}^{T}, i = 1, \dots N \tag{5.18}$$

B) Time waveform recovery

In order to obtain waveform estimates of the sources, we merge the amplitude information $\widehat{\boldsymbol{S}}_{\boldsymbol{i}}$ with the phase information θ available from the STFT of the input signal. The individual phases can be recovered from θ on the basis of the assumption that over a small time-frequency region one source is dominant i.e. the maximum of the individual sub-spectrograms over each point is approximately equal to the sum of all the sub-spectrograms [67]. Accordingly, we generate a binary mask $\boldsymbol{M}_i$ for each source:

$$(\boldsymbol{M}_{\boldsymbol{i}})_{pq} = \begin{cases} 1, & i = argmax(\widehat{\boldsymbol{S}}_{\boldsymbol{i}})_{pq}, k = 1, \dots N \\ 0, & otherwise \end{cases} \tag{5.19}$$

with *p = 1, …m* and *q = 1, …n*. Next, the estimated STFT of the sources is obtained:

$$\boldsymbol{STFT}\{\boldsymbol{x}_{\boldsymbol{i}}\} = \widehat{\boldsymbol{X}}_{\boldsymbol{i}} \circ \boldsymbol{M}_{\boldsymbol{i}} \circ \boldsymbol{\theta}, i = 1, \dots, N \tag{5.20}$$

$$\widehat{\boldsymbol{X}} = (\widehat{\boldsymbol{S}}_{\boldsymbol{i}})^{\frac{\boldsymbol{1}}{\boldsymbol{2}}}, i = 1, \dots, N \tag{5.21}$$

and the desired waveforms are yielded by applying the overlap-add algorithm to (5.20) [105].

5.2.5 Example

An illustration of the algorithm performance on estimating the baseline noise component (presently referred to as the i^{th} signal component) from the input data is shown in Figure 5.4.

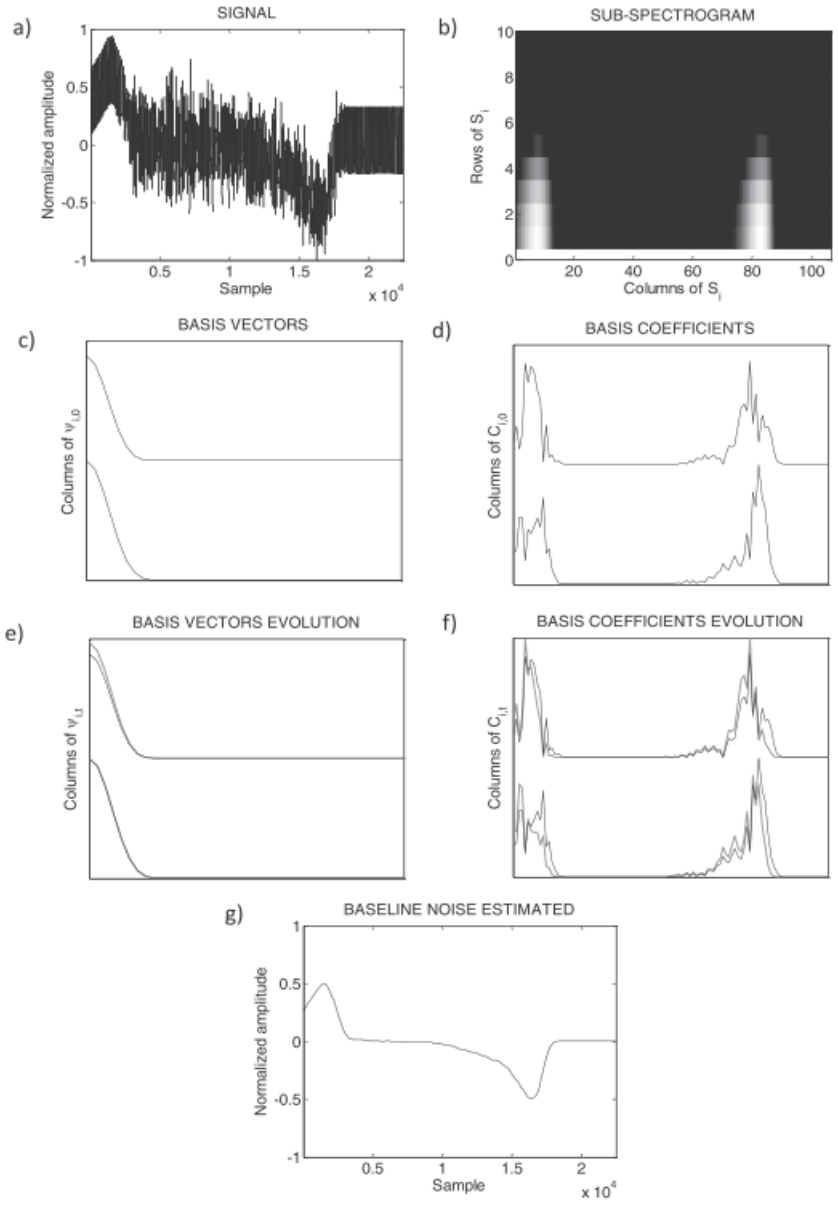

Figure 5.4 Illustration of the algorithm separation performance on a baseline noise. (a) and (b) input data and the baseline noise sub-spectrogram (spectrogram segmentation); (c) and (d) basis vectors and coefficients obtained by minimizing (6) (source grouping); (e) and (f) original basis vectors and coefficient (grey) and after 5 iterations (black) (sub-spectrogram interference removal); (g) estimated baseline noise (time-waveform recovery).

The choice was motivated by the fact that baseline noise is typically described by only a few basis vectors and coefficients, which keeps the graphical representation clear and concise. One can immediately establish a visual correlation between the input signal waveform (Figure

5.4 (a)) and the sub-spectrogram $\boldsymbol{S_i}$ of the baseline noise (Figure 5.4 (b)): most of the energy is uniformly distributed around the DC component except towards the beginning and the end of the recording where a strong variation in the baseline noise is mapped onto a larger frequency bandwidth in $\boldsymbol{S_i}$. For the $rank_+ = 2$ the cost function minimization in (32) delivers the matrices $\{\boldsymbol{\psi_{i,0}}, \boldsymbol{C_{i,0}^T}\}$. whose columns/rows are shown in Figure 5.4 (c) and (d) respectively. Fig. 5.4 (e) and (f) show the content of the matrices $\{\boldsymbol{\psi_{i,0}}, \boldsymbol{C_{i,0}^T}\}$. before (grey) and after sub-spectrogram interference removal $\{\boldsymbol{\psi_{i,t}}, \boldsymbol{C_{i,t}^T}\}$. (black). The relatively small difference is explained by the fact that the estimates $\{\boldsymbol{\psi_{i,0}}, \boldsymbol{C_{i,0}^T}\}$ are situated in the neighborhood of the cost function minimum. Finally, the recovered baseline noise time- waveform shown in Figure5.4 (g) captures the drift in the input data very well.

Algorithm summary:

(1) Spectrogram segmentation

- For each source:
  - Construct the spectrogram shaping vector;
  - Compute the sub-spectrogram.
  - Non-negative rank estimation
- For each source:
  - Calculate the singular value decomposition of the sub-spectrogram;
  - Estimate the non-negative rank by thresholding the accumulated singular value variance.

(2) Source grouping

- For each source:
  - Compute the sub-spectrogram decomposition by randomly initialized rank-constrained NMF;
- Generate the basis vectors matrix and activation coefficients matrix by stacking the results of the previous step.

(3) Separation

- Obtain noise-suppressed sub-spectrograms by the Euclidean-distance NMF constrained to the basis vectors matrix and activation coefficients matrix.
- For each source:

(4) Obtain the time-waveform by applying binary masks on the noise-suppressed sub-spectrogram.

5.3 Results

5.3.1 Data

We used two sets of surface EMG signals, recorded under different experimental and measurement conditions. In both cases the experimental procedure was conducted in accordance with the Declaration of Helsinki and was approved by the Local Ethics Committee. Each subject provided an informed written consent before participation in the study. The first set of EMG signals (EMG set I) was obtained from the vastus medialis obliquus during a sustained fatiguing contraction at 30% of the maximal voluntary contraction (MVC) during 50 seconds for ten healthy subjects. The maximum MVC was calculated as the highest value of two MVCs of the right knee extension over a period of 5 seconds, separated by 2 min of rest. The signals were recorded using three Ag/AgCl sintered electrodes (4 mm in diameter). The skin surface was abraded before the electrode fixation. Next, the signals were band-pass filtered (−3 dB bandwidth, 1–500 Hz), sampled at 2048 Hz and digitalized with 12 bits resolution. The presence of harmonic and baseline noise in the recordings is practically negligible; therefore, they were used for an objective algorithm performance comparative study through controlled signal-noise mixing. The second set of EMG signals (EMG set II) was obtained from biceps brachii during short contractions (3–5 seconds) at 10%, 20%, 40% and 60% of the MCV separated by 30 seconds of rest for 8 healthy subjects. The maximum MVC measure, recorded three times with 2 min rest in between was the reference for the definition of submaximal contraction levels. The signals were recorded by a 2D adhesive array of 13 × 5 equally spaced electrodes (inter-electrode distance 8 mm), sampled at 2048 Hz and stored by a 12-bit analogue-to-digital conversion. Because no specific signal accommodation had been performed, the recordings contained both baseline and harmonic perturbation. Accordingly, this set of signals was used for a subjective algorithm performance comparison.

The ECG signals were taken from the PTB Diagnostic ECG database, which is part of the Physionet project [106]. The database contains 549 recordings from 290 subjects, each subject represented by one to five recordings. Each recording includes 15 simultaneously measured

signals by the conventional 12 electrodes. The recordings are digitized at 1 kHz with 16-bit resolution over the ±16.384 mV range. The harmonic noise was generated s a sum of two-time variant sinusoids with variable instantaneous amplitude and frequency at 50 Hz and 100 Hz respectively. The maximum frequency deviation was 2 Hz and 4 Hz respectively, whilst the maximum amplitude deviation was 20% of the root mean squared value. The amplitude of each harmonic was set to be inversely proportional to its harmonic number. The baseline noise was generated by low-pass Butterworth 4^{th}-order filtering of a Gaussian noise. The variance of the noise sources was set according to analysis scenarios (Sections 5.3.3 and 5.3.4).

5.3.2 Methods for the comparative study

For the present performance comparative study, we have selected the following state-of-the-art reference methods based on different simultaneous harmonic and baseline noise removal mechanisms:

(1) the sinusoidal modeling method (SM) [5],

(2) the fractal and empirical mode decomposition method (FEMD) [107],

(3) the proposed low-rank matrix factorization method (LRMF from now on).

The SM, which operates on both ECG and EMG recordings, models both noise sources as time-variant sinusoids through low-degree polynomials. The sinusoidal frequencies and polynomial coefficients make up model parameters, which are estimated by means of linear least squares in short analysis windows (a few seconds, typically). The FEMD was designed to operate in ECG denoising scenarios only, where the harmonic and baseline noise are modeled as a 1^{st} and 2^{nd} order fractional Brownian motion process respectively. Such fractal modeling allowed for the generation of a projection matrix for mitigating the baseline noise. Furthermore, the algorithm performs an amplitude-frequency decomposition onto a set of intrinsic mode functions (IMF), from which the strongest component is utilized to mitigate the harmonic noise. For the SM, we used the analysis window of 1 second duration and the polynomial order equal to 3. Regarding the FEDM we had to modify slightly the original algorithm, to account for more than one component in the harmonic noise. This modification consisted in processing the two strongest IMFs.

For the LRMF, the STFTs were calculated on the basis of a 2-second Hanning window with 75% overlap. The shaping vectors h_i for spectrogram segmentation were constructed by means of the combined action of 3rd order Butterworth filters in the frequency domain according to Table 5.1. In the same table, the estimated non-negative ranks are given.

Table 5.1 Third-order Butterworth filter types and cutoff frequencies (Hz) for the generation of spectrogram shaping vectors (Figure 5.2), together with the estimated ranks.

Source	Baseline noise	Harmonic noise	ECG	EMG	
Filter type	Low-pass	Band-pass	Band-pass	High-pass	Stop-band
Cutoff frequency	3	46–54 92–108	2–50	3	46–54 92–108
Rank	2	3	6	21	

5.3.3 Removing noise from ECG

A total of forty ECG signals of variable duration from different subjects contaminated simultaneously by the harmonic and baseline noise, were analyzed. As the performance evaluation parameter, we used the output signal-to-interference ratio (SIR out) which quantifies the energy of the non-contaminated ECG over the energy of the residual noise in the ECG after denoising [5]. The SIR_{out} was evaluated as a function of the input signal to-interference ratio (SIR_{in}), defined as the energy of the non-contaminated ECG over initial noise energy, equally split between both noise sources. The analysis was carried out for the SIR in [−15,10] dB with 5 dB resolution step and the overall average scores are shown in Figure 5.5. For the SIR in larger than 10 dB approximately, the SM and LRMF method are situated on practically the same performance level. As the noise power increases, the LRMF algorithm clearly outperforms the reference methods: at SIR in = −15 dB it gains around 8 dB and 17 dB regarding the SM and FEMD respectively.

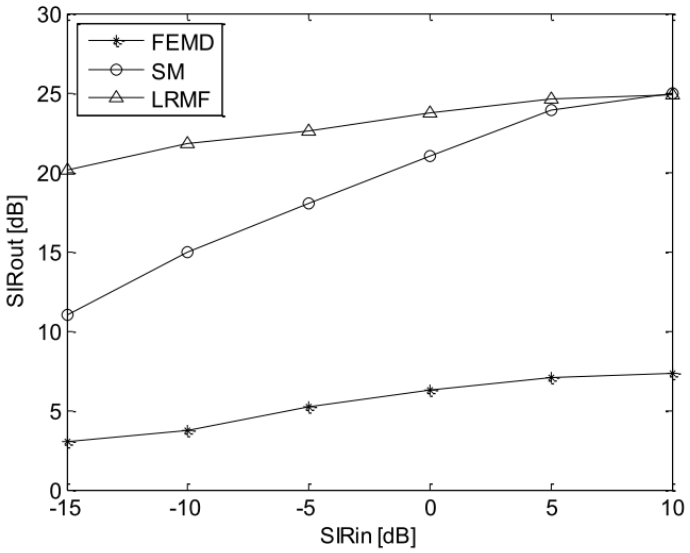

Figure 5.5 Average SIR_{out} = SIR_{out} (SIR_{in}) for removing the noise from the ECG signals.

As an illustration, consider Figure 5.6 where the two uppermost rows represent a clean ECG and contaminated ECG signal with $SIR_{in} = -10$ dB respectively; the remaining rows show output of the analysis methods as labeled. All the methods correctly localize the QRS complexes on the time scale; nevertheless, they are attenuated/distorted with respect to the clean ECG. Moreover, the ST segments undergo important distortion, which is especially noticeable with the FEMD. The LRMF, on the contrary, preserves most of the original ECG characteristics. In addition, we carried out a comparison in terms of average execution time for processing a 1 min recording (60,0 0 0 samples at 1 kHz sampling rate) on a personal computer running at 3.2 GHz processor with 1.5 GB of memory. The methods were run on MATLAB(c) R2013b under Windows 7 (c).

The results, which appear in Table 5.2, show that the SM is computationally the most efficient (less than a second), followed by the LRMF (more than 3 s) and the FEMD (around 25 s). Although these results should be interpreted with care because they are implementation-dependent, the execution time for the FEMD might be considered as an outlier.

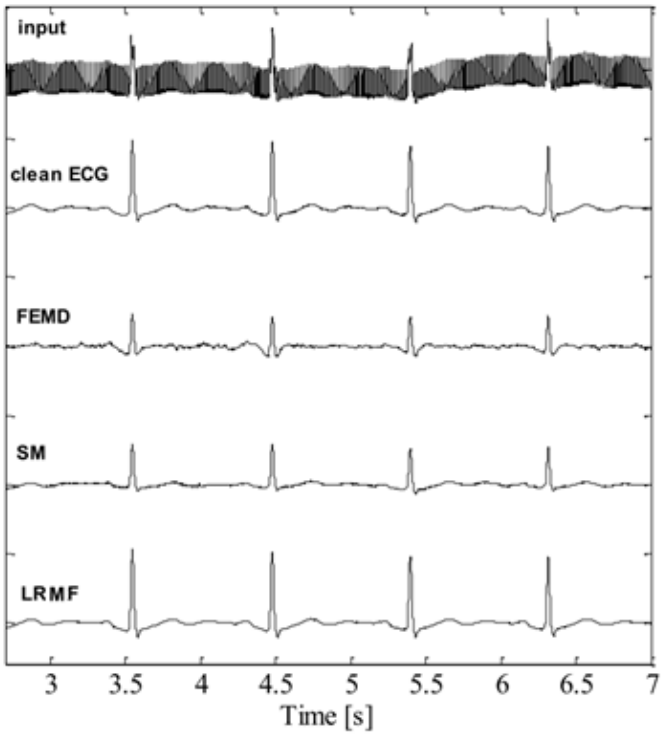

Figure 5.6 Two uppermost signals represent a noisy and clean ECG; the remaining signals are the results obtained by the comparison methods. The SIR_{in} was set to −10 dB.

The reason is that the spline interpolation (which is used for representing intrinsic mode functions) of a relatively large number of points takes a lot of computer resources. Therefore, for processing long signals and/or working with acquisition systems at a high sampling frequency one needs to seek more advanced algorithm implementations in order to cut on the time consumption. On the other hand, the SM and LRMF exhibit much lower computational complexity, which makes them adequate candidates for online processing.

Table 5.2 Average execution time for processing 1 min recording (60 samples at 1 kHz sampling frequency) evaluated on an Intel 3.2 GHz processor.

Method	Time (s)
SM	0.79
FEMD	24.6
LRMF	3.27

5.3.4 Removing noise from EMG

We analyzed thirty EMG signals, each 50-second-long (EMG set I), contaminated simultaneously by the harmonic and baseline noise with the SIR_{in} in [−15, 10] dB range. To evaluate the noise suppression quality, the same measure as in Section 5.3.3 was used (SIR out as a function of SIR_{in}). The corresponding figures of merit are shown in Figure 5.7.

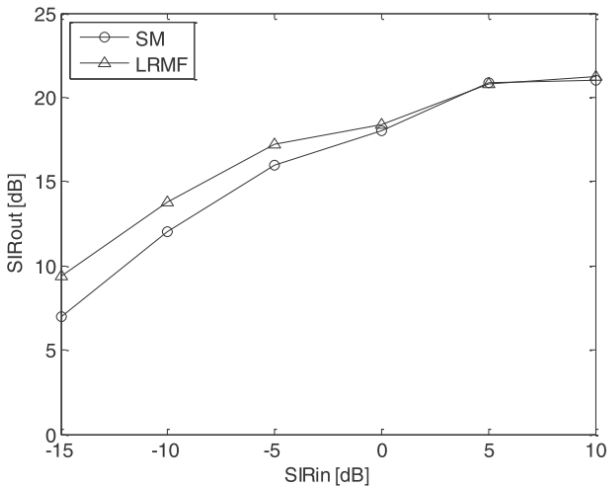

Figure 5.7 Average SIR_{out} = $SIR_{out}(SIR_{in})$ for removing the noise from the EMG signals.

We observe that for the SIR_{in} below 0 dB approximately the LRMF method reaches about 4 dB above the SM. As the SIR_{in} gets larger, both methods perform practically the same. To support these findings, we show in Figure 5.8 an EMG noise removal scenario for SIR_{in} = −10 dB.

The upper row shows a clean and contaminated EMG signal, whilst the lower row shows the goodness-of-fit of the SM and LRMF method for a small waveform portion (for the sake of clarity). Observe how the SM distorts the instantaneous amplitude around the salient peaks, which means that the estimated noise still contains a fraction of the EMG energy. Regarding the LRMF, the quality of the reconstructed EMG is clearly superior, thus indicating that most of the noise was successfully retrieved from the input data. The performance of the methods was also evaluated on the EMG set II recordings by means of subjective comparison (note that an objective comparison could not be carried out because we were unaware of the way the signal components were mixed in the recordings). We processed the total of 1240 contraction bursts from all subjects and acquisition channels and we show next two illustrative examples describing different analysis scenarios.

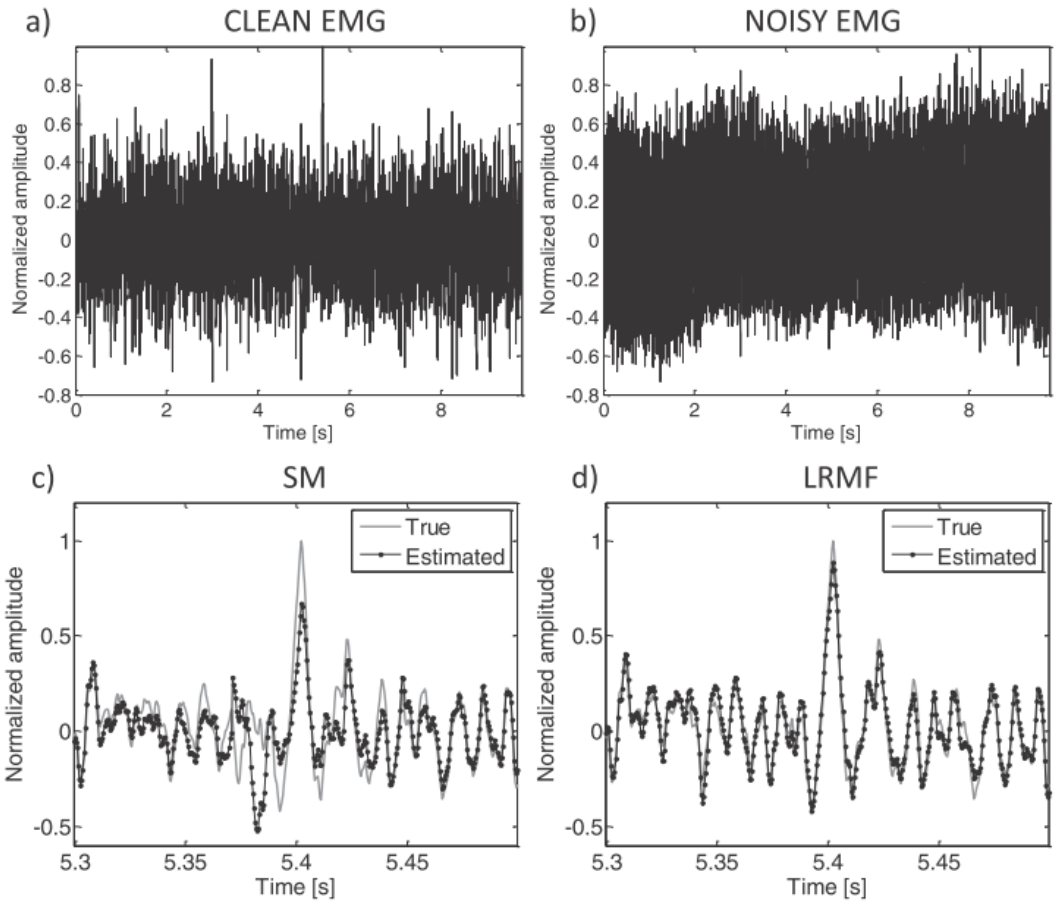

Figure 5.8 The upper row represents (a) a clean and (b) noisy EMG signal (set I); the lower row shows the goodness-of-fit for (c) the SM and (d) LRF method, zoomed around t = 5.4 s. The SIR_{in} was set to −10 dB.

In Figure 5.9 we show the outcome of the SM and LRMF method applied to an EMG recording at 20% MVC. The top row shows the input wave- form and its spectrum, whilst the middle and bottom row show the outcome of the SM and LRMF method respectively. The presence of harmonic noise is clearly visible (Figure 5.9 (b)) as it is the dominant perturbation component in the data. While the time domain waveforms do not provide much insight, a visual inspection of the spectra (Figure 5.9 (b), (d) and (f)) brings out the impact of the noise components removal onto the EMG signal. Both methods succeed in mitigating most of the unwanted signal component energy. However, the SM creates important dips around the harmonic frequencies in the EMG spectrum. As a consequence, it also removes a fraction of the signal of interest, thus generating distortions in the corresponding waveform (recall Figure 5.8).

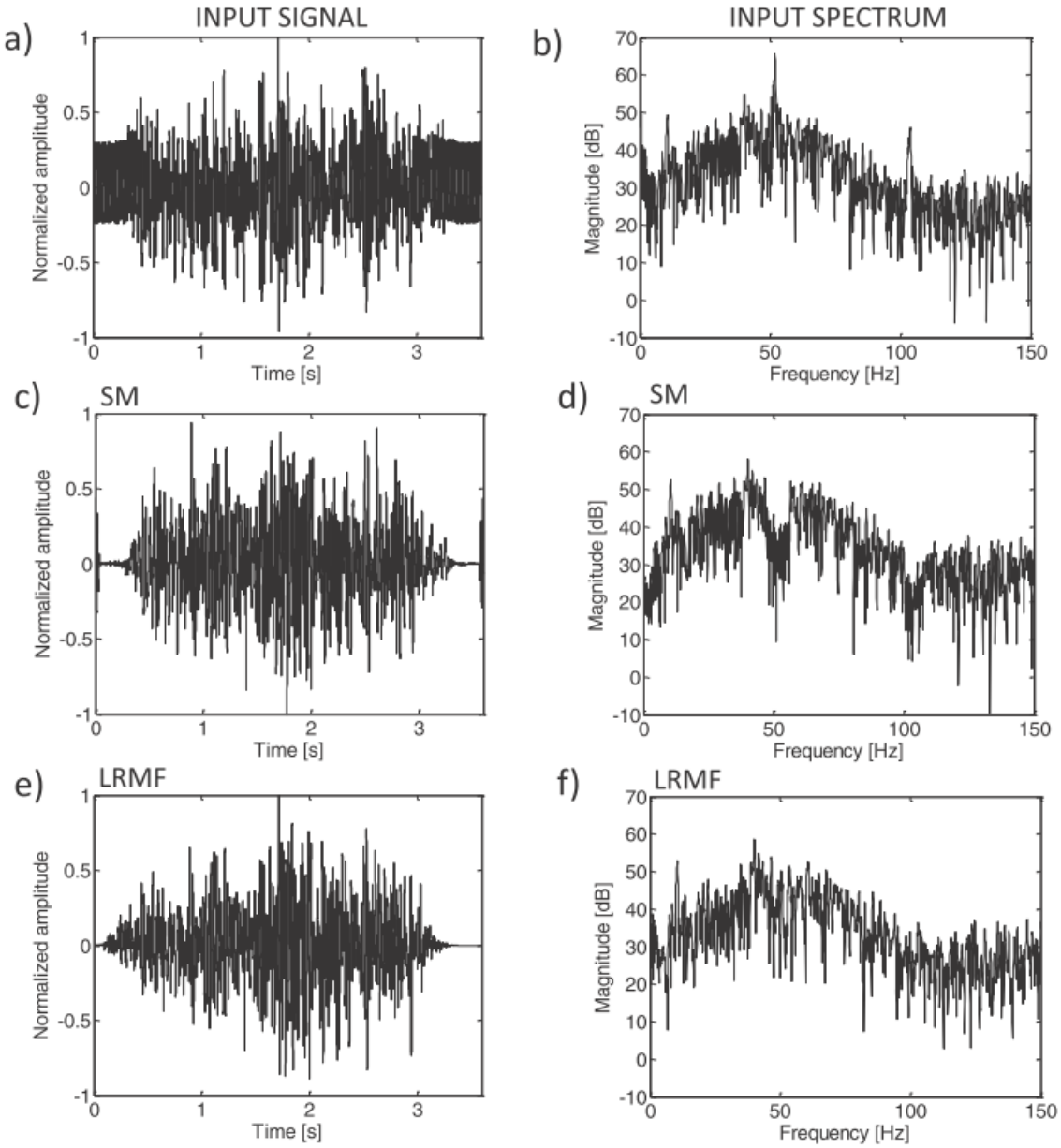

Figure 5.9 EMG set II example at 20% MVC: input waveform and spectrum (upper row), estimated waveform and spectrum by the SM (middle row) and LRMF (bottom row) respectively.

Moreover, the SM generates the short time-domain artifacts visible on the edges of the recording. They are due to the fact that the SIR_{in} is very poor at the recording boundaries, which largely amplifies the uncertainties in the sinusoidal model parameter estimates. The LRMF, on the contrary, introduces minimum altering in the analysis bandwidth, ensuring that all features of the signal of interest are preserved. In addition, the EMG onset and offset turn out to be artifact-free.

Another example, shown on Figure 5.10, features an EMG recording at 60% MVC and its spectrum (upper row) and the outcome of the SM and LRMF method (middle and bottom row respectively). In this case both harmonic and baseline noise components are clearly present (observe that the energy of the baseline drift is clustered in a small bandwidth around the spectrum origin).

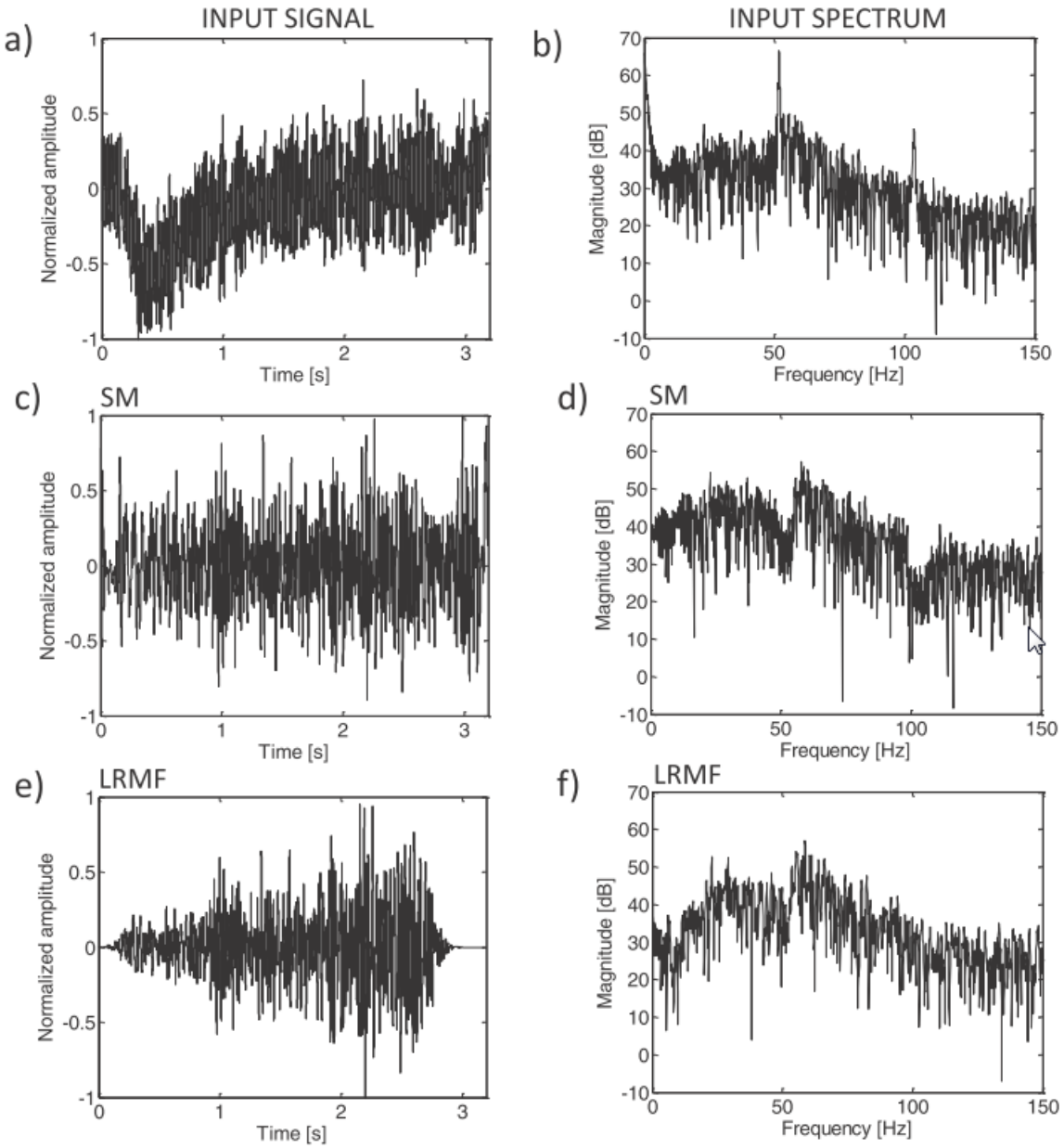

Figure 5.10 EMG set II example at 60% MVC: input waveform and spectrum (upper row), estimated waveform and spectrum by the SM (middle row) and LRMF (bottom row) respectively.

Seemingly both methods accomplish a reasonably good baseline noise removal, as no apparent drift can be seen in the estimated waveforms (Figure 5.10 (c) and (e)). The estimated spectrum by the SM (Figure 5.10 (d)) exhibit the same unwanted harmonic dips, which cause an excessive harmonic noise reduction and EMG signal distortion. The recording-edge artifacts are very strong because the overall noise component contribution is larger compared to the previous example. We observe that the LRMF delivers the EMG signal with no recording-edge artifacts and minimum distortion.

5.5 Summary

We presented a novel approach to joint harmonic and baseline noise removal from biopotential signals in the framework of the low-rank matrix factorization. We showed that suitable biopotential spectrogram modifications generate sparse non-negative representations, which admit decomposition in low-rank matrices. Such matrices convey the information about concurrent sources in the input data and can easily yield the corresponding time waveforms. We introduce a novel spectrogram segmentation procedure which preserves the phases of the input data. Such an approach allows for almost distortionless time-waveform signal component recovery. Moreover, we propose a simple and robust scheme for estimating the optimal non-negative rank for sub-spectrogram decomposition. Experimentally, we establish a comprehensive comparative study against two recent state-of-the-art methods for joint harmonic and baseline noise removal from biopotential signals. We conducted both an objective and a subjective performance analysis on a large number of real and synthetic signal-noise mixtures. The proposed method exhibited superior overall performance, especially in conditions of low signal-to-noise ratios. In terms of output signal-to-interference ratio, the ECG noise removal set the proposed method between 8 dB and 17 dB above the reference methods. Regarding EMG noise reduction, the performance improvement was about 4 dB.

CHAPTER 6

CONCLUSIONS AND FUTURE WORK

In this concluding chapter the main conclusions and guidelines for future research are presented.

6.1 Conclusions

In the following lines we present the most representative conclusions from this research work where we address the aforementioned drawbacks.

6.2 Shortcomings of NMF as an "off-shelf" tool

A straightforward use of existing NMF algorithms for source separation task in biomedical applications turned out to be very inadequate. A thorough research of the core of the NMF algorithms brought out the following evidences:

- A time-frequency representation of the data should emphasize characteristic patterns in the dynamics of the underlying sources: the more significant differences in patterns between sources the better quality of separation could be obtained.
- An initial guess for the iterative process should put the algorithm as close as possible to the global minimum of a cost function. A default random algorithm initialization cannot guarantee a convergence to a global minimum.
- A non-negative matrix decomposition rank should optimally characterize the true dimensions of the sources in the input data. It turned out that when initialization is done with carefully designed structures, the factorization rank can significantly improve separation quality.

Moreover, there was a serious problem regarding phase conservation needed by the inverse STFT for synthesizing time domain waveforms.

6.2.1 Initialization

We have discovered that spectrogram parameters, mainly duration of analysis window, have an impact on NMF efficiency. This parameter controls how the time-frequency pattern of a signal appears in the spectrogram. By modifying this parameter, we were able to change the input "image" and in this way, improve separation quality.

A random-noise initialization of the NMF could not yield reproducible results, even for the same analysis settings. Our first attempt was to design approximate time-frequency structures of the signal sources presented in the mixture. Accordingly, the separation performance improved and the results became predictable.

Later on, we introduced an alternative to the STFT, the Wavelet transform (WT) with adequately chosen basis functions according to the source signals (in our case Cauchy-type non-linearly scaled wavelets to capture ECG source signals). The WT mitigated two problems: it relaxed constrains on the optimal settings for the STFT parameters and ensured correct reconstruction of the time-waveforms by means of its inverse form.

Finally, we have improved the initialization with a spectrogram segmentation scheme what ensured that no spectral phase modifications occur; accordingly, the estimated signal component waveform were virtually distortionless.

6.2.2 Non-negative rank

We immediately noticed the importance of optimal rank selection as we started to design initialization matrices adapted to data. In case of rather simple time-frequency source patterns or spectrogram reshaping that imposed sparsity, the rank set to unity was justified.

Accordingly, we developed a study which presented a general relationship between standard and non-negative matrix rank and showed under which circumstances those ranks could be used interchangeably. A major benefit of this study is that non-negative rank estimation can

be carried out by economy-size singular value decomposition SVD, which significantly improves the algorithm's overall performance i.e. the separation quality and computational efficiency.

6.3 Guidelines for future research

Based on this work, two future research directions can be drawn.

Since proposed by us algorithms need only a few information of source signals, we think that they could be easily adapted to operate on wearable devices to measure electromyogram activity. It could be also useful to innovate existing systems as [108] and to apply our algorithms for ECG denoising tasks.

Although we devoted this research to only single channel acquisition, it still might be interesting to analyze multichannel data in terms of spatial kernels. Indeed, in the last decades, several techniques based on multichannel superficial EMG recordings have been developed for the study of single motor unit (MU) properties. For example, assessment of the characteristics of surface MU potentials (MUPs) along the muscle fiber direction provides information on the location of the innervation zone, fiber length, and muscle fiber conduction velocity, whereas the changes of surface MUPs parameters along the direction perpendicular to the fibers have been used to estimate the MU depth. Therefore, analysis of high density surface EMG data can provide the spatiotemporal profiles of action potentials, which can be interesting for a fundamental research in physiology of muscles. To that end, a natural approach is to extend and generalize matrix factorization models to multi-dimensional matrices - tensor decompositions. Such decompositions are nowadays commonly used in fields of biomedicine, where large amount of multi-dimensional data is available e.g. electroencephalogram signal processing [109] [110]. Probably the most frequently used tensor decomposition is PARAFAC [111] [112], considered as a high-order generalization of the matrix principal component analysis (PCA) [113]. Especially important for biomedical applications is the non-negative PARAFAC method, which imposes non-negativity constraints on factor matrices [114]. This method allows for combining different modes, e.g. space (channels), time and frequency, in order to bring out the interactions and relationship between the signal components. Moreover, it provides a meaningful decomposition results

which have physical interpretation [115]. Such a decomposition strategy is an extension of the classical NMF approach [116] [117] [118] [119]. By adding extra dimensions, the resulting decomposition components can be described not only by the time-frequency signature, but also by the relative contribution from different subjects and channels.

6.4 Conclusiones

A continuación, presentamos las conclusiones más relevantes de este trabajo.

Análisis de algoritmos NMF

El uso de los algoritmos NMF utilizados hasta ahora en la separación de fuentes, en aplicaciones biomédicas, resulta inadecuado. El estudio exhaustivo de dichos algoritmos mostró que:

• Una representación de tiempo y frecuencia de los datos debería enfatizar los patrones característicos de la dinámica de las fuentes: cuanto mayor es la diferencia entre los patrones de las fuentes, se podría obtener una mejor calidad de separación.

• Una inicialización del proceso iterativo debe colocar el algoritmo lo más cerca posible del mínimo global de una función de costo. Por otro lado, la inicialización de algoritmo aleatorio no puede garantizar una convergencia a un mínimo global.

• Un rango de descomposición de matriz no negativa debe caracterizar de manera óptima las verdaderas dimensiones de las fuentes en los datos de entrada. Resultó que cuando la inicialización se realiza con estructuras cuidadosamente diseñadas, el rango de factorización puede mejorar significativamente la calidad de la separación.

Además, había un problema serio con respecto a la conservación de fase necesaria por el STFT inverso para sintetizar las señales en el dominio temporal.

Tratando de solventar los inconvenientes que presentaban este tipo de algoritmos nos hemos centrado en:

Inicialización

Hemos descubierto que los parámetros del espectrograma, principalmente la duración de la ventana de análisis, tienen un impacto en la eficiencia del NMF. Este parámetro controla cómo

aparece el patrón de tiempo-frecuencia de una señal en el espectrograma. Al modificar este parámetro, pudimos cambiar la "imagen" de entrada y, de esta manera, mejorar la calidad de la separación.

La inicialización aleatoria del NMF no podría obtener resultados reproducibles, incluso para los mismos ajustes de análisis. Nuestro primer intento fue diseñar estructuras de tiempo-frecuencia aproximadas de las fuentes de señales en la mezcla. En consecuencia, el rendimiento de separación mejoró y los resultados se volvieron predecibles.

Más adelante, presentamos una alternativa al STFT, la transformada Wavelet (WT) con funciones básicas elegidas adecuadamente de acuerdo con las señales fuente (en nuestro caso, wavelets de escala no lineal de tipo Cauchy para capturar señales fuente de ECG). El WT mitigó dos problemas: elimino las restricciones sobre los ajustes óptimos para los parámetros de STFT y aseguró la reconstrucción correcta de las señales de domino temporal mediante transformada inversa.

Finalmente, hemos mejorado la inicialización con un esquema de segmentación de espectrogramas lo que aseguró que no ocurran modificaciones de fase espectral; en consecuencia, le señal recuperada era sin distorsiones.

Rango

Descubrimos la importancia de la selección óptima de rango cuando comenzamos a diseñar matrices de inicialización adaptadas a los datos. En el caso de patrones de fuente de tiempo-frecuencia simples o en caso de remodelación del espectrograma que imponía la dispersión, el rango igual a la unidad estaba justificado.

Luego desarrollamos un estudio que presentaba una relación general entre el rango de matriz estándar y el rango non negativo y enseñamos en qué circunstancias esos rangos se podían usar indistintamente. Un beneficio importante de este estudio es que la estimación de rango no negativo se puede llevar a cabo mediante la descomposición SVD, lo que mejora significativamente el rendimiento general del algoritmo, es decir, la calidad de separación y la eficiencia computacional.

BIBLIOGRAPHY

[1] C. J. P. Comon, Handbook of Blind Source Separation: Independent Component Analysis and Applications, Academic Press, 2010.

[2] M. Zivanovic, M. Gonzalez-Izal, „Nonstationary Harmonic Modeling for ECG Removal in Surface EMG Signals," *IEE Transactions on Biomedical Engineering,* tom 59, nr 6, pp. 1633-1640, 2012.

[3] A. Cichocki, R. Zdunek, AH Phan, S. Amari, Nonnegative Matrix and Tensor Factorizations: Applications to Exploratory Multiway Data Analysis and Blind Source Separation, John Wiley & Sons, Ltd, 2009.

[4] D.D. Lee, H.S. Seung, „Learning the parts of objects by non-negative matrix factorization," *Nature,* tom 401, p. 788—791, 1999.

[5] M. Zivanovic, M. González-Izal, „Simultaneous powerline interference and baseline wander removal from ECG and EMG signals by sinusoidal modeling," *Medical Engineering and Physics,* tom 35, nr 10, pp. 1431-1441, 2013.

[6] T. Schweitzer, J. Fitzgerald, J. Bowden. P. Lynne-Davies, „Spectral analysis of human inspiratory diaphragmatic electromyograms," *The Journal of Physiology,* tom 46, pp. 152-165, 1979.

[7] C. Roberts, A. Bartolo, R. Dzwonczyk, E. Goldman, „Analysis of diaphragm EMG signals: comparison of gating vs. subtraction for removal of ECG contamination," *ournal of Applied Physiology,* tom 80, nr 6, p. 1892–1902, 1996.

[8] S. Levine, J. Gillen, P. Weiser, M. Gillen, E. Kwatny, „Description and validation of an ECG removal procedure for EMGdi power spectrum analysis," *Journal of Applied Physiology,* tom 60, p. 1073–1081, 1986.

[9] M. Redfern, R. Hughes, D. Chaffin, „High-pass filtering to remove electrocardiographic interference from torso EMG recordings," *Clinical Biomechanics,* tom 8, pp. 44-48, 1993.

[10] J.D.M. Drake, J.P. Callaghan, „Elimination of electrocardiogram contamination from electromyogram signals: An evaluation of currently used removal techniques," *Journal of Electromyography and Kinesiology,* tom 16, nr 2, pp. 175-187, 2006.

[11] S. Sanei, T.K.M. Lee, V. Abolghasemi, „A new adaptive line enhancer based on singular spectrum," *IEEE Transactions on Biomedical Engineering,* tom 59, nr 2, pp. 428-434, 2012.

[12] J. Barrios-Muriela, F. Romeroa, F.J. Alonso, K. Gianikellis, „A simple SSA-based de-noising technique to remove ECG interference in EMG signals," *Biomedical Signal Processing and Control,* tom 30, pp. 117-126, 2016.

[13] B. Widrow, J.R. Glover, M. Mccool, J. Kaunitz,C.S. Williams, R.H. Hean, J.R. Zeidler, E. Dong Jr, R.C. Goodlin R, „Adaptive noise canceling: Principles and applications," *Proceedings of the IEEE,* tom 63, nr 12, p. 1692–1716, 1975.

[14] Y. Deng, W. Wolf,R. Schnell, U. Appel, „New aspects to event-synchronous cancellation of ECG," *IEEE Transactions on Biomedical Engineering,* tom 47, nr 9, p. 1177–1184, 2000.

[15] C. Marque, C. Bisch, R. Dantas, S. Elayoubi, V. Brosse and C. Perot, „Adaptive filtering for ECG," *Journal of Electromyography and Kinesiology,* tom 15, nr 3, pp. 310-315, 2005.

[16] G. Lu, J. Brittainb, P. Holland, J. Yianni, A. Greenb, J. Steina, T. Aziza, S. Wanga, „Removing ECG noise from surface EMG signals using adaptive filtering," *Neuroscience Letters,* tom 462, nr 1, pp. 14-19, 2009.

[17] P. Zhou, B. Lock, T.A. Kuiken, „Real time ECG artifact removal for myoelectric prosthesis control," *Physiological Measurement,* tom 28, nr 4, 2007.

[18] L. Cuiwei, Z. Chongxun, T. Changfeng, „Detection of ECG characteristic points using wavelet transforms," *IEEE Transactions on Biomedical Engineering,* tom 42, nr 1, pp. 21-28, 1995.

[19] P. Ravier, O. Buttelli, „Robust detection of QRS complex using Klauder wavelets," *12th European Signal Processing conference,* p. 2199–2202, 2004.

[20] L. Brechet, M.F. Lucas, C. Doncarli, D. Farina, „Compression of biomedical signals with mother wavelet optimization and best-basis wavelet packet selection," *IEEE Transactions on Biomedical Engineering,* tom 54, nr 12, pp. 2186-2192, 2007.

[21] K Daqrouq, AR Al-Qawasmi, „ECG Enhancement using Wavelet Transform," *ransactions on Biology and Biomedicine,* tom 7, nr 2, p. 62–72, 2010.

[22] PS Gokhale, „ECG Signal De-noising using Discrete Wavelet Transform for removal of 50Hz PLI noise," *International Journal of Emerging Technology and Advanced Engineering,* tom 2, nr 5, p. 81–85, 2012.

[23] C. Zhan, L. F. Yeung, Z. Yang, „A wavelet-based adaptive filter for removing ECG interference in EMGdi signals," *Journal of Electromyography and Kinesiology,* nr 20, p. 542–549, 2010.

[24] Y. Slim, K. Raoof, „Removal of ECG interference from surface respiratory electromyography," *IRBM,* nr 31, p. 209–220, 2010.

[25] J. Taelman, S. Van Huffel, A. Spaepen, „Wavelet-independent component analysis to remove electrocardiography contamination in surface electromyography," *IEEE Engineering in Medicine and Biology Society,* p. 682–685, 2007.

[26] V. Von Tscharner, B. Eskofier, P. Federolf, „Removal of the electrocardiogram signal from surface EMG recordings using nonlinearly scaled wavelets," *Journal of Electromyography and Kinesiology,* tom 21, nr 4, pp. 683-688, 2011.

[27] P. Akbary, H. Rabbani, „Removing power line interference and ECG signal from EMG signal using matching pursuit," *International Conference on Signal Processing,* pp. 1714-1717, 2010.

[28] A. Elloumi, Z. Lachiri, N. Ellouze, „Denoising ECG contaminated with EMG components based on pitch synchronous wavelet analysis," *IEEE International Conference on Industrial Technology ,* tom 3, p. 1660–1663, 2004.

[29] A Awal, SS Mostafa, M Ahmad, „Performance Analysis of Savitzky-Golay Smoothing Filter Using ECG Signal," *International Journal of Computer and Information Technology ,* tom 1, nr 2, p. 24–29, 2011.

[30] S. Hargittai, „Savitzky-Golay least-squares polynomial filters in ECG signal processing," *Computers in Cardiology,* p. 763–766, 2005.

[31] J. Piskorowski, „Suppressing harmonic powerline interference using multiple-notch filtering methods with improved transient behavior," *Measurement.,* tom 45, nr 6, p. 1350–1361, 2012.

[32] YV Joshi, SC Dutta Roy, „Design of IIR multiple notch filters," *International Journal of Circuit Theory and Applications,* tom 26, nr 5, p. 499–507, 1998.

[33] R Deshpande, B Kumar, SB Jain, „On the design of multi notch filters," *International Journal of Circuit Theory and Applications,* tom 40, nr 4, p. 313–327, 2012.

[34] R Deshpande, B Kumar, SB Jain, „Highly narrow rejection bandwidth finite impulse response notch filters for communication," *IET Communications,* tom 4, nr 18, p. 2208–2216, 2010.

[35] J Piskorowski, „Digital Q-varying notch IIR filter with transient suppression," *IEEE Transactions on Instrumentation and Measurement,* tom 59, nr 4, p. 866–872, 2010.

[36] S.C. Pei, C.C. Tseng, „Elimination of AC interference in Electrocardiogram using IIR Notch filter with transient suppression," *IEEE Transactions on Biomedical Engineering,* tom 42, nr 11, 1995.

[37] P.S. Hamilton, „A comparison of adaptive and nonadaptive filters for reduction of power line interference in the ECG," *IEEE Transactions on Biomedical Engineering,* tom 46, nr 1, pp. 105 - 109, 1996.

[38] Y. W. Bai, W.Y. Chu, C.Y. Chen, Y.T. Lee, Y.C. Tsai, C.H. Tsai, „Adjustable 60Hz noise reduction by a notch filter for ECG signals," *Proceedings of the IEEE Instrumentation and Measurement Technology Conference,* 2004.

[39] D.P. Allen, „A frequency domain Hampel filter for blind rejection of sinusoidal interference from electromyograms," *Journal Neuroscience Methods,* tom 155, nr 177, pp. 303-310, 2009.

[40] M. H. Costa, M. C. Tavares, „Removing harmonic power line interference from biopotential signals," *Computers in Biology and Medicine,* nr 39, pp. 519-526, 2009.

[41] IS Badreldin, DS El-Kholy, AA El-Wakil, „A modified adaptive noise canceler for electrocardiography with no power-line reference," *Proceedings of the 5th Cairo International Biomedical Engineering Conference,* p. 13–16, 2010.

[42] IS Badreldin, DS El-Kholy, AA Elwakil, „Harmonic adaptive noise canceler for electrocardiography with no power-line reference," *Proceedings of the 16th IEEE Mediteranean Electrotechnical Conference,* p. 1017–1020, 2012.

[43] SMM Martens, M Mischi, SG Oei, JWM Bergmans, „An improved adaptive power line interference canceller for electrocardiography. IEEE Transactions on Biomedical Engineering," *IEEE Transactions on Biomedical Engineering,* tom 53, nr 11, p. 2220–2231, 2006.

[44] M Maniruzzaman, KMS Billah, U Biswas, B Gain, „Least-Mean-Square algorithm based adaptive filters for removing power line interference from ECG signal," *Proceedings of the International Conference on Informatics, Electronics & Vision ,* p. 737–740, 2012.

[45] G Liangling, Z Nanquan, W Haotian, „Application of interference canceller in bioelectricity signal disposing," *Procedia Environmental Sciences,* tom 10, nr A, p. 814–819, 2011.

[46] G Li, X Zeng, X Zhou, Y Zhou, G Liu, X Zhou, „Robust suppression of nonstationary power-line interference in electrocardiogram signals," *Physiological Measurement,* tom 33, nr 7, p. 1151–1169, 2012.

[47] H Hajimolahoseini, MR Taban, H Soltanian-Zadeh, „Extended Kalman Filter frequency tracker for nonstationary harmonic signals.," *Measurement,* tom 45, nr 1, p. 126–132, 2012.

[48] JJ Galiana-Merino, D Ruiz-Fernandez, JJ Martinez-Espla, „Power line interference filtering on surface electromyography based on the stationary wavelet packet transform," *Computer Methods and Programs in Biomedicine,* tom 111, nr 2, p. 338–346, 2013.

[49] P Karthikeyan, M Murugappan, S Yaacob, „ECG signal denoising using wavelet thresholding techniques in Human Stress Assessment," *International Journal on Electrical Engineering and Informatics,* tom 4, nr 2, 2012.

[50] M Alfaouri, K Daqrouq, „ECG signal denoising by wavelet transform thresholding," *American Journal of Applied Sciences,* tom 5, nr 3, p. 276–281, 2008.

[51] S Pal, M Mitra, „Empirical mode decomposition based ECG enhancement and QRS detection," *Computers in Biology and Medicine,* tom 42, nr 1, pp. 83-92, 2012.

[52] MA Kabir, C Shahnaz, „Denoising of ECG signals based on noise reduction algorithms in EMD and wavelet domains.," *Biomedical Signal Processing and Control,* tom 7, nr 5, p. 481–489, 2012.

[53] J Arturas, M Vaidotas, L Arūnas, „Ensemble empirical mode decomposition based feature enhancement of cardio signals," *Medical Engineering & Physics,* tom 35, nr 8, p. 1059–1069, 2012.

[54] S Poungponsri , XH Yu, „n adaptive filtering approach for electrocardiogram (ECG) signal noise reduction using neural networks," *Neurocomputing,* tom 117, pp. 206-213, 2013.

[55] J Mateo, C Sánchez, A Torres, R Cervigon, JJ Rieta , „Neural network based canceller for powerline interference in ECG signals," *Proceedings of the Annual International Conference on Computers in Cardiology,* p. 1073–1076, 2008.

[56] YD Lin , CY Hsu , HY Chen , KK Tseng, „Efficient block-wise independent component analysis with optimal learning rate," *Neurocomputing,* tom 117, p. 22–32, 2013.

[57] MPS Chawla, „PCA and ICA processing methods for removal of artifacts and noise in electrocardiograms: a survey and comparison," *Applied Soft Computing Journal,* tom 11, nr 2, p. 2216–2226, 2011.

[58] A Hyvärinen, „Fast and robust fixed-point algorithms for independent component analysis," *IEEE Transactions on Neural Networks,* tom 10, nr 3, p. 626–634, 1999.

[59] C Levkov, G Mihov, R Ivanov, I Daskalov, I Christov, I Dotsinsky, „Removal of power-line interference from the ECG: a review of the subtraction procedure," *BioMedical Engineering Online,* tom 50, p. 4, 2005.

[60] G Mihov, I Dotsinsky, T Georgieva, „Subtraction procedure for powerline interference removing from ECG: improvement for non-multiple sampling," *Journal of Medical Engineering and Technology,* tom 29, nr 5, p. 238–243, 2005.

[61] D.D. Lee, H.S. Seung, „Algorithms for nonnegative matrix factorization," *Advances in Neural Information Processing Systems,* tom 13, pp. 556-562, 2001.

[62] Z. Zheng, J. Yang, Y. Zhu, „Initialization enhancer for non-negative matrix factorization," *Engineering Applications of Artificial Intelligence,* tom 20, pp. 101-110, 2007.

[63] J. Yoo, S. Choi, „Nonnegative Matrix Factorization with Orthogonality Constraints," *Information Processing and Management,* tom 46, nr 5, pp. 559-570, 2010.

[64] M. Asteris, D.Papailiopoulos, AG. Dimakis, „Orthogonal NMF through Subspace Exploration," *Advances in Neural Information Processing Systems ,* tom 28, pp. 343--351, 2015.

[65] H Li, T Adal, W Wang, D Emge, A Cichocki, „Non-negative Matrix Factorization with Orthogonality Constraints and its Application to Raman Spectroscopy," *The Journal of VLSI Signal Processing Systems for Signal, Image, and Video Technology ,* tom 48, p. 83–97, 2007.

[66] N. Bertin, R. Badeau, E. Vincent, „Fast bayesian nmf algorithms enforcing harmonicity and temporal continuity in polyphonic music transcription," *IEEE Workshop on Applications of Signal Processing to Audio and Acoustics,* 2009.

[67] T. Virtanen, „Monaural sound source separation by non negative matrix factorization with temporal continuity and sparseness criteria," *IEEE Transactions on Audio, Speech, and Language Processing,* tom 15, nr 3, p. 1066–1074, 2007.

[68] J. Eggert, E. Korner, „Sparse Coding and NMF," *Neural Networks,* 2004.

[69] M. Schmidt, J. Larsen, F. Hsiao, „Wind Noise Reduction using Non-negative Sparse Coding," *IEEE Workshop on Machine Learning for Signal Processing,* 2007.

[70] S. Li et al, „Learning Spatially Localized, Parts-Based Representation," *Computer Vision and Pattern Recognition,* 2001.

[71] P. Smaragdis, „Non-negative Matrix Factor Deconvolution Extraction of Multiple Sound Sources from Monophonic Inputs," *International Symposium on ICA and BSS,* 2004.

[72] D. Griffin,.J Lim, „Signal estimation from modified short-time Fourier transform," *IEEE Transactions on Acoustics, Speech, and Signal Processing,* tom 32, p. 236–242, 1984.

[73] K. Achan, S. Roweis, B. Frey, „Probabilistic inference of speech signals from phaseless spectrograms," *Proceedings of Neural Information Processing Systems,* p. 1393–1400, 2003.

[74] T. Virtanen, „Sound Source Separation in Monaural Music Signals," *PhD Thesis,* 2006.

[75] P. Smaragdis, J. Brown, „Non-negative matrix factorization for polyphonic," *IEEE Workshop on Applications of Signal Processing to Audio and Acoustics,* p. 177–180, 2003.

[76] N. Bertin, R. Badeau and E. Vincent, „Enforcing Harmonicity and Smoothness in Bayesian Non-Negative Matrix Factorization Applied to Polyphonic Music Transcription," *IEEE Transactions on Audio, Speech, and Language Processing,,* tom 3, p. 18, 2010.

[77] S. Wild, J. Curry, A.Dougherty, „Improving Non-negative Matrix Factorizations Through Structured Initialization," *Pattern Recognition,* tom 37, nr 11, pp. 2217-2232, 2004.

[78] A. Janecek, Y. Tan, „Using population based algorithms for initializing nonnegative matrix factorization," *The Second International Conference on Swarm Intelligence,* p. 307–316, 2011.

[79] H. Qiao, „New SVD based initialization strategy for non-negative matrix factorization," *Pattern Recognition Letters,* tom 63, nr 1, pp. 71-77, 2015.

[80] A.L.Goldberger, L.A.N.Amaral, L. Glass, J.M. Hausdorff, P.Ch. Ivanov, R.G. Mark, J.E.Mietus, G.B.Moody,CK.Peng, H.E.Stanley, „PhysioBank, PhysioToolkit, and PhysioNet; Components of a New Research Resource for Complex Physiologic Signals," *Circulation Electronic Pages,* tom 101, pp. 215-220, 2000.

[81] M Porteous, „Introduction to Digital Resampling," *RF Engines Ltd,* 2011.

[82] DA Winter, „Biomechanics and motor control of human movement," *New York: John Wiley & Sons, Inc,* pp. 191-212, 1990.

[83] R. Karthik, „ECG simulation using Matlab," *Online.*

[84] M. S. Redfern, R. E. Hughes, D. B. Chaffin, „High-pass filtering to remove electrocardiographic interference from torso EMG recordings," *Clinical Biomechanics,* tom 8, pp. 44-48, 1993.

[85] B. Wang, W. Lu, „A fixed-point ICA algorithm with initialization constraint," *Conference on Computer and Communications Security,* pp. 891-894, 2005.

[86] A. Teolis, Computational Signal Processing With Wavelets, Boston: Birkhaeuser, 1998.

[87] E. C. Karvounis, M. G. Tsipouras, D. I. Fotiadis, K. K. Naka, „An automated methodology for fetal heart rate extraction from the abdominal electrocardiogram," *IEE Transactions on Biomedical Engineering,* tom 11, nr 6, p. 628–638, 2007.

[88] M.Zivanovic, M.González-Izal, „Simultaneous powerline interference and baseline wander removalfrom ECG and EMG signals by sinusoidal modeling," *Medical Engineering & Physics ,* tom 35 , p. 1431– 1441, 2013.

[89] M. Niegowski, M. Zivanovic, „ECG-EMG separation by using enhanced non-negative matrix factorization," *Conference proceedings: Annual International Conference of the IEEE Engineering in Medicine and Biology Society,* pp. 4212-4215, 2014.

[90] M. González-Izal, A. Malanda, I. Navarro-Amézqueta, E.M. Gorostiaga, F. Mallor, J. Ibañez, M. Izquierdo, „EMG spectral indices and muscle power fatigue during dynamic contractions," *Journal of Electromyography and Kinesiology,* tom 20, pp. 233-240, 2010.

[91] M. Izquierdo, M. González-Izal, I. Navarro-Amézqueta, A.L. Calbet Jose, J. Ibañez, A. Malanda, F. Mallor F, K. Hakkinen, W.J. Kraemer, E. Gorrostiaga, „Effects of Strength Training on Muscle Fatigue Mapping from Surface EMG and Blood Metabolites," *Medicine & Science in Sports & Exercise,* tom 43, nr 2, pp. 303-311, 2011.

[92] D. Farina, F. Negro, „Estimation of muscle fiber conduction velocity with a spectral multidip approach," *IEEE Transactions on Information Technology in Biomedicine,* tom 54, nr 9, pp. 1583-1589, 2007.

[93] C.L. Christodoulou, P.A. Kaplanis, V. Murray, M.S. Pattichis, C. S.Pattichis, T. Kyriakides , „Multi-scale AM-FM analysis for the classification of surface electromyographic signals," *Biomedical Signal Processing and Control,* tom 7, nr 3, p. 265–269, 2012.

[94] E. Carotti, J.C. De Martin, R. Merletti, D. Farina, „Compression of surface EMG signals with algebraic code excited linear prediction," *Medical Engineering & Physics,* tom 29, nr 2, pp. 253-258, 2007.

[95] M. Niegowski, M. Zivanovic, M. Gomez, P. Lecumberri, „ Unsupervised learning technique for surface electromyogram denoising from power line interference and baseline wander," *Proceedings of the Thirty-seventh Annual International Conference of IEEE Engineering in Medicine and Biology Society,* 2015.

[96] I. Markovsky, „Applications of structured low-rank approximation," *Proceedings of International Federation of Automatic Control,* 2009.

[97] Z. Zhang, Y. Xu, J. Yang, X. Li, D. Zhang,, „A survey of sparse representation: algorithms and applications," *IEEE Access 3,* p. 490–530, 2015.

[98] D.A. Gregory , N.J. Pullman, „Semiring rank: Boolean rank and nonnegative rank factorizations," *Journal of Combinatorics, Information & System Sciences,* tom 8, p. 223–233, 1983.

[99] M.M. Lin, M.T. Chu, „On the nonnegative rank of Euclidean distance matrices,," *Linear Algebra Appl,* tom 433, nr 6, p. 81–86 89, 2010.

[100] S.A. Vavasis, „On the complexity of nonnegative matrix factorization," *The SIAM Journal on Optimization ,* tom 20, p. 1364, 2010.

[101] B. Dong, M.M. Lin, M.T. Chu, „ Nonnegative rank factorization-a heuristic approach via rank reduction," *Numerical Algorithms,* p. 1–24, 2013.

[102] J.S. Williams, D. Child, „The essentials of factor analysis," *New York Continuum,* 2003.

[103] A.S. Beavers , J.W. Lounsbury , J.K. Richards , S.W. Huck , G.J. Skolits , S.L. Esquivel, „Practical considerations for using exploratory factor analysis in educational research," *Practical Assessment, Research and Evaluation ,* tom 18, p. 1–13, 2013.

[104] J.D. Dixon, „Problems in Group Theory," *Dover Publications,* 1973.

[105] W. Verhelst, „Overlap-add methods for time-scaling of speech," *Speech Communication,* tom 30, p. 207–221, 2000.

[106] A .L. Goldberger, L.A .N. Amaral, L. Glass, J.M. Hausdorff, P.C. Ivanov, R.G. Mark,J.E. Mietus, G.B. Moody, C.-K. Peng, H. Stanley, „PhysioToolkit and PhysioNet: components of a new research resource for complex physiologic signals," *Circulation,* tom 101, pp. 215-220, 2000.

[107] S. Agrawal, A. Gupta, „ Fractal and EMD based removal of baseline wander and powerline interference from ECG signals," *Computers in Biology and Medicine,* tom 43, pp. 1889-1899, 2013.

[108] S.Led, M.Martínez-Espronceda, J.Redondo, A.Baquero, M. Niegowski, L. Serrano, L.Cabezas, „A Wearable Electrocardiogram Recorder (ECG) Using ISO / IEEE 11073 Interoperability Standard," *Lecture Notes in Computer Science: International Workshop on Ambient Assisted Living,* tom 7657, pp. 175-182, 2012.

[109] K. Nazarpour, Y. Wongsawat, S. Sanei, J.A. Chambers, S. Oraintara, „Removal of the eye-blink artifacts from EEGs via STF-TS modeling and robust minimum variance beamforming," *IEEE Transactions on Biomedical Engineering ,* tom 55, nr 9, pp. 2221-2231, 2008.

[110] K. Nazarpour, H.R. Mohseni, C.W. Hesse, J.A. Chambers, S. Sanei , „A novel semi-blind signal extraction approach for the removal of eye-blink artifact from EEGs," *EURASIP Journal on Advances in Signal Processing,* tom 857459, pp. 1-12, 2008.

[111] R.A. Harshman, M.E. Lundy, „ PARAFAC: Parallel factor analysis," *Computational Statistics & Data Analysis,* tom 18, pp. 39-72, 1994.

[112] R. Bro, „PARAFAC: Tutorial and applications," *Chemometrics and Intelligent Laboratory Systems,* tom 38, p. 149–171, 1997.

[113] R. Pardo, B.A. Helena, C. Cazurro, C. Guerra, L. Deban, C.M. Guerra, M. Vega, „Application of two- and three-way principal component analysis to the interpretation of chemical fractionation results obtained by the use of the B.C.R. procedure," *Analytica Chimica Acta,* tom 523, pp. 125-132, 2004.

[114] J.D. Carroll, G. De Soete, S. Pruzansky, „Fitting of the latent class model via iteratively reweighted least squares CANDECOMP with nonnegativity constraints," *Multiway data analysis,* p. 463–472, 1989.

[115] A.H. Phan, A. Cichocki, „Multi-way nonnegative tensor factorization using fast hierarchical alternating least squares algorithm (HALS)," *International Symposium on Nonlinear Theory and its Applications,* 2008.

[116] M. Welling, M. Weber, „Positive tensor factorization," *Pattern Recognition Letter,* tom 22, nr 12, pp. 1255-1261, 2001.

[117] D. FitzGerald, M. Cranitch, E. Coyle, „Non-negative tensor factorisation for sound source separation," *In proceedings of Irish Signals and Systems Conference,* pp. 8-12, 2005.

[118] M.R. Parry, I. Essa, „Estimating the spatial position of spectral components in audio," *In proceedings Independent Component Analysis and Blind Signal Separation – Lecture Notes in Computer Science,* tom 3889, pp. 666-673, 2006.

[119] A. Cichocki, R. Zdunek, S. Choi, R. Plemmons, S. Amari, „Nonnegative tensor factorization using alpha and beta divergencies," *IEEE International Conference on Acoustics, Speech, and Signal Processing,* tom 3, pp. 1393-1396, 2007.

[120] J. A. Van Alste, T. S. Schilder, „Removal of base-line wander and power-line interference from the ECG by an efficient FIR filter with a reduced number of taps," *IEEE Transactions on Biomedical Engineering,* tom 32, nr 12, pp. 1052-1060, 1985.

[121] J. Mak, Y. Hu, and K. Luk, „An automated ECG-artifact removal method for trunk muscle surface EMG recordings," tom 32, nr 8, p. 840–848, 2010.

[122] C. Levkov, G. Mihov, R. Ivanov, I. Daskalov, I. Christov, I. Dotsinsky, „Removal of power-line interference from the ECG: a review of the subtraction procedure," *BioMedical Engineering OnLine,* tom 4, p. 50, 2005.

[123] M.Martínez-Espronceda, S. Led, M. Niegowski, L.Serrano, L. Cabezas, „A Novel Software Development Kit (SDK) to Foster Adoption of Health Informatics Standards in Personal Health Device (PHD) Communications," *Lecture Notes in Computer Science,* tom 7657, pp. 66-73, 2012.

List of publications

- Miroslav Zivanovic, ***Maciej Niegowski***, Pablo Lecumberri, Marisol Gómez: A low-rank matrix factorization approach for joint harmonic and baseline noise suppression in biopotential signals. Computer Methods and Programs in Biomedicine 141: 59-71 (2017)

- ***Maciej Niegowski***, Miroslav Zivanovic: Wavelet-based unsupervised learning method for electrocardiogram suppression in surface electromyograms. Medical Engineering & Physics 38 (3), 248–256 (2016)

- ***Maciej Niegowski***, Miroslav Zivanovic, Marisol Gómez, Pablo Lecumberri: Unsupervised learning technique for surface electromyogram denoising from power line interference and baseline wander. EMBC 2015: 7274-7277

- ***Maciej Niegowski***, Miroslav Zivanovic: ECG-EMG separation by using enhanced non-negative matrix factorization. EMBC 2014: 4212-4215

- Miguel Martínez-Espronceda, Santiago Led, ***Maciej Niegowski***, Luis Serrano, Luis Cabezas: A Novel Software Development Kit (SDK) to Foster Adoption of Health Informatics Standards in Personal Health Device (PHD) Communications. IWAAL 2012: 66-73

- Santiago Led, Miguel Martínez-Espronceda, Javier Redondo, Alfonso Baquero, ***Maciej Niegowski***, Luis Serrano, Luis Cabezas: A Wearable Electrocardiogram Recorder (ECG) Using ISO / IEEE 11073 Interoperability Standard. IWAAL 2012: 175-182